SCUOLA SUPERIORE DI CATANIA
International PhD in Nanoscience
XXIV cycle

Micro and Nano patterns for Biosensing: from enzymatic assays to single cells interaction arrays

Giuseppe Domenico Arrabito

Coordinator of PhD:
Prof.ssa M.G. Grimaldi

Tutor:
Prof.ssa M.G. Grimaldi
Prof. B. Pignataro

a.a. 2009/2011

Micro and Nano patterns for Biosensing: from enzymatic assays to single cells interaction arrays

Author:

Giuseppe, Domenico Arrabito

Ph.D. Thesis - Università degli Studi di Catania - Scuola Superiore di Catania

al piccolo Carlo
alle piccole Helena ed Isabella

a Marco Simoncelli

Contents

List of Figures

Abstract

In this thesis work, solution dispensing techniques have been employed for the realization of complex biological arrays. Inkjet printing techniques were employed for the generation of drug screening platforms. In particular, picoliter drops containing a model substrate (D-glucose)/inhibitor (D-glucal) couple were accurately dispensed on a single layer consisting of the enzymatic target (glucose oxidase) covalently linked to a functionalized silicon oxide support. A simple colorimetric detection method allowed one to prove the screening capability of the microarray with the possibility to assay with high reproducibility at the single spot level. Measurements of the optical signal as a function of concentration and of time verified the occurrence at the solid-liquid interface of the competitive enzymatic inhibition with a similar behavior occurring for this system in a solution phase along with overcoming competition effects. Afterwards, this methodology has been extended to CYP450 enzymes like CYP3A4, one of the main targets for the phase I drug metabolism via a droplet microreactors arrays contain-

ing CYP3A4 enzyme mixed with inhibitors (1-aminobenzotriaozle and erythromycin) and a luminogenic enzymatic substrate (Luciferin-IPA). Detection of the enzymatic reaction was carried out via a simple luminometric optical method that exploited the bioluminescence given by D-luciferin upon reaction with oxygen in a reaction catalyzed by Luciferase enzyme. In parallel, High-throughput and Multiplexed Dip Pen Nanopatterning methodologies were combined with DNA-Directed Immobilization for the creation of complex protein biochips on modified glass surfaces displaying spots of cell-specific ligands with feature size of less than five micrometer diameter. The method takes advantage of a highly modular biomolecular assembly system comprised of covalent ssDNA conjugates of the biotin-binding protein streptavidin (STV) and biotinylated polypetide ligands for specific interactions with living cells. In particular, biotinylated epidermal growth factor (EFG) was coupled with covalent ssDNA-STV conjugates by means of biotin-STV interaction. As second application, an experimental strategy has been developed to build a protein chip inside individual living cells. This protein-chip is constructed by recruiting designed receptors to micrometer-scale patterns of immobilized ligands. Each receptor presents an arbitrary intracellular protein domain of interest, which acts as bait. A cytosolic, fluorescently tagged binding partner serves as prey. The interaction between the two proteins is monitored via TIRF microscopy. As a proof of principle experiment, it has been possible to measure alterations in the interaction between the catalytic and regulatory subunit of the cAMP-dependent protein kinase in living cells via pharmacological manipulation.

Introduction

Micro- and nano- patterning of biomolecules on surfaces, along with retention of activity and structural integrity of the deposited molecules, has been particularly investigated in these years. In particular, a bio-array can be defined as a 2D micro-/nano- ordered pattern of biomolecules on the surface of a substrate. These top-down man-made biological surfaces have profoundly influenced both life sciences and biotechnologies because of their ability to permit a simultaneous, low cost and high sensitivity detection of a large number (hundreds or even thousands) of molecular species in a single experiment [1, 2]. Nowadays they are fundamental tools for research in areas as genomics, proteomics, drug screening, lab-on-chip diagnostic, food chemistry, environmental monitoring, forensic investigation, military defence, and so forth [3]. Modern biomolecular array fabrication technologies enable the realization of low cost, integrated and complex bio-arrays with high density of reaction sites on surface, requiring extremely smaller analyte sample volumes - with respect to conventional assay methodologies - and higher detec-

tion sensitivity and throughput screening. Fabrication techniques for biomolecular arrays are typically categorized into top-down and bottom-up approaches. The top-down approach creates micro- or nanoscale structures from a starting biomaterial, whereas the bottom-up approach is based on super-molecular interactions of molecules to self-assemble structures of interest. The most common fabrication techniques are based on top-down approaches such as photolithography, electron beam lithography and focused ion beam lithography: conventional methods commercially available and widely implemented in manufacturing, but often limited by their high cost, difficult multiple-steps processes, and accessibility to the clean room facilities necessary for processing [4]. These limitations motivate the development of new, original unconventional micro- nano- fabrication methods with higher flexibility, ambient condition operations and lower costs, as for example nano-imprint lithography, soft lithography, scanning probe nanolithography (including dip-pen nanolithography). In any case, every bio-array fabrication technique targets the same objective: efficient deposition of uniform, dense arrays of probe molecules with low dispensed reagent consumption, preventing solution contamination and biomolecular damage. It is possible to summarize these techniques (see the the table 1 reproduced from [5]) according to the discrimination contact/non contact technique. In contact printing techniques, a printing device comes in physical con-

Contact		Non-Contact	
Serial	Parallel	Serial	Parallel
Solid/Split Contact Pins		Dynamic Controlled Pins	Photochemical Printing Electro-Printing
	Microstamps		
Nano-Tips		Laser Writing	Inkjet/Nozzle Printing Electrospray Deposition

Figure 1: **Array fabrication techniques. Figure reproduced from [5].**

tact with the substrate to deposit biological material (e.g., pin printing and dip pen nanopatterning). Instead, in non-contact printing no physical contact between the device and the substrate occurs (e.g., photolithography, ink-jet printing, and laser writing). Moreover, each of these array fabrication techniques can be sub-classified as serial or parallel according to the patterning strategy. Parallel methods enable the robust large area and high-throughput duplication of a pre-designed and not arbitrarily modifiable pattern on a surface. In serial deposition, serially repeated movements of the printing device permit to create patterns with high resolution and registration however, in principle, with limited fabrication throughput. Recently, it has been demonstrated the feasibility of 2-D cantilever arrays devices for dip-pen nano-lithography approaches for enabling a robust production of patterned structures over areas as large as square centimetres [6]. A fundamental discriminant for patterning methodologies is constituted by the attainable lateral resolution. Accordingly, conventional micro- array fabrication techniques as pin printing, thermal or piezoelectric inkjet printing typically permit droplet volumes of 1-10 picoliters, spot resolution of 10-20 μm at the best - based on these resolution biochemical assays at the microscale permit to save time, costs and reagents with respect to established micro-well based assays time and reagent consuming that work with micro-, nanoliter scale volumes [7]. Nanoarray based devices would still permit a dramatic further decrease in the cost of the assay since - in comparison to micro-arrays - still less volumes of reagents and analytes are required (down to the atto- liter scale), shorter response times are to be considered and importantly much higher sensitivity can be obtained reaching the sub-femtomolar level. At tens of nanometers patterning

resolution, nanoarrays would even enable to probe the activity of biological entities at spots whose lateral dimensions would be the same or one higher order of magnitude compared to the biomolecules typical dimensions - this meaning performing biomolecular recognition individually, as it happens in natural systems, rather than collectively in lumps - i.e. micron scale sized spots. The 10000 to 100000-fold increase in areal density - that could be achieved with the use of nanoscale patterns dispensing techniques (see fig. 2) - would allow an assay to screen for a correspondingly larger number of targets and a fixed number of targets to be screened with a correspondingly smaller sample volume, and in a shorter amount of time [8]. High-resolution patterning would greatly facilitate the development of high-throughput, high-resolution screening tools [2].
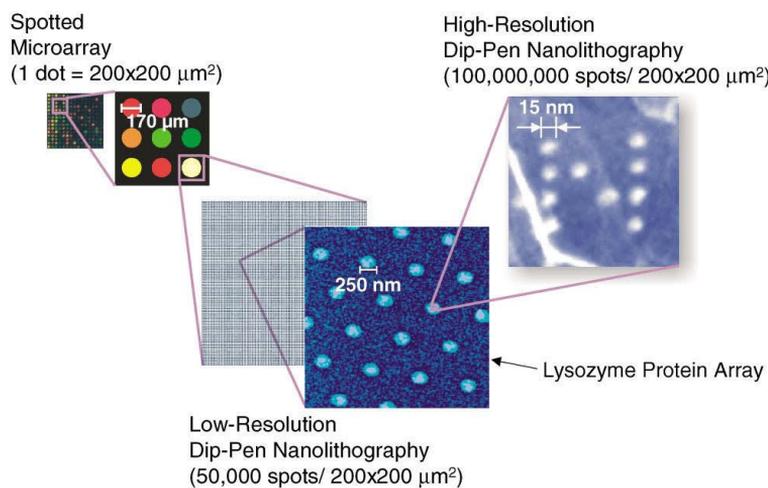
Figure 2: **Scheme of the effect of patterning resolution in spot surface density for biological array fabrication. The figure is reproduced from [8].**

However, in order to fully appreciate and apply the potentialities of nanoscale arrays, it is mandatory to establish an appropriate read-

out to scheme and finally interpret the data employing bioinformatics tools. To address the detection issues, there are many possible solutions [1]. When a feature composed of receptors is miniaturized to the scale of the biological analytes or their attached labels, almost every mechanical, electrical, and chemical property of the receptor feature is changed upon reaction with the analyte. These properties, which include size, shape, electrical conductivity, and hydrophilicity, all can be monitored in situ with an AFM or with on-chip electronic circuitry. Examples of microscale detection in this sense include micro cantilevers that translate biomolecular interactions into mechanical bending, silicon field effect sensors that measure intrinsic biomolecular charge, electrochemical sensors that translate biomolecular adsorption to changes in redox current and microchannel resonators for measuring mass [9]. In addition, detectors on the nanoscale, such as silicon nanowires [10], require far fewer target molecules, and protein sensibitivity till the femtomolar level has been reported [11]. Recently, sub-femtomolar detection with single-molecule resolution was achieved with a micron-sized optical cavity resonator. Nanoparticle binding has also been used for oligonucleotide detection by patterning single strand DNA using DPN and exposing this array to gold nanoparticles showing a label with the complementary DNA strand [12]. As far as to the bioinformatics topics, fortunately, there exist tools for both collecting and processing large amounts of high-resolution data rapidly [2]. Finally, motivations below

---

[1] apart from the conventional colorimetric or fluorimetric methodologies nowadays employed in microarray technologies

[2] For example, electronic components such as CCD chips, CMOS devices, and high-density integrated circuits provide the ability to collect enormous amounts of data on short time scales. Data storage capacity has increased to enable these data to be collected and stored. In addition, the ability to process data rapidly has kept

the advancement in bio-arrays fabrication and utilization come from several fronts in Life Sciences. Increasing data are needed to solve increasingly complex problems coming from biological sciences. Nowadays it is necessary to collect an enormous amount of data to understand the interactions and connections between biological pathways inside living cells. The ability to produce patterns of certain complexity and with multiple materials at sub-cellular levels enables the possibility to address fundamental studies - at the single-cell level - of cellular migration, focal adhesion, cellular polarization and proliferation, studies neuronal development, and stem cell differentiation. Chemically patterned surfaces can also be used to study highly specific cell-cell and cell-substrate interactions or to create increasingly densely packed biosensors. From a biological standpoint, these methods enable fabrication of elaborate interfaces to mechanistically study the effects of cell adhesion ligand density, spacing, clustering, and spatial distribution on cell fate and function. In addition, the completions of the Human Genome Project and the HapMap Project have provided a rich database of human genetic variation. Only by collecting millions of pieces of data from many thousands or millions of individuals will permit to uncover the causes of disease at a molecular level. High density and multiplexed bio-arrays technologies could permit to unravel the fundamental molecular mechanisms at the basis of human pathologies thus providing an exceptional tool for the medicine of the future.

In this thesis work, solution dispensing techniques have been employed for the realization of complex biological arrays. The first ob-

---

pace. Without these corresponding improvements in data storage and processing capability, there would be no need to collect more data.

jective was to employ Inkjet printing techniques for the generation of advanced drug screening platforms. This approach was initially proved with a model enzyme system like Glucose Oxidase substrate covalently linked to a functionalized silicon oxide support. On this support an enzymatic substrate (D-glucose)/inhibitor (D-glucal) couple was accurately dispensed. A simple optical detection method was used to prove the screening capability of the microarray with the possibility to assay with high reproducibility at the single spot level. Afterwards, this methodology has been extended to CYP450 enzymes like CYP3A4, one of the main targets for the phase I drug metabolism via a droplet microreactors arrays containing CYP3A4 enzyme mixed with model inhibitors (erythromycin) and enzymatic chemiluminescent substrates (Luciferin-Isopropylacetate). The enzymatic activity was again detected by using easy and low cost optical measurements of spot brightness. As a second main objective, high-throughput and multiplexed Dip Pen Nanopatterning methodologies in liquid format were combined with Proteic Ligand DNA-Directed Immobilization for the creation of complex protein biochips on modified glass surfaces displaying spots of cell-specific ligands with lateral dimensions minor than one single cell. In a first application the epidermal growth factor (EFG) protein arrays were realized to display specific single cell adhesion activity. As a second application, immobilized proteic ligands were used to recruit designed cellular receptors which presented intracellular protein domain (regulatory subunit of cAMP-dependent protein kinase) whose interaction with a cytosolic binding partner (catalytic subunit of cAMP-dependent protein kinase) was monitored and pharmacologically perturbated.

In order to facilitate the reading of this thesis, the work has been

divided into a first Part (State of the Art) and a second Part (Experimental Section). The first Part is composed of two chapters Chapter 1 and Chapter 2. Chapter 1 - **Biopatterning fabrication methodologies** - gives general notions regarding patterning methodologies at the micron scale and at the nano scale. In particular, ink-jet printing and dip pen nanopatterning are considered and discussed in detail. Chapter 2 - **Array technologies in Life Sciences** - focuses on applications of micro- and nano- array technology in relevant fields of Life Sciences, like Drug Discovery and Cell Biology reporting examples from Literature in the subject. The second Part is composed of two Chapters, Chapter 3 and Chapter 4, dealing with the Experimental Section of the Thesis. Chapter 3 - **Enzymatic arrays by Inkjet printing** - reports on a general drug screening methodology based on microarray realized by ink-jet printing for screening drug candidates on protein target. We show the principle of this approach with a model enzymatic system like Glucose Oxidase and envisage the application to relevant systems for pharmaceutics like CYP3A4. Finally, Chapter 4 - **Single Cell Interaction Arrays by DPN** deals with the set-up of a robust methodology for the realization of complex protein biochips usable as platforms for single cells experiments. This is achieved by combining multiplexed direct Dip Pen Nanopatterning of single strand oligonucleotides with DNA-directed immobilization of a supra-molecular construct between a complementary DNA sequence conjugated with a streptavidin molecule and a biotinylated polipeptide ligand. Bibliography is provided at the end of each chapter. Finally, Conclusions, Acknowledgments and a *Curriculum Vitae* are presented.

References

[1] Ogaki R.; Alexander M.; Kingshott P., *Materials Today* **13**, 22 (2010).

[2] Hong J.; Edell J.B.; deMello A.J., *DDT* **14**, 134 (2009).

[3] Albala J.S.; Humpheiy-Smith I., *Protein Arrays, Biochips, and Proteomics: The Next Phase of Genomic Discovery* (Marcel Dekker, New York, 2003).

[4] Kim S. M.; Suh K. Y., *Front. in Bioscienc.* 406 (2009).

[5] M.; Sun Y.; Zhang M.; Wheeler A.R.; Bussmann M. Barbulovic-Nad, I.; Lucente, *Crit. Rev. in Biotechnol.* **26**, 237 (2006).

[6] Haaheim J. R.; Tevaarwerk E. R.; Fragala J.; and Shile R., in *Micro (MEMS) and Nanotechnologies for Defense and Security* (Orlando, Florida, 2007).

[7] Arrabito G.; Pignataro B., *Anal. Chem.* **82**, 3104 (2010).

[8] Ginger D. S.; Zhang H. and Mirkin C.A., *Angew. Chem. Int. Ed.* **43**, 30 (2004).

[9] Squires T.M.; Messinger R.J.; Manalis S.R., *Nat. Biotech.* **26**, 417 (2008).

[10] Cui Y.; Wei Q.Q.; Park H.K.; Lieber C.M., *Science* **293**, 1289 (2001).

[11] Zheng G.; Patolsky F.; Cui Y.; Wang W. U.; Lieber C. M., *Nat. Biotechnol.* **23**, 1294 (2005).

[12] Zhang H.; Li Z.; Mirkin C.A., *Adv. Mater.* **14**, 1472 (2002).

Part I

State of the Art

1

Biopatterning fabrication methodologies

This chapter presents a the state of the art about bio-array fabrication methods, especially focusing on the solution-based approaches. Specifically, Ink-jet printing and Dip Pen Nanopatterning (DPN) techniques are described in detail. In particular, as far as the ink-jet printing, details on the piezoelectric technology for biological array fabrication, mechanisms of droplet formation and impact on hard and soft surfaces are provided. As to the Dip Pen Nanopatterning, writing mechanism is analyzed focusing on the difference between diffusive and liquid ink depositions. Evolution in high-throughput patterning by employing 1D and 2D pen arrays are also presented.

Glossary and list of acronyms:

DPN: acronym for Dip Pen Nanopatterning, a scanning-probe based patterning technique in which molecules are directly transported from a molecule-coated atomic force microscope tip to a receiving surface.

Multiplexing: increase of the number and of the density of tested biological targets in a single array experiment.

1.1 Ink-jet printing

Ink-jet printing is a flexible, gentle and robust micropatterning technique featured with rapidity and cost-effectiveness, not requiring the use of masks, stamps or other costly and time-consuming conventional processing equipment [1, 2]. Ink-jet printing has been implemented in many different designs and has a wide range of potential applications: fundamentally, ink-jet printing is divided into the continuous and the drop-on-demand ink-jet methods: the last one being the most employed one, in which a series of electrical signals is employed to control the actuation at the moment of drop ejection. Depending on the mechanism used in the drop formation process, the technology can be categorized into four major methods: thermal, piezoelectric, electrostatic, and acoustic ink-jet. Most, of the drop-on-demand ink-jet printers use either the thermal or piezoelectric principle [3]. However, for Life Science applications thermal ink-jet mode is not the best choice because of the heat stress that would affect printed bio-materials; then piezoelectric dispensing remains the most used method [4, 5].

1.2 Piezoelectric Ink-jet printing

Piezoelectric ink jet printing is a thermally constant process that is carried out at a constant temperature. The piezoelectric print-head consists of a piezoelectric transducer, nozzles, manifolds, ink pumping

chambers, and fluid inlet passages. When a voltage is applied to a piezoelectric transducer - typically lead zirconate titanate (PZT)-, the transducer deforms and creates mechanical vibrations. The electric signal applied to the piezoelectric is called waveform: a complex pattern of electrical impulses consisting in a series of square waves. Each square wave is characterized by a voltage value V_i, a time interval t_i and a slope p_i. The absolute value of the voltage is correlated to the entity of the compression inside the fluid chamber. The slope is correlated to the compression rate, while the time interval is correlated to the time the piezoelectric transducer remains in a defined position. These vibrations create acoustic waves, which in turn force ink out of the chamber through the nozzle. Piezoelectric print heads (see fig. 4.3 taken from [6]) are categorized based on the deformation mode of the transducer in squeeze mode (a), bend mode (b), push mode (c), or shear mode (d).
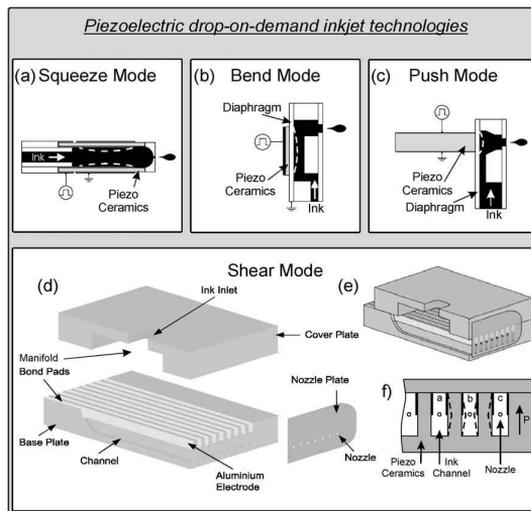
Figure 1.1: **Piezoelectric drop-on-demand technologies.** **Figure reproduced from [6].**

The volume of the emitted droplet is in relation to the nozzle size typically lying in the picoliter to nanoliter range. During droplet formation, energy is distributed between viscous flow, the drop surface tension, and the drop kinetic energy. In turn this leads to a liquid jet resolving into a droplet hitting the substrate surface. Unlike other patterning methods, ink-jet printing has the great advantage to allow precise and controlled parallel deposition of small volumes (typically picoliter to nanoliter range) of multiple biological materials using independent jets (i.e. independent controlled micro-channels) on almost any possible type of substrates solid, gel, liquid surfaces being a conctacless in nature. Moreover, the hardware integration with automated translation stages enable precise pattern placement and registration for preparing multilayer patterns with different printed biomaterials. Several papers report on the realization of multiplexed arrays via piezodispensing nanoliter-picoliter droplets for realizing accurate biomolecular assays involving DNA hybridization on functionalized surfaces [7, 8] and characterize interactions involving delicate proteins: in particular MacBeath set up a high throughput microarray-based strategy for measuring the equilibrium dissociation constant of different recombinant PDZ domains for fluorescently labeled peptides [9, 10]. M.S. Hasenbank et al. [11] showed multi-protein patterning ink-jet printing for setting-up a biosensor assay. The method involved a two sequential patterning steps, consisting in the initial deposition onto gold-coated surface of a mixed thiol layer (BAT/PEG thiol solution) to provide oriented binding capabilities in a non fouling background and a second deposition of multiple biotinylated proteins (b-HRP and b-BSA). Antibodies specific to each of the two proteins were introduced in a development step in the SPR microscope in

order to execute detection. Highly specific binding of the antibodies to the immobilized proteins was observed. In addition, Sukumaran et al. showed the advantage given by the combination of enzyme encapsulation techniques in alginate and microarraying methods for an integrated screening platform for CYP450 [12] while Lee et. al prepared a miniaturized 3D cell-culture array (the Data Analysis Toxicology Assay Chip or DataChip) for high-throughput toxicity screening of drug candidates and their cytochrome P450-generated metabolites [13].

Together with heterophase assays, piezo ink-jet droplet formation enable droplet microarray fabrication: an innovative technique that permits to conduct enzymatic assays in liquid droplets. Accordingly, the this approach was firstly developed by Gosalia et al. [14] who arrayed chemical compounds inside nanoliter droplets fo glycerol and by aerosol deposition, added reagents and water to assemble different multiple biochemical reactions without requiring chemical linkage of the protein to the surface. They were able to execute kinetic profiling of protease mixtures, protease-substrate interactions and high throughput reactions showing the suitability of the method by the identification of an inhibitor of caspases 2, 4 and 6. Based on this approach, Mugherli et al. set-up a robust microarray platform in which multiple reactions are conducted in piezo deposited nanoliter droplets maintained on a glass slide for the in situ preparation of derivatives of thousands of derivatives of phenylboronic acid and their successive activity screening on the NS3/4A protease of the hepatitis C virus [15] and, in a subsequent paper they were able to identificate new type of fluorescent pharmacophores by multicomponent reactions using combinatorial synthesis and screening of chemical libraries in droplet microarrays [16].

In particular, the assembly by a multicomponent reaction is a unique potential for synthesizing thousands of structurally different fluorescent molecules. Since they are based upon a druglike scaffold, these fluorophores maintain their molecular recognition potential and, thus their suitability as bioimaging probes. Despite its simplicity, ink-jet printing deposition has some drawbacks. Nozzles tendency to produce undesirable satellite droplets that contaminate surrounding spots and thus, reduce printing resolution. In addition, it is difficult to completely flush printing nozzles before a new solution is loaded. This problem is more serious in piezoelectric printers since the nozzle is separated from the ink reservoir and all linking channels must be flushed clean. In addition, droplets experience high shear rates while passing through the nozzle and impacting the substrate surface: under these shear rates, there is a risk of denaturing biomolecules in the solution [17]. Accordingly, for achieving high resolution and good morphology spots and avoid the formation of undesirable satellites together with the primary droplet, its rheological properties have to be optimized being those of typical biological solutions (that have low viscosities and high surface tensions), with the addition of viscous, surfactant and bio-compatible additives in the buffer solution. In this sense we showed that additives like glycerol can increase fluid viscosity at a sufficient level in order to permit satellites free droplet formation and retaining of the biological activity [18].

The main stages of Drop-on-demand drop formation are ejection and stretching of liquid, pinch-off of liquid thread from the nozzle exit, contraction of liquid thread, breakup of liquid thread into primary drops and satellites, and recombination of primary drop and satellites. The final phase of the process consists in the impact of the ejected droplet

towards the substrate.

1.2.1 Droplet formation

When the piezoelectric transducer expands, liquid in the nozzle is accelerated and pushed out of the nozzle orifice. Initially, the meniscus extends outward until a liquid column with a round leading edge is formed. After a short time, the liquid flow rate from the nozzle decreases. The speed of liquid at the nozzle exit falls until no additional liquid flows into the column. The volume of the liquid column remains constant, and the inertia of the liquid extends the column: during the stretching of the liquid column, the liquid at the tail necks. This necking position remains at the nozzle exit, and the radius of the liquid thread here continuously thins. Finally, the tail of the liquid thread pinches off from the nozzle exit, creating a free liquid thread with a bulbous head. The time required for the ejected fluid to stretch and then pinch off from the nozzle exit is called pinch off time. Subsequently, recoil of the free liquid thread occurs because pressure is high in the tail tip at pinch-off so that the tail recoils toward the head of the drop. During the shrinkage of the liquid thread, the liquid thread tends to break up into two parts, a primary drop and a free secondary and unsymmetrical liquid threads that may shrink into a smaller drop or satellite, or break up into two or more parts. So the breakup of the free liquid thread leads to the generation of a primary drop and satellite(s) [19]. During the contraction of the liquid thread after it has pinched off from the nozzle, two modes of breakup are possible: end-pinching where the liquid thread pinches off from an almost spherical head, and multiple breakups of the liquid thread due to capillary waves. The evolution of

the liquid thread depends on the length of the liquid thread at pinch-off, which increases with voltage. For the shorter water threads, a capillary wave is not observed, and satellite formation results from end-pinching. For longer water threads, a wave-like instability typically occurs along the thread. As the amplitude of the capillary wave increases, the liquid thread breaks up at several locations at slightly different times, forming several satellites. The longer the liquid thread, the more satellites are formed. Multiple breakups evolving from the wave-like instabilities complicate the printing performance due to the generation of satellites and are unfavorable for Drop-on-demand formation. Multiple breakups and end-pinching both originate from the growth of disturbances along the liquid thread. Using the results from the linear instability analysis, it is possible to derive the following equation that permits to quantify the pinch off time:

$$t_b = \frac{1}{\alpha_{max}^*} \left(\frac{\rho R_{noz}^3}{\gamma} \right)^{1/2} ln \left(\frac{R_{noz}}{\epsilon_{max}} \right) = C \frac{t_{ca}}{\alpha_{max}^*} \qquad (1.1)$$

where $C = ln(R_{noz}/\epsilon_{max})$ and $t_{ca} = \left(\rho R_{noz}^3/\gamma \right)^{1/2}$ is referred to as the capillary time. α_{max}^* is the fastest temporal growth rate of the disturbance along the surface of the thread. ϵ_{max} is the (typically unknown) initial amplitude of the disturbance corresponding to α_{max}^*. This is the expression for α_{max}^* :

$$\alpha_{max}^* = \left\{ \left[\frac{1}{2} x_{max}^2 (1 - x_{max}^2) + \frac{9}{4} Oh^2 x_{max}^4 \right]^{1/2} - \frac{3}{2} Oh x_{max}^2 \right\} \qquad (1.2)$$

where $Oh = \frac{\mu}{(\rho \sigma D^{1/2})}$ is the Ohnesoger number (μ, ρ,σ are respectively dynamic viscosity, density and surface tension of the printed liquid) and $x_{max}^2 = \frac{1}{2+\sqrt{18Oh}}$. According to these equations, the breakup time of a

liquid thread should only depend on the capillary time and α^*_{max} . The C_i coefficients can be associated to the breakup times. These coefficients are defined as follows:

$$C_i = \frac{t_{bi} - t_e}{t_{ca}/\alpha^*_{max}} \tag{1.3}$$

In this expression, the ejection time t_e is subtracted from the breakup time because typically little stretching occurs in the ejected liquid during the ejection stage, as the ratio of the surface area to volume of the ejected liquid is almost constant during the ejection-stage. C_1 (the first breakup) refers to t_{b1} , the time required for the pinch-off of the liquid thread, while C_2 (the second breakup) refers to the end-pinching. After the liquid snaps off from the nozzle exit and becomes a free-flying thread, the thread tail recoils rapidly under the action of the surface tension. The expression for retraction speed is given by this equation:

$$v_r = \left(\frac{2\gamma}{\rho r_0}\right)^{1/2} \tag{1.4}$$

where r_0 is the radius of the liquid thread. Being the radius of the liquid thread scaled by the radius of the nozzle, R_{noz} , then

$$v_r \approx a v_{ca} \tag{1.5}$$

where a is a constant and $v_{ca} = (\gamma/\rho R_{noz})^{1/2}$, referred to as the capillary speed. The evolution of the free-flying liquid thread depends on the liquid and driving voltage. If the driving voltage is sufficiently low, no satellites are formed. At higher voltages, the breakup of the free-flying liquid thread occurs, and satellites form.

1.2.2   Droplet impact on a surface

Droplet impact phenomena considerably differ in function of the aggregation state of the receiving surface, being it solid or liquid. The

main dimensionless groups (see [20] for further details) governing drop impact here employed for the discussion are: Weber number $We = \frac{\rho D_0 U_0^2}{\sigma}$, Ohnesorge number $Oh = \frac{\mu}{\sqrt{D_0 \sigma \rho}}$ and Reynolds number $Re = \frac{\rho D_0 U_0}{\mu} = \frac{\sqrt{We}}{Oh}$, where ρ is the density of the fluid D_0 and U_0, respectively, are the diameter and the velocity of the droplet before impact, μ is the dynamic viscosity and σ is the fluids surface tension. The typical operating regime for ink-jet printing operation is characterized by high Reynolds numbers ($O(10) < Re < O(10^3)$) and intermediate to high Weber number ($O(1) < We < O(10^2)$). The Weber and Reynolds numbers for the droplet generation process are equal to those of the impact process. In order to obtain sufficient ballistic accuracy of a droplet, the Weber number of droplet generation should be typically $We > \sim 1$, while the integrity of the droplet determinates an upper limit on the Weber number. In other words, excessively slow jetting drops could lead to an inaccurate trajectory, while a high drop speed may lead to the formation of undesirable tails along with drop satellites. The piezo-acustic generation mechanism must have $Re > \sim 1$ in order to prevent excessive viscous damping, while the need for some damping of the fluid after droplet generation puts un upper bound on the Reynolds number [21].

1.2.3   Impact on a solid surface

The impact of the droplet on a solid substrate can be subdivided in three phases (for further details see [21]]). In the initial impact phase, the droplet hits the substrate with air bubbles entering inside the droplet at the very moment of impact. In second phase, the radial extent of the droplet-substrate interface becomes of the order of

magnitude of the initial droplet radius and there is a rapid radial fluid flow in which a blob of fluid is formed near the contact line. After the fluid has reached its maximum radial extent, oscillations set in after a rebound in which the droplet remains intact as one volume. In the case of high-contact angle surfaces and large Weber numbers, the droplet can move beyond its equilibrium advancing contact angle. When the droplet has low speed ($We < 1$), the droplet deforms as a whole and flattens somewhat, already during the first stage of impact - this behavior being explained by considering capillary force as the important driving mechanism for spreading. For these impacts, the time scales for capillary-driven spreading and deformation of the whole droplet are the same. The final radius becomes larger for experiments with a larger Weber number and is a function of the surface contact angle. At high Weber numbers ($We > 8$), in the first stage of impact the upper part of the droplet remains undisturbed. Then for high speed impacts, the time scale for spreading R_0/U_0 becomes considerably smaller then the time scale for deformation of the droplet by surface tension $\sqrt{\rho R_0^3/\sigma}$. In the third phase, the fluids comes to rest in a process of rebound followed by inertial oscillations, damped by viscous dissipation. A high amount of the initial energy in the droplet before spreading is dissipated by viscosity through the oscillations. The value of the final radius can be calculated by considering an energy balance based on surface energy, kinetic energy, and viscous dissipation in the following form:

$$\frac{2}{3}\pi R_0^3 \rho U_0^2 + 4\pi R_0^2 \sigma = \pi R_f^2 (f_s\sigma + \sigma_{ls} - \sigma_{sv}) + \triangle E_u \qquad (1.6)$$

where R_f is the final radius after impact has completed, f_s is the ratio of the fluid-vapor surface and the fluid-solid surface, and $\triangle E_u$ is the

dissipated energy in the impact process by viscosity, σ_{ls} and σ_{sv} are the surface energies of the liquid-solid and solid-vapour interfaces, respectively. After impact, the fluid flow velocity is zero and the droplet has taken the shape of a spherical cap with contact angle θ, which can take values between the equilibrium advancing contact angle θ_{adv} and the receding contact angle θ_{rec}. A special case is constituted by the impact of a droplet on a porous substrate: in this case, the liquid in the droplet is imbibed due to capillary suction in an initially dry and undeformed substrate: then deformation of the substrate occurs as the liquid fills the pore space. For more details see [22]

1.2.4   Impact on a liquid surface

The drop impact on a liquid surface is a slightly more complicated case; a good review dealing with the physics underneath is the one of Yarin [22]. Briefly, a fundamental parameter for the impact on a liquid surface is the droplet velocity. At low impact velocities ($10^{-2} - 1$ m/s) practically no rim is visible, and the droplet is simply deposited on the liquid film. At velocities of the order of 1-30 m/s, the motion initiated by the drop is virtually unconstrained and capable of pushing apart a significant liquid mass under the impact site (conditions of droplet spreading): the drop takes the shape of lamellae with a visible outer rim. At higher impact velocities (conditions of droplet splashing), the lamellae take the shape of crowns consisting of a thin liquid sheet with an unstable free rim at the top, from which numerous small secondary droplets are ejected. The threshold for a droplet splashing in a train of

frequency f is given this expression:

$$V_{0S} = 18 \left(\frac{\sigma}{\pi} \right)^{\frac{1}{4}} \nu^{\frac{1}{8}} f^{\frac{3}{8}}$$ (1.7)

where π, ν, and σ denote liquid density, kinematic viscosity, and surface tension, respectively. Drop spreading occurs at the impact velocities $V_0 < V_{0S}$, whereas at $V_0 > V_{0S}$ splashing and formation of a crown and multiple secondary droplets occur. Following the impact, mixing between the droplet and the liquid surface occurs: this phenomenology is strictly dependent upon the molecular diffusion in liquids and then, assuming Brownian motion ($x_2 = 2D{\cdot}\tau$, where x is the distance traveled, D is the coefficient of diffusion, and τ is the time), it depends upon the dimension - and then the volume - of the considered droplet. For example, a small molecule like fluorescein needs about 36 s to diffuse across 215 μm (that is a 10-nL droplet), but only 3.6 ms for diffusing on a 2.15 μm droplet (10 fL volume) [23].

1.3   Nano tip printing techniques: Nanoshaving lithography

Nano Tip printing techniques are an ensemble of methodologies that permit to achieve submicron resolution, high spot density and more complex arrays, being initially developed from the atomic force microscope (AFM), the master tool for nanoscale investigation of materials surfaces. These methods are able either to perform adding process of molecules to a substrate - i.e. dip pen nanolithography - or removing self-assembled molecules nanoshaving.

Nanoshaving is a destructive method, thus not allowing direct mul-

tiple features patterning but it can be adapted by using careful ex-
perimental procedures. Accordingly, Tinzali et al. [21] set-up a proof-
of-concept double protein nanopattern experiment: they developed a
write, read and erase method in which uniformly oriented His-tagged
proteins immobilized on a NTA-functionalized (i.e. Oligoethylene alkyl
thiols with nickel-N-nitrilotriacetic acid moieties) surfaces are removed
with an AFM tip in contact oscillation mode and replaced simultane-
ously or sequentially with other His-tagged proteins. In one experiment,
the affinity-captured matrix protein (N-His6 proteosome) was locally
replaced by a maltose-binding protein (MBP) with a C-terminal His10
tag (MBP-His10); additionally they monitored specific protein-protein
interactions between a ligand and its receptor for instance the extra-
cellular domain of the human type I interferon receptor (ifnar-His10)
was nano arrayed and then binding of interferon-2 (IFN 2) was mon-
itored with fluorescence microscopy. In [24], F. Bano et al. used a
combination of DNA-directed immobilization - a technique for immobi-
lizing proteins on surfaces by means of covalent DNA-streptavidin coni-
ugates - and DPN to execute a decoration of nanometer sized areas of
single-stranded DNA (ssDNA) prepared by nanografting on alkylthiol-
modified gold surfaces, with different cDNA-protein conjugates. The
authors showed the multiplex patterning feasibility of the method by the
simultaneous DNA-directed immobilization of DNA-HRP (horseradish
peroxidase) and DNA-GOx (Glucose oxidase) with nanografted patches
and subsequent probing with an HRP specific antibody. More recently,
Unruh et al. showed an electrochemical tip based patterning method in
which, depending on the surface bias, a redox-sensitive surface bound
molecule - i.e. a triethoxysilane derivative featuring a redox-active

trimethylbenzoquinone moiety - can be electrostatically reduced to an amine or instead oxidized to produce oxygen-rich species [25] to create surfaces functionalities usable in an independent way to deposit complementary materials like electron- or hole- transporting molecules via self-assembly. The above presented methods enable multiplexing but they are quite laborious and not robust enough for high-throughput biological applications.

1.4 Nano tip printing techniques: Dip Pen Nanopatterning

Introduced by Mirkin et al. in 1999 [26], Dip-pen nanolithography (DPN) is a powerful atomic force microscope based constructive patterning technique that permits to fabricate nano- and micro- scale patterns in ambient conditions along with high registration and recently high-throughput capabilities. Dip pen nanolithography enables the realization of devices as diverse as nano-scale electronic circuits, chemical sensors, micro- nano- arrays of organic and biological molecules for cell biology studies and so forth.

The method is based on the ink transportation from an ink-coated AFM tip to a receiving surface. Two possible deposition mechanisms exist diffusive or liquid. In the diffusive regime, the tip is dipped into the ink solution with subsequent solvent evaporation leading to molecules coated on the DPN tip to be deposited on the surface substrate by the naturally occurring water meniscus at the interface with the receiving surface. The ink deposition rate is then directly function of the molecular diffusion rate, which is molecule-specific this feature complicating the implementation of multiplexed-patterning [28]. Moreover,
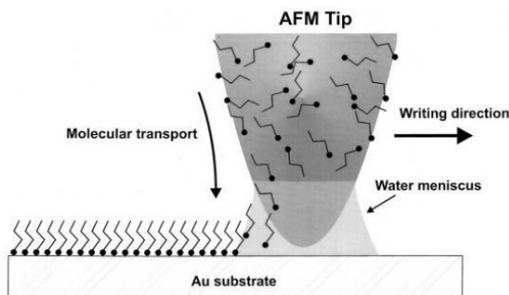
Figure 1.2: **Schematic representation of DPN for molecular inks. A water meniscus forms between the AFM tip - coated with the organic molecule ODT - and the Au substrate. The dimension of the meniscus is controlled by relative humidity affecting the molecular transport rate and the lateral resolution. Figure reproduced from [27].**

the patterned feature size depends on temperature, relative humidity, tip/surface dwell-time, ranging from micro- till nano- scale (< 100 nm). Specifically, the molecular or liquid aggregation state of the ink gives rise to significant changes in deposition mechanism. In the present section, the physical mechanisms involved in the DPN deposition process are discussed by summarizing the experimental and theoretical results obtained so far.

1.4.1 Molecular inks

Molecular inks are composed of small molecules coated onto a DPN tip and are dispensed to the surface through a water meniscus that forms naturally when the tip is brought in contact to the surface. Molecular dynamic simulations have also indicated the existence of such a nucleating process. Also, a thin aqueous film (of the order of one or two molecular layers) is believed to adhere on all surfaces under ambient conditions, which can also aid in the formation of a capillary bridge.

On the other side, a liquid ink is a material that is always liquid at the deposition conditions. The liquid deposition properties are determined by the surface energies of interactions between the liquid and the tip, the liquid and the surface, and the viscosity of the liquid itself. The crucial point for the transfer of material from a tip to a substrate is the formation of a liquid bridge (or meniscus) between the tip and the sample due to the capillary condensation. This meniscus plays a fundamental role since it forms the transfer path for the ink molecules. Its size increases with increasing humidity and by decreasing the distance between the tip and the sample. This point has been estimated by computer simulations and confirmed by experiments of environmental scanning electron microscopy as well as by STM. The shape of the meniscus is also influenced by the hydrophilic/hydrophobic character of the substrate. In case of hydrophilic surface, the small contact angle leads to a spreading of the meniscus, so providing a larger volume meniscus which is beneficial for the material transfer. On hydrophobic surfaces, however, the contact area of the meniscus is reduced, so limiting the cross section of the water bridge and then reducing the material transfer. Double ink DPN experiments with MHA (hydrophilic) and ODT (hydrophobic) were performed for verifying this process. Firstly, a dot pattern was produced with one molecular ink. Afterwards, a second pattern was deposited on the top of the first one using the complementary ink. For ODT the deposition rate was increased when patterning on top of the hydrophilic MHA as compared to deposition on the bare gold substrate. MHA patterning exactly showed the opposite trend, i.e. higher transfer rate on naked gold surface as compared to on top of hydrophobic ODT The formation of the meniscus also has pronounced consequences on th

tip-sample interactions due to capillary forces- that can determine tip abrasion leading to lager radii of curvature. This, in turn changes the contact area and the size of the meniscus leading to changes in the ink transport from the tip to the sample. A full theoretical approach, based on the experimental data has been developed for estimating the amount of the force. [29]. Custom made modification of the radius of curvature by laser ablation allowed investigating the influence of the tip size on the deposition. A sub-proportional increase in the deposition rate was observed for increasing size of the tip - for tips showing radii between 40 and 500 nm - leading to larger feature sizes during the patterning process. Assumed the meniscus to be the natural pathway for molecular ink deposition from the tip to the surface, the material transfer itself depends upon several experimental parameters. As was mentioned above, higher humidity leads to a larger meniscus. This feature can be quite advantageous for transferring hydrophilic molecules (as MHA) while for hydrophobic inks (i.e. ODT) there is no increase in the rate of diffusion to the surface. Instead, the transfer rate seems to remain constant or even to decrease slightly with increasing humidity. This observation is attributed to the dissociation of the ink molecules from the cantilever and their subsequent dissolution in the meniscus fluid. For hydrophobic compounds however, this transition is not favourable. Notwithstanding the dependence of the meniscus on the humidity, even under 0 % relative humidity (i.e. nitrogen-purged atmosphere) a residual water layer is present on the surface [30] which is enough for the formation of a meniscus, and deposition had in fact been carried out successfully under these conditions. Since the material transport is based on desorption, solubilization and diffusion, a strong dependence on the temperature can be

expected. Simulations investigating the deposition of ODT during short contact times were performed: it was found that most of the transferred material comes from the ruptured meniscus. An increase in temperature from 300 to 500 K led to an increase in the deposited amount by a factor of three. The transfer rate also varies over the course of the experiment [31] even if all environmental parameters are kept constant. The presence of ink already on the surface can slow the transport rate for additional ink. A further consequence of this observation is that the exact nature of the substrate used for a particular DPN experiment can affect the behaviour of the ink during patterning. Although DPN enables the fabrication of nanopatterns of diverse chemical nature on a wide selection of substrates, the transfer of material from the tip to the surface is successful if the choice of ink fits the substrate properties. The main requirement in this respect is the similarity in the hydrophilicity/hydrophobicity of the involved materials. In order to improve this compatibility, use of a surfactant can be required for the effective transport of molecules to the surface for the effective transport of molecules to the surface. Studies on the transport of maleimide-linked biotin to mercaptosilane modified glass substrates investigated the effect on deposition abilities of small amounts of Tween-20 (a non ionic surfactant) in the ink solution. The surfactant was found to decrease the contact angle with increasing concentration, leading to a larger spreading of the meniscus and, hence, promoting the transfer of the hydrophilic biotin derivative on the surface [32]. Once the ink molecule has been transferred to the surface, surface diffusion will determine the material spreading and then the final shape of the pattern. The diffusion can occur in two different ways, termed as serial pushing and hopping down

process. In the case of serial pushing mode, a newly transferred molecule will displace a molecule that has been previously deposited, pushing it outward. This displacement continues for other molecules till the pattern boundary is reached. In the case of hopping down, the molecules that are transferred to the substrate are immediately bound strongly to the surface. New molecules thus diffuse on the top of the first monolayer and then hop down to the substrate once they reach the board of the patterned area, again becoming bound to the substrate. Commonly, a mixture of these two processes will occur, the extent of the contribution of each of these mechanism being determined by the molecule-substrate binding energy and the number of binding sites: according to simulation, low binding energies will lead to fractally shaped structures, intermediate energies will lead to patterns related to the substrate anisotropy whereas high binding energies lead to circular shapes. The process of ink dispensing on surface depends on the specific diffusion rate of the molecule, this complicating the deposition of different molecules [33], and hence, preventing implementation of robust multiplex patterning processes.

1.4.2 Liquid inks

A liquid ink is a material that is defined as always liquid at the deposition conditions. Molecules are always dissolved in a liquid during the deposition conditions - this being advantageous especially for patterning biomolecules as they would always remain in their natural hydrated state. The deposition mechanism is function of the surface tension occurring between the liquid and the tip, the liquid and the surface and the viscosity of the liquid [26] - these interactions finally determining a

lateral resolution in the micron range scale and not nanoscale. Viscosity is the crucial parameter for the ink writing: higher viscosity leads to lower flow rate from the tip to the surface permitting to pattern for a long time without need of re-inking the tips. Raising ink viscosity also permits to decrease the written features dimensions (till about one micron) and, importantly, to increase the number of spots so allowing to pattern on large areas (mm^2). Relative humidity affects the meniscus size formed between tip and surface. Importantly, unlike molecular inks, multiplexed depositions can be easily realized since the deposition rates are mainly governed by the liquid properties and not by specific molecular diffusion: this significantly simplifying multiple features patterning on the microscale resolution. In this way, the ink diffusion in molecule-indipendent; different molecules can be printed con temporarily producing same features sizes. Considering that expensive, high-resolution technologies would be required to acquire data from nano-scale arrays since conventional fluorescence detectors have a resolution down to 1 μm, this method is already able to fulfil the needs of accessible and easy-implementable multiplexed biological assays in array format [34]. The liquid must not have an affinity to the surface that is neither too weak nor too strong. If surface affinity is too weak, the deposition will not occur and if it is too strong, the liquid will transfer from tip to surface as the tip immediately contacts the surface, resulting in uncontrollable ink spreading. These interactions limit the minimum feature size of the liquid ink to about one micron, depending on the contact angle of the liquid to the surface. The meniscus between the tip and the surface is essentially composed of the actual liquid to deposit, and not by the water meniscus found in the molecular diffusion mechanism

of the diffusive ink-DPN.

Despite several basic studies concerning molecular ink are reported in literature, like for instance [30, 35], as far as we know, there are no good comprehensive basic investigations regarding liquid ink transfer mechanism. Thus far, successful control in liquid ink printing has been possible through using additives such as glycerol, agarose, tricine and even hexane for PDMS polymer printing to influence viscosity, wettability and the ink-surface interactions [36–38]. With the benefit of a solid knowledge platform about liquid DPN printing mechanism, we can anticipate the liquid-ink deposition to be the prime method of choice for enabling multi patterning biological molecules in friendly conditions and at low cost in order to realize robust complex array devices. In the following sections, a survey of the current State-of-the-Art DPN-based fabrication methods for biological applications is presented.

1.4.3   Serial multiplexed printing via single tips

Proof-of-concept multiple biomolecular printing by DPN in diffusive conditions has already been shown in literature for single tips in a serial printing approach- notably a tedious procedure suffering from intrinsic slowness and extremely low-throughput. Demers et al. used a DNA diffusive ink (containing 90% dimethyformamide/10% water solution) coated on a 3-amino propyl trimethoxysilane functionalized tip to produce covalently anchored arrays via DPN of modified oligonucleotide sequences on metallic and insulating substrates [39], showing the possibility to execute double-feature DNA array: figure A shows the epifluorescence image of two different fluorophore-labeled sequences (Oregon Green 488-X and Texas Red-X) hybridized to the respective comple-
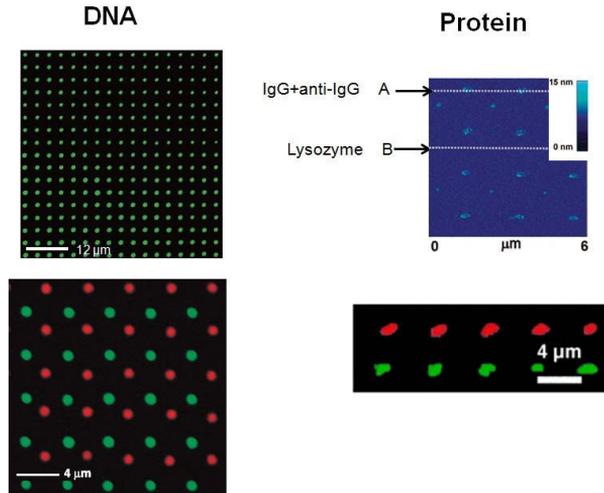
Figure 1.3: **On the left, serial patterning of two different DNA sequences hybridized to their complementary fluorolabeled DNA- complementary sequences (Oregon Green 488-X and Texas Red-X) by single pen DPN on SiO$_x$ from [39]. Top right: dual protein array made up of IgG and then lysozime features by serial deposition. Reproduced from [40]. Bottom right: serial deposition of Antirabbit IgG (Alexa Fluor 594 -red) and antihuman IgG (Alexa Fluor 488 - green) on silicon surfaces from [41].**

mentary sequences deposited on SiOx. As concerns protein printing, Lee et al. [40]generated dual protein nanoarrays on gold surfaces by serially generating rabbit IgG nanoarrays and then lysozime features in between the IgG spots. Importantly, they functionalized tip surface with a a monolayer of PEG which prevents adsorption of proteins on the reflective Au surface of the cantilever by soaking the gold-coated cantilever in symmetric 11-mercapto-undecylpenta(ethylene glycol)disulfide (PEG). To prove the biorecongnition properties of the IgG in the spots, the array was incubated with a solution containing anti-rabbit IgG: a height increase due to the anti-rabbit IgG binding was observed only on the rabbit IgG features and not on the lysozyme patterned areas. Lim

et al. [41] employed a modified AFM tip-covered with 2-[methoxypoly (ethyleneoxy) propyl] trimethoxysilane (Si-PEG) - that forms a biocompatible and hydrophilic layer - that was dipped in a buffer solution containing the protein of interest with glycerol at 5% - this one to increase the hygroscopicity of the solution. They showed multiple protein-ink capabilities by serially patterning two different fluorophore-labeled proteins, antirabbit IgG (Alexa Fluor 594) and antihuman IgG (Alexa Fluor 488) on an aldehyde-derivatized surface (see figure B). Recently, C. Xang et al. combined bias-assisted DPN with aptamer-protein recognition (Aptamers are nucleic acids which are able to bind specifically to their targets, which range from small organic molecules to proteins) to fabricate dual protein protein patterns(Nanoscale Patterning of Multicomponent Proteins by Bias-Assisted Atomic Force Microscopy Nanolithography [42]. Two different types of aptamber arrays to anchor PDGF-BB and thrombin were successfully fabricated by two-step bias lithography and two-step assembling of thiol-functionalized aptamers. Thanks to biorecognition between the two proteins (PDGF-BB and thrombin) and the respective specific aptamers, a multicomponent protein pattern with two different protein was realized.

Hollow tip nanodispensing

Dip Pen Nanopatterning suffers from the limit of periodic ink refilling - both in liquid and diffusive cases. In this sense, nanofountain probes (NFB) constitute a natural evolution of DPN coat and write technique towards a continuous ink delivery mode in contact mode. Liquid molecular inks stored in an on-chip reservoir are constantly fed through integrated microchannels to apertured dispensing tips by capillary ac-

tion, this allowing continuous delivery either to a substrate. Like in liquid DPN, solutions are deposited in liquid state, with an attainable lateral resolution consistently from the micrometer till the sub 100 nm scale. The deposition mechanism can be interpreted as liquid diffusion to the surface as in DPN, also if application of electric fields between the pen and the surface have been show to permit a more consistent fluid dispensing via electrophoretic (EPF) or electro-osmotic flow (EOF) as described by Loha et al. [43]. Consistent control of the spot size at the nanoscale can be achieved by employing hollow AFM probes milled by focused ion beam lithography [44] as K. Kaisei et al. recently showed in depositing liquid droplets with a volume in zeptoliters scale by applying an electric field between the liquid and a conductive surface [45]. As already shown with DPN, also nanofountain probes enable scalability to 1- and 2-D probe arrays for enhancing the throughput. Moldovan et al. fabricated 1D nanofountain pens array with twelve cantilever probes with microfluidic channels connecting two on-chip reservoirs (that can be filled with two different inks) to volcano-shaped nanofountain pens [46]: in a recent evolution of this system, authors showed the possibility, in principle, to dispense till four different biological inks - each of them inking six pens [47]. As a perspective, NFP could be expanded to 2D arrays by optimization of suitable a network of reservoirs and microchannels with the advantage that NFP cantilevers having protruding tips that eliminate the need for tilting cantilevers against the substrate surface minimize the problems associated with 2D DPN probe alignment [48]. Since microfluidics elements of NFP are enclosed, multiple inks can be used in adjacent channels without cross contamination and negligible evaporation rates; however big issues derive from easy pen clogging and

difficult channel cleaning procedures. This methodology is still prone to advancements and optimization; in fact, solving these hurdles, it could become a broad-applicable liquid nanodeposition tool with applications in direct in vitro single cell injection [49].

1.4.4   1D Pen Arrays for Multiplexing Patterning
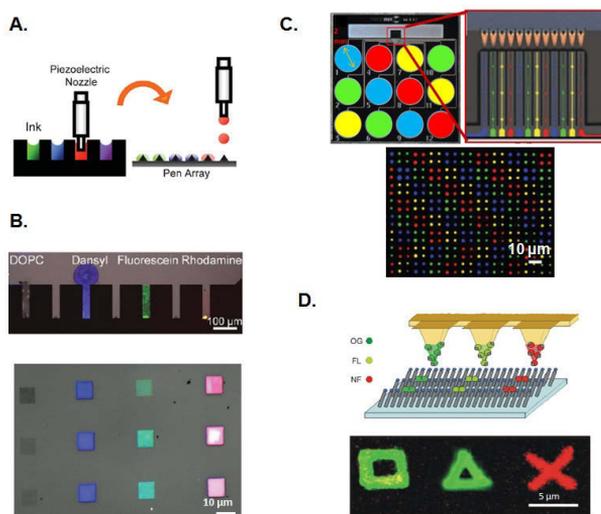
Figure 1.4: **A. Scheme for addressable inking of pen arrays by ink-jet printing and B. inking of a 1D pen array with four different inks (DOPC, Dansyl, Fluorescein, Rhodamine) and corresponding multiplexed parallel patterns written on glass. Pictures adapted from [50]. C. At the top: optical image of a 1D cantilever tip array overlaid with a fluorescence image of a micro-channel Inkwell containing solutions of four different dye-labeled IgG antibodies. At the bottom: fluorescence image of the same four antibodies deposited [51]. D. Scheme for the fabrication of a combinatorial pH indicators array (OG, FL and NF- see text for the chemical names) by direct-writing parallel DPN on glass substrates with a fluorescence image of OG square-, FL triangle- and NF cross-like structures. Pictures reproduced from [52].**

To be really useful for biological application, DPN should enable parallel and speed writing of different inks in a single step procedure rather than serial writing of single inks in multiple steps. This goal

can be achieved by the enhancing high-throughput attributes of DPN permitted the realization of devices as 1D (i.e. linear array of pens) or 2D (i.e. array of pens in a plane) pen arrays for the simultaneous writing of ink on large areas at the best on one square centimeter area reported by employing the 2D array of 55,000 pens [53] and combining this with multiplexing capabilities. Conventionally, inking process involves pen soaking in single ink solution for few seconds and subsequent blow drying with nitrogen. This method can introduce variability due to in-homogeneous solvent drying depending on the duration and angle of N2 blowing, as well as the manner of soaking. An efficient method should deliver well-defined amounts of ink to each pen to overcome the problem due to lack in reproducibility with inking from a solution. In this sense, challenges are then associated with addressing and inking each pen of a such designed array with different inks, assuring uniform ink coating for different inks on different pens and controlling ink transport rates (this being in principle resolved by employing liquid inks as explained before). Two possible approaches for multiple pen inking have been investigated: via ink-jet printer addressing or microfluidic inkwells. The ink-jet printer addressing approach has been shown by Wang et al. [54]to be an easy and reproducible method to deliver independent inks to each pen or to several pens within a 1D or 2D pen array. Cantilevers were alternating inked within a 7-pen array each with different fluorophore-labeled phospholipids diluted (1 wt%) in a carrier lipid, 1,2-dioleonyl-sn-glycero-3-phosphocholine (DOPC) this last one allowing uniform transport properties for different dye labeled lipid inks. The inked pen array was then used to pattern the four different inks in arrays of squares (10 μm wide) and made of 300 nm parallel line features. To

improve selective pen inking, authors functionalized each pen anisotropically rendering the pyramidal tip hydrophilic (MHA functionalization) and the remaining area hydrophobic (ODT functionalization) so that ink molecules are preferentially driven to the hydrophilic area due to differences in surface energy in order to improve spatial resolution of ink droplet confinement to a single tip. On the other side, microfluidic inking protocol is a more robust and rather well established method to selectively and precisely confine different inks at separation scales of the same order of distance between pens in a 1D pens array in order to load different ink on individual pens at the same time. This methodology is based on the employment of inkwell loading chips, microfluidic devices etched out of silicon wafers using a Deep Reactive Ion Etch process that creates nearly vertical side walls. Trenches are etched 100 microns deep and are deep enough that a water-based ink remains usable for at least 10 minutes in ambient conditions. Fluid actuation occurs by open-channel capillary flow (wicking) from reservoirs - where different inks can be loaded with a conventional micropipette - to individual microchannels that run out from microchannels and ultimately to microwells where tips are inked. The system is designed to keep the microwells full of ink even as the ink supply slowly evaporates from the reservoir. 1D Pens array is dipped into micron-sized cavities or microwells to load inks in a single step [51]. Being microfluidics elements in open configuration, they are relatively clog-free, easy to fabricate and in principle, it is possible to reuse them by appropriate cleaning procedures. However, especially if used in multiplexing, they can suffer from cross contamination in particular for adjacent channels and also solvent evaporation this problem being resolved by employment of high-boiling or hygroscopic co-solvents

or high relative humidities. There are some examples in literature as the applications J.-W. Jang et al. [55] showed multifeatures hydrogel and phospholipid structure patterning with precise registration. In particular they printed four different dye-labeled hydrogel inks (PEG-DMA) within a small area of 50 x $50\mu m^2$ on hexamethyldisilazane (HMDS) spin-coated silicon substrates. Rhodamine, FITC, Alexa347, and a mixture of rhodamine and FITC were used as red, green, blue, and orange dyes, respectively. The volume mixture ratio between dyes and PEG-DMA solutions was balanced to exhibit similar fluorescence intensity at each dye-labeled ink. A. Martinez-Otero et al. [52] showed the possibility of realizing miniaturized combined arrays of three different pH indicators for sensitive and robust acidity detection using parallel dip-pen nanolithography. The authors employ different amino-reactive of Oregon Greens 514 (OG), fluorescein (FL) and 5-carboxynaphthofluorescein (NF) covalently immobilized on the amino group of a functionalized glass support (N-(6- aminohexyl)-3-aminopropyltrimethoxysilane SAM on the surface), which show different protonation states with distinct emissive properties and complementary pKa values, so that the combined use of these compounds allows for a pH monitoring within the pH 3.0 - 9.0 range.

1.4.5   2D Pen Arrays for High-throughput Multiplexing Patterning

Being throughput the biggest limitation of the DPN technology, research developed large area parallelization capabilities in order to realize its full potential for Life Science applications. The first parallel probe investigation was conducted at IBM and Stanford in the known IBMs
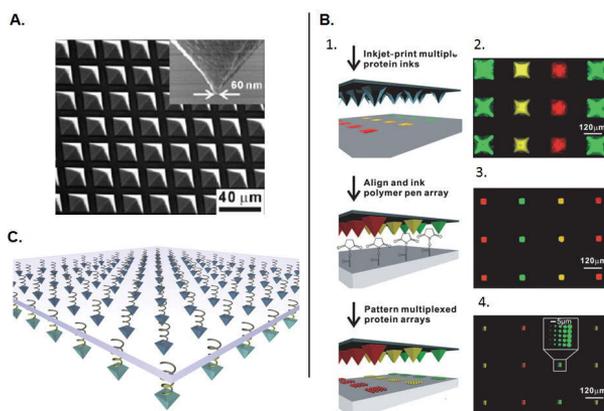
Figure 1.5: **A. Scanning electron microscope image of a Polymer Pen Array for Lithography. Reproduced from [56]. B. Multiplexed protein patterning via Polymer Pen Lithography. (B.1) Scheme for multiple proteins PPL patterning. Fluorescence images of a Si mold inked with three proteins by ink-jet (B.2); a polymer pen array dipping inside the Si mold (B.3); and multiplexed proteins arrays made by PPL (B.4). Reproduced from [57]. C. Scheme of a Hard-tip soft-spring tip array supported by a transparent, PDMS backing layer that provides mechanical flexibility to each tip and alleviates alignment issues [58].**

millipede project in the field of high-density data storage: researcher were able to realize a 32 x 32 probe array with each cantilever assigned to read and write its own approximately 100 x 100 μm area. As to the lithography applications, Quate and coworkers [59] developed 1D and 2D probe arrays for imaging and lithographic applications: the approach they followed was the one of current-induced lithography in which each pen is independently actuated for delivering material on the surface. Since the independent control of the on/off state of each cantilever requires actuation of the force applied to, and height of, the cantilever above the surface, this approach finally results in a quite challenging operative principle. On the other side, patterning in DPN simply occurs whenever a coated tip is held in contact with a surface: applying

this principle on the scale of a 2D array of pens, this means that pens are not actuated independently but are simultaneously brought into contact with the surface and scanned together, which allows the duplication of a single pattern a number of times equal to the number of probes in the array. This solution is defined as passive probe array and results in a simple and robust implementation of parallel-pen DPN [60] that importantly, can be integrated with standard AFM systems. Accordingly, efforts led Mirkin and coworkers to the realization of 2D cantilevers arrays [53] a bi-dimensional array of 55,000 with a pen spacing of 90 and 20 m in the x and y directions, respectively. However, in order to get reproducible patterning results, the plane of the array of pens has to be as parallel as possible to the plane of the surface in order that all the pens exert the same amount of force on the surface this resulting in ideal uniform spot sizes across the array in extended periods of writing time. The procedure to align a pen array with respect to the surface is defined **leveling** procedure. While this can be accomplished quite easily via optical methods for 1D pen arrays, the opacity of Si and Si_3N_4 cantilvers makes it very challenging to align a 2D cantilver array on a surface. In addition, although being capable of parallel patterning of a single feature on 1 cm^2, this systems suffers from hurdles in multiplexing via inkwell devices since the micro-fabricated area occupancy for a chip containing the ink reservoir of a inkwell for a 2D nano tip device would be larger than 0.5 m^2 thus making the realization of such device not realistic. It is remarkable that, by employing ink-jet printing techniques, it is possible, in principle, to coat individual pens also within 2D pen arrays with different materials [61]. In a newer version of this device, holes have been constructed inside the 2D nano array to permit the user

to look at the cantilevers to see if and how they touch the surface and evaluate their deflection. Moreover, the 2D nano array is also quite expensive and fragile: these are further impediments for its applications in Life Science [62].

Evolutions 2D Pen Arrays: from Polymer Pen Lithography to Hard-Tip Soft Spring Lithography

A significant evolution for multiple 2D patterning is then constituted by Polymer-Pen Lithography (PPL): instead of employing hard Si_3N_4 cantilevers, PPL uses a relatively soft elastomeric polymer (typically Polydimethylsiloxane) to deliver inks onto a surface by controlling the movement of the pen array with a scanning probe microscope. A typical polymer pen array contains thousands of pyramid-shaped tips made with a master prepared by conventional photo-lithography and subsequent wet chemical etching. These pyramids are connected by a thin PDMS backing layer (thickness around 50 to 100 nm) that is adhered to a glass support. The feature size not only depends on the dwell time (i.e. probe-surface time of contact) but also on the contact force (that results with the reversible flattening of the tip). In addition, the same mould used to fabricate the array can be used as inkwell that can be addressed and filled with different inks by employing ink-jet printing so achieving perfect registry between the pens on the array and the inkwells [63]. Leveling these pen arrays with respect to the surface by optical methods can still produce misalignment, however X. Liao et al. showed a leveling method based on the evaluation of the exerted force between the pen array and the surface that significantly improves the alignment achieving a tilt of less than 0.004 [64]: in this way, array

features can vary no more than 50 nm over 1 cm.

A proof-of-principle multiplexed PPL enabled printing in high-throughput and low cost manner has been shown by Zheng et al. [57] in one step writing with control over feature size (spanning the sub-100 nm to the μm scale length scale) by varying tip-substrate contact time and contact force. The pyramid-shaped wells in Si mould were first filled with three different dye-labeled proteins inks by ink-jet printing i.e. yellow: TRITC-conjugated anti-mouse IgG (TRITC = tetramethylrhodamine isothiocyanate); green: Alexa Fluor 488-conjugated anti-prostate specific antigen (anti- PSA); red: Alexa Fluor 647-conjugated anti-cholera toxin beta (anti-CT). In such a way by fluorescence microscopy authors showed that the inks have been properly addressed with the ink-jet printer and printed on surface, for instance a Codelink slide. Moreover PSA dot arrays have been fabricated and subsequently labeled by its corresponding dyelabeled antibody; anti-PSA selectively binds onto the PSA regions with undetectable background this meaning that PPL-patterned protein maintain their structural integrity.

As future advancements of 2D pen arrays, it is remarkable the possibility to integrate Polymer-Pen Lithography with the concepts of near-filed scanning optical microscopy (NSOM) to generate patterns by passing 400-nm light through nanosized apertures at each tip in the array. The technique has been called beam pen lithography and is able to toggle between near and far field distances, allowing the generation of both sub-diffraction limit (100 nm) and larger features [65]. However, an impressive evolution versus a versatile cantilever-free tip-based nanopatterning method has been recently shown by Shim et al. [58] in which an array of hard silicon tips is mounted onto an elastomeric backing. The

approach - termed hard-tip, soft-spring lithography - can overcome the throughput issues of cantilever-based scanning probe systems and the resolution limits imposed by elastomeric stamps and tips, being able to deposit materials on a surface reaching a sub-50 nm lateral resolution over centimeter-scale areas.

References

[1] Sumerel J.; Lewis J.; Doraiswamy A.; Deravi L. F.; Sewell S. L.; Gerdon A. E.; Wright D. W.; Narayan R. J., *Biotechnol. J.* **1**, 976 (2006).

[2] Boland T.; Xu T.; Damon B.; Cui X., *Biotechnol. J.* **1**, 910 (2006).

[3] Brünahl J.; Grishin A.M., *Sens. and Act. A* **101**, 371 (2002).

[4] Lemmo A.V.; Rose D.J. and Tisone T.C., *Curr. Opin. Biotechnol.* **9**, 615 (1998).

[5] Arrabito G.; Pignataro B., *Anal. Chem.* **82**, 3104 (2010).

[6] Brünahl J.; Grishin A.M., *Sens. and Act. A* **101**, 371 (2002).

[7] Beier M.; Hoheisel J.D., *NAR* **27**, 1970 (1999).

[8] Beier M.; Hoheisel J.D., *NAR* **32**, e9 (2004).

[9] Stiffler M.A.; Grantcharova V.P.; Sevecka M. and MacBeath G., *J. Am. Chem. Soc.* **128**, 5913 (2006).

[10] Gordus A. and MacBeath G., *J. Am. Chem. Soc.* **128**, 13668 (2006).

[11] Hasenbank M.S. et al., *Anal. Chim. Acta* **611**, 80 (2008).

[12] Sukumaran S.M.; Potsais B.; Lee M.-Y.; Clark D.S. and Dordick J.S., *J. Biomol. Screen.* **14**, 668 (2009).

[13] Lee M.-Y.; Kumar R.A.; Sukumaran S.M.; Hogg M.G.; Clark D.s S.; Dordick J.S., *PNAS* **105**, 59 (2008).

[14] Gosalia D.N.; Diamond S.L., *PNAS* **100**, 8721 (2008).

[15] Mugherli L.; Burchak O.N.; Balakireva L.A.; Thomas A.; Chatelain F.; Balakirev M.Y., *Angew. Chem. Int. Ed.* **48**, 7639 (2009).

[16] Mugherli L.; Burchak O.N.; Balakireva L.A.; Thomas A.; Chatelain F.; Balakirev M.Y., *J. Am. Chem. Soc.* **133**, 10058 (2011).

[17] Nishioka G. M.; Markey A. A.; Holloway C. K., *J. Am Chem. Soc.* **126**, 16320 (2002).

[18] Barbulovic-Nad I.; Lucente M.; Sun Y.; Zhang M.; Wheeler A.R.; Bussmann M., *Crit. Rev. in Biotechnol.* **26**, 237 (2006).

[19] Dong H.; Carr W. W.; Morris J. F., *Phys. Fluids* **18**, 072102 (2006).

[20] Schiaffino S.; Sonin A. A., *Phys. Fluids* **9**, 3172 (2003).

[21] D. B. van Dam; C. Le Clerc, *Phys. Fluids* **16**, 3403 (2004).

[22] Anderson D. M., *Phys. Fluids* **17**, 087104 (2005).

[23] Chiu D.T.; Lorenz R.M. and Jeffries G.D.M., *Anal. Chem.* **81**, 5111 (2009).

[24] Bano F.; Fruk L.; Sanavio B.; Glettenberg M.; Casalis L.; Niemeyer C. M. and Scoles G., *Nanolett.* **9**, 2614 (2009).

[25] Unruh D.A.; Mauldin C.; Pastine S.J.; Rolandi M.; Frchet J.M.J., *J. Am. Chem. Soc.* **132**, 6890 (2010).

[26] Piner R.D.; Zhu J.; Xu F.; Hong S.; Mirkin C.A., *Science* **132**, 661 (1999).

[27] Piner R.D.; Zhu J.; Xu F.; Hong S.; Mirkin C., *Science* **283**, 661 (1999).

[28] Hampton J.R.; Dameron A.A.; Weiss P.S., *J. Am. Chem. Soc.* **128**, 1648 (2006).

[29] Fabi L.; Durou H. and Ondarçuhu T., *Langmuir* **26**, 1870 (2010).

[30] Weeks B.L. and DeYoreo J.J., *J. Phys. Chem. B* **110**, 10231 (2006).

[31] Hampton J.R.; Dameron A.A. and Weiss P.S., *J. Phys. Chem. B* **109**, 23118 (2005).

[32] Hampton J.R.; Dameron A.A. and Weiss P.S., *Nano Lett.* **4**, 2171 (2004).

[33] Hampton J.R.; Dameron A.A.; Weiss P.S., *J. Am. Chem. Soc.* **128**, 1648 (2006).

[34] Irvine J.; Hernandez-Santana A.; Faulds K. and Graham D., *Analyst* **136**, 2925 (2011).

[35] Rozhok S.; Piner R. and Mirkin C.A., *J. Phys. Chem. B* **107**, 751 (2003).

[36] Hernandez-Santana A.; Irvine E.; Faulds K. and Graham D., *Chem. Sci.* **2**, 211 (2011).

[37] Senesi A.J.; Rozkiewicz D.I.; Reinhoudt D.N. and Mirkin C.A., *ACS Nano* **3**, 2394 (2009).

[38] Li H.; He Q.; Wang X.; Lu G.; Liusman C.; Li B.; Boey F.; Venka-traman S.S. and Zhang H., *Small* **7**, 226 (2011).

[39] Demers L.M.; Ginger D.S.; Park S.-J.; Li Z.; Chung S.-W.; Mirkin C. A., *Science* **292**, 1836 (2002).

[40] Lee K.B.; Lim J.H.; Mirkin C.A., *J. Am. Chem. Soc.* **125**, 5588 (2003).

[41] Lim J.H.; Ginger D.S.; Lee K.B.; Heo J.; Nam J.M.; Mirkin C.A., *Angew. Chem. Int. Ed.* **42**, 2309 (2003).

[42] Xing C.; Zheng Z.; Zhang B.; and Tang J., *ChemPhysChem* **12**, 1262 (2011).

[43] Loha O.Y.; Ho A.M.; Rima J.E.; Kohlib P.; Patankara N.A. and Espinosa H.D., *PNAS* **105**, 16438 (2008).

[44] Fang A. et al., *Nanoletters* **6**, 2368 (2006).

[45] Kaisei K.; Satoh N.; Kobayashi K.; Matsushige K. and Yamada H., *Nanotechnology* **22**, 175301 (2011).

[46] Moldovan N.; Kim K.-H. and Espinosa H.D., *J. Micromech. Micro-eng.* **16**, 1935 (2006).

[47] Loha O.Y.; Ho A.M.; Rima J.E.; Kohlib P.; Patankara N.A.; Espinosa H.D., *PNAS* **105**, 16438 (2008).

[48] Kim K.-H.; Sanedrin R.G.; Ho A.M.; Lee S.W.; Moldovan N.; Mirkin C.A., *Adv. Mater.* **20**, 330 (2008).

[49] Loh O.; Lam R.; Chen M.; Moldovan N.; Huang H.; Ho D. and Espinosa H.D., *Small* **5**, 1667 (2009).

[50] Sekula S.; Fuchs J.; Weg-Remers Su.; Nagel P.; Schuppler S.; Fragala J.; Theilacker N.; Franzreb M.; Wingren C.; Ellmark P.; Borrebaeck C. A. K.; Mirkin C. A.; Fuchs H.; Lenhert S., *Small* **4**, 1785 (2008).

[51] Gandor S.; Reisewitz S. et al., *Manuscript in Preparation* (2012).

[52] Martnez-Otero A.; Gonzlez-Monje P.; Maspoch D.; Hernando J. and Ruiz-Molina D., *Chem. Commun.* **47**, 6864 (2011).

[53] Loh O.; Lam R.; Chen M.; Moldovan N.; Huang H.; Ho D. and Espinosa H.D., *Angew.Chem.Int.Ed.* **45**, 7220 (2006).

[54] Wang Y.; Giam L.R.; Park M.; Lenhert S.; Fuchs H.; and Mirkin C.A., *Small* **4**, 1666 (2008).

[55] Jang J.W.; Smetana A.; Stiles P., *Scanning* **32**, 24 (2010).

[56] Huo F.; Zheng Z.; Zheng G.; Giam L.R.; Zhang H.; Mirkin C.A., *Science* **321**, 1658 (2008).

[57] Zheng Z.; Daniel W.L.; Giam L.R.; Huo F.; Senesi A.J.; Zheng G. and Mirkin C.A., *Angew. Chem.* **121**, 7762 (2009).

[58] Shim W.; Braunschweig A.B.; Liao X.; Chai j.; J. Kuk Lim J.K.; Zheng G. and Mirkin C.A., *Nature* **469**, 516 (2011).

[59] Chow E.M.; Yaralioglu; G.G.; Quate C.F.; Kenny T.W., *Appl. Phys. Lett.* **80**, 664 (2002).

[60] Ginger D. S.; Zhang H. and Mirkin C.A., *Angew. Chem. Int. Ed.* **43**, 30 (2004).

[61] Sekula S.; Fuchs J.; Weg-Remers S.; Nagel P.; Schuppler S.; Fragala J.; Theilacker N.; Franzreb M.; Wingren C.; Ellmark P.; Borrebaeck C.A.K.; Mirkin C.A.; Fuchs H. and Lenhert S., *Small* **4**, 1785 (2008).

[62] Braunschweig A.B.; Huo F. and Mirkin C.A., *Nature Chem.* **1**, 353 (2009).

[63] Huo F.; Z. Zheng Z.; G. Zheng G.; Giam L.R.; Zhang H.; Mirkin C.A., *Science* **321**, 1658 (2008).

[64] Liao X.; Braunschweig A.B. and Mirkin C.A., *Nano Lett.* **10**, 1335 (2010).

[65] Huo F.; Zheng G.; Liao X; Giam L.R.; Chai J.; Chen X.; Shim W. and Mirkin C.A., *Nature Nanotech.* **5**, 637 (2010).

Array technologies in Life Sciences

This chapter deals with the applications of micro- and nano- array technology in relevant fields of Life Sciences, like Drug Discovery and Cell Biology. As to the drug discovery process, we focus on micro-array based approaches for target discovery and high throughput screening via chemical microarrays. Moreover, as to cell array, the discussion deals with the evolution from micro-well based assays to high-tech array-based single cell measurements.

Glossary and list of acronyms:

Biological array: array of biomolecular entities (oligonucleotides, proteins, etc.) immobilized on a surface at known, discrete locations that are used to measure or detect a series of biological interactions in a single experiment.

Drug Discovery: the process by which drugs are discovered and/or designed, involving the identification of candidates, synthesis, characterization, screening, and assays for therapeutic efficacy.

Protein array: array of different proteins or specific capture probes for the proteins affixed at separate locations on a solid surface for identifying protein protein interactions, enzymatic substrates of protein kinases, transcription

factor protein-activation, targets of biologically active small molecules.

Chemical array: collection of organic chemical compounds spotted on a solid surface that provides a multiplex tool to search potential drugs for therapeutic targets.

Cellular array: array of different biological materials (such as antibodies, proteins, or lipids) which can interact with the cells, leading to their capture on specific spots. They allow for the multiplex interrogation of living cells on the surface of a solid support.

2.1   Microarrays in Drug Discovery

2.1.1   Drug Discovery Process

Drug discovery is a lengthy, expensive and complex procedure that entails a series of serial and/or parallel operations which include target selection, hit identification, lead optimization, compound synthesis, characterization, screening, assays for therapeutic efficacy, pre-clinical and clinical studies. The journey from initial concept to a marketed drug is a long one, and is statistically more likely to end in failure than success [1] On average, the discovery and development process for a drug takes 10 to 12 years and costs as much as US one billion of dollars and only 1 in 5,000 compounds screened in early-stage discovery successfully makes it through to market, although both figures vary dramatically with disease area. Therefore, the search for and the development of new technologies to accelerate drug discovery is of fundamental importance. In fig. 2.1, the complete pipeline for modern drug discovery is presented. The process of drug discovery can roughly be divided into an early and late phase. The early phase is mainly represented by target and lead discovery, whereas the later phase deals mainly with clinical evaluation (Phases I, II, III) and development. Considering early phase drug discovery, identification of a target biomolecule is the first step in the drug

discovery process. Target identification consists in the discovery and se-
lection of a suitable drug target. Such targets are protein biomolecules
such as receptors, enzymes and ion channels but can also be DNA. The
chosen target must be of relevance to the disease under study and its
modulation must lead to effective disease treatment: in this way the
target is validated. The initial steps of target validation are usually ob-
tained *in vitro* and in animal models but the ultimate validations are
usually obtained only in clinical experiments in humans [2].
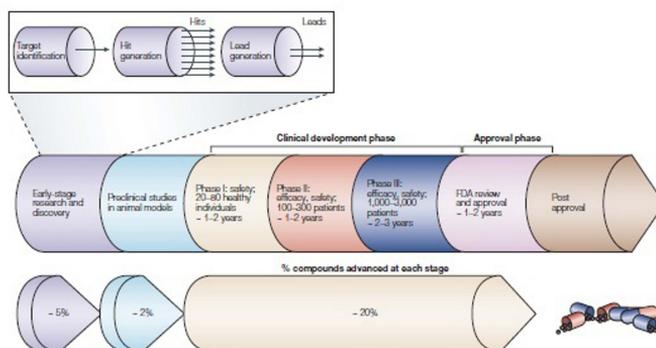
Figure 2.1: **The drug discovery and development pipeline.**

After target selection and validation, modulators of the target have
to be identified. Such modulators are chemical compounds that can be
agonists or antagonists in the case of receptors, activators on inhibitors
of enzymes, and openers or blockers of ion channels. This phase starts
with the design and development of suitable assays to monitor the target
under study. By employing high-throughput screening (HTS) method-
ologies, the target is exposed to compound libraries - a large number of
chemical compounds (in the order of 10^5) that come from high-speed
parallel combinatorial synthesis. Successful compounds (called hit com-

pounds) are those who exceed a certain threshold value in a given assay for activity modulation on the validated target are progressed into leads. At this step, hit compounds are assessed for relevant biological and drug-like properties, such as chemical integrity, functional behavior and structure-activity relationships in order to become lead compounds. Lead discovery can also be realized by virtual screening, that is the computer based process of scoring and ranking molecules in large chemical libraries according to the likelihood of having affinity for a determined target. Lead compounds are subsequently confirmed by a more detailed assessment of chemical integrity, accessibility, dose-dependent and selective target modulation, structure-activity relationships (SARs) as well as physicochemical and pharmacokinetical properties (absorption, distribution, metabolism and excretion). The lead compounds that demonstrate activity and selectivity in the secondary screens are tested in progressively more complex systems as cells and whole animals before reaching clinical trials. At this stage, only a few drug candidates continue into the drug development stage for clinical trials. The clinical development phase is composed of three phases, is costly and time-consuming (it lasts several years). It is followed by the Approval phase: at the end of the process the drug is approved for manufacturing and marketing [3].

Nowadays, by employing microarray based technologies on system biology level, many new possible drug targets can be discovered every day and in the meanwhile being new compounds daily synthesized by high-throughput synthesis. Admittedly, drug discovery process is critically dependent upon the ability to identify chemical compounds (hit compounds) acting on specific targets, that is drug screening is one of

the bottlenecks in the process of drug discovery [4]. So, there is an urgent need to find high throughput screening (HTS) methodologies to profile the activity of large numbers of chemicals against hundreds of biological targets in a fast, low-cost fashion. The recent development of microarray and also microfluidic technologies has permitted the development of high-density, low volume assays to achieve this goal. In particular, the reduction in cost, rather than increase in throughput, is the primary driving force within most HTS groups to move to higher density, lower volume assays. By the way, the number of new drugs approved per year by regulatory agencies has not increased in a significant way in the last years especially if comparing to the financing investment in pharmaceutical research and development [5]. Tough causes for this low productivity can be ascribed to the complexity of related biological targets systems inside cells, one major issue derives from the extremely high rate of toxicity among drug candidates in the late clinical trials stage. In this sense, miniaturization high-throughput and multiplexing in are highly desirable features for cell-based assays whose aim is to identify potential toxic compounds much earlier in the drug development pipeline, in order to exclude these unsuccessful compounds from further pharmaceutical consideration, and finally saving significant financial resources. In this scenario, liquid dispensing in the microarray format plays a fundamental role in all of the potential bottlenecks for drug discovery procedure as a general tool for low cost biological solution dispensing in a microarray format. Thanks to the inherent simplicity, multiplexing attributes, ability to handle minute amounts of liquids (from hundreds of nanoliters till femtoliters), it can be considered as a tool for speeding-up and reducing the financial investments of the drug

discovery process.

2.1.2 Target identification by Protein Biochips

Modern drug discovery is focused on the search or design of drug-like molecules, which selectively interact and modulate the activity of one or a few selected therapeutic targets [6]. Genomic and proteomic studies have indicated the potential existence of about 10,000 druggable targets; however, less than 500 of these targets have corresponding FDA-approved drugs. One of the biggest challenges in drug development is to choose and explore promising targets from a growing number of potential targets. In general a good drug target has to be efficacious for the considered disease, safe, meet clinical and commercial needs and be druggable. A target is defined druggable only if accessible to drug molecules that upon binding elicit a biological response which can be measured both *in vitro* and *in vivo*. Correct target identification derives from careful data mining of available biomedical data: namely, the use of bioinformatic approaches for identification, selection and prioritizing potential disease targets [7]. The data come from a variety of sources but include publications and patent information, gene expression data, proteomics data, transgenic phenotyping and compound profiling data. Through the study of cellular protein expression - proteomics, it is possible to identify novel proteins involved in key biological processes in the cell that may serve as potential drug targets. Despite its considerable theoretical promise, individual cells/tissues have the potential to generate many millions of proteins while the current analytical technologies that involve the use of time-consuming two dimensional gel electrophoresis (2DIGE) and mass spectrometry (MS) techniques are not able to handle

complex biological samples without multiple high-resolution purification steps to reduce their complexity. This significantly limits the speed of data generation and replication and requires the use of bioinformatic algorithms to reconstitute the parent proteome, a process that does not always result in a reproducible outcome [8]. In addition, membrane bound proteins, like G-protein coupled receptors and ion channels, that are the targets of almost 70% of currently existing drugs, are not amenable to study due, in part, to limitations in current proteomic techniques and also to these being present in low abundance and thus disproportionally represented in proteome profiles. Target selection and validation are important not only for achieving therapeutic efficacy but also for increasing drug development odds, given that few innovative targets have made it to the approved list each year: twelve innovative targets have been discovered between 1994 and 2005 [9] while only ten new human targets have been retrieved between 2006 and 2010 [10]]. Apart from target selection and validation, drug discovery efforts might be facilitated by a molecular level knowledge of active molecular scaffolds, SAR, multi-target agents and synergistic drug combinations against selected target or multiple targets, and information about the sources of drug leads such as the species origins of natural product-derived drugs [11] in order to fulfill the system-biology driven approach to drug discovery. In this more and more complex scenario one needs a far deeper understanding of the molecular mechanisms of diseases, taking into account the full biological context of the drug target and moving beyond individual genes and proteins [12] towards a Systems biology approach consisting in the systematic interrogation of the biological processes within the complex, physiological milieu in which they function. Insight into

the combined behavior of these many, diverse, interacting components is achieved through the integration of experimental, mathematical and computational sciences in an iterative approach: through this contextual understanding of the molecular mechanisms of disease, a systems approach has the potential to further facilitate the identification and validation of the therapeutic modulation of regulatory and metabolic networks and hence help identify targets and biomarkers, as well as off-target and side effects of drug candidates [13]. Thus new technologies are needed that can utilize microscopic amounts of cellular material: in this regard protein microarrays represent the best tool for identifying the components of a system and their interactions, and monitoring the effect of perturbations on these components [14–16]. The ability of protein microarrays in the identification and characterization of entire interconnecting protein pathways and networks in cells gives the possibility to expand the comprehension of physiological processes and essential diseases mechanisms so leading to the rational and speed identification of new drugs and drug targets. In the following section, protein array technologies will be discussed in detail concerning the specific challenges in fabrication and detection methods.

Protein Biochip Technology

In Comparison with DNA microarrays, protein array technologies(see Fig. 2.2 from [17]) have additional challenges with the image analysis, primarily due to both low signal to noise ratio and limited number of abundant protein signal spots to align grids. A protein array image usually consists of one or multiple blocks of arrays. The variety of array formats, spot shapes, and intensity profiles makes it quite chal-

lenging to extract spot signal correctly [18]. In addition, the different substrates, printing mechanisms and protocols, staining/blocking processes, and broad applications result in varied kinds of complex images which make it difficult to develop a silver bullet solution-one algorithm to be applied to all scenarios. Proteome microarrays are an excellent way to discover drug targets. The rate of drug development can be accelerated by screening potential drug candidates against their putative protein targets, while at the same time, ensuring that the candidates exhibit no cross-reactivity with secondary proteins. In this way a primary drug screen can be used to rule out compounds which carry the potential for causing side-effects. Microarrays can be used for screening small molecule binders to protein targets while simultaneously analyzing its binding to other cellular proteins that may be structurally and functionally related to the protein of interest. Entire proteomes printed on a chip can be probed with small molecules in one experiment to discover interactions. Huang et al. [19] used yeast proteome microarrays to study protein-drug interactions. They probed the array with a biotinylated small molecule inhibitor of rapamycin (SMIR) to find proteins targets that may be involved in the target-of-rapamycin (TOR) dependent nutrient response network. They discovered a protein of previously unknown function to be a target of SMIR. They followed up the array probing experiment with gene deletion experiments to prove that the target protein was indeed a legitimate target of the SMIR.

Fundamental issues in protein chips fabrication are: substrate surface preparation, protein handling, detection methods and data acquisition.

Proteins can be attached to various kinds of surfaces via diffusion,
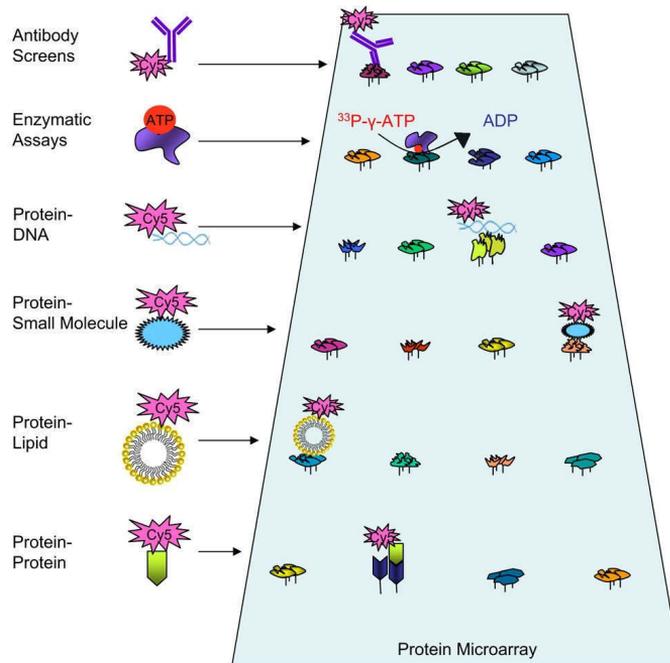
Figure 2.2: **Representative samples of the different assays performed on functional protein microarrays are shown. Proteins are immobilized at high spatial density onto a surface. Albeit only Cy5 is shown, any other fluorophore can be used for detection.**

adsorption/absorption, covalent bonding and affinity interactions (see fig. 2.3 taken from [20]).

Protein diffusion in 3D gels and agarose thin films is a methodology with high binding capacity without requiring protein modification. Anyway, gel fabrication can be quite tough and expensive. Protein adsorption/absorption is used with surfaces which have a high inherent binding energy to proteins in general. The most common of these substrates are hydrophobic plastics such as polystyrene, to which most proteins physically adsorb by van der Waals, hydrophobic and hydrogen-bonding interactions. This type of physical adsorption is used to immobilize capture
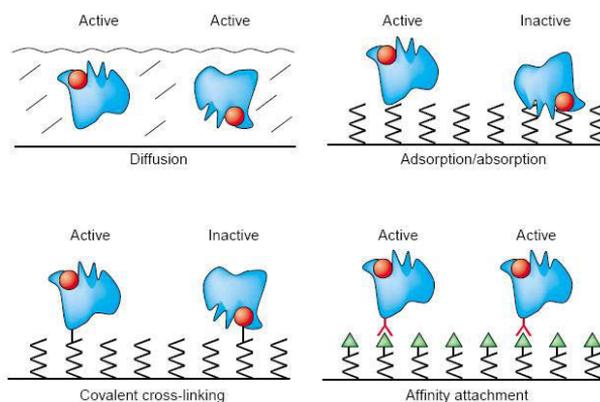
Figure 2.3: **Comparison of protein attachment methods. Except from affinity attachment, proteins are usually laid on the surface in a random fashion, which may alter their native conformation, reducing their biological activity, or make them inacessible to probes.**

antibodies in enzyme-linked immunosorbent assays (ELISA). This immobilization is very simple to perform, because it does not require any modification of the protein for its attachment to the surface. The disavantage is that proteins can be inactivated because of surface-induced denaturation and steric occlusion. Protein covalent linking to surfaces is the most adoperated protein attachement method for protein biochips. The immobilization procedure must be optimized to obtain the maximum surface coverage preventing the biological molecule denaturation and/or the loss of its specific properties, e.g., for an enzyme its enzymatic activity. The surface-linked protein must be oriented on the surface such that the active site or binding site faces away from the protein thin film and can therefore interact optimally with proteins in the biological sample. This is most easily achieved when using recombinant proteins, in which amino-, caboxy- or His-tag terminal tags are introduced to realize highly specific affinity interactions. Proteins fused with

a high-affinity tag at their amino or carboxy terminus are linked to the surface via this tag, and hence, all of the attached proteins should orient uniformly away from the surface. For non recombinant proteins, one must take advantage of existing functional groups on the protein, as for example the amino or hydroxyl groups. For silicon dioxied surfaces, for example, a bifunctional silane cross-liner is used to form a self assembled monolayer (SAM) which possesses one functional group that reacts with hydroxyl surface groups, and another free one that can either react wih primary amine groups of proteins or can be used to react with a liker molecule which is reactive towards primary amine groups of proteins. For example, there exist several methods to orient antibodies and their fragments on surfaces: antibodies contain a conserved glycosylation site on the Fc domain, and this can be oxidized and them biotynylated using biotin hydrazide. Alternatively, antibodies can be cleaved by pepsin into dimeric Fab' fragments (antigen-binding fragments of immunoglobulin G) which are linked together by disulfide bonds in the hinge region.

As regards detection methods, high-quality assay methods are required for translating specific biomolecular phenomena into observable and quantitative parameters. Typically, this is achieved through measurements of radioactivity, photon absorption, or photon emission. Although radioactive methods were successfully applied in High-throughput screening, they have become less popular primarily because of the handling radioactive materials and the availability of non-radioactive alternatives. Photon emission is by far the dominant assay methodology due to its broad adaptability to biological targets and automation methods, and its ability to deliver the speed, accuracy, and sensitivity necessary for successful High-Throughput Screening. Photon emission is achieved

primarily through fluorescence and chemiluminescence (which includes bioluminescence). Fluorescence detection methods are generally the most diffused methodology in research labs, because they are simple, safe, extremely sensitive and and can have very high resolution [20]. Although assays based on either fluorescence or chemiluminescence can yield high sample throughput, fluorescence has been used more commonly because of its broader familiarity and easier implementation into assay designs. The most used fluorescent dyes include Cy3 and Cy5, the same dyes that have found application in DNA arrays. However, the expensive instrumentations required for fluorescence methods, such as laser confocal microarray scanner have limited the wide applications of DNA and protein microarray technologies, especially in clinical diagnosis. Although both fluorescence and luminescence processes create photons through energy transitions from excited states to their corresponding ground states, they differ in how the excited states are generated. In fluorescence, the energy needed for producing excited states is gained through the absorption of light, whereas in chemiluminescence, the energy results from exothermic chemical reactions (see fig. 2.4). This
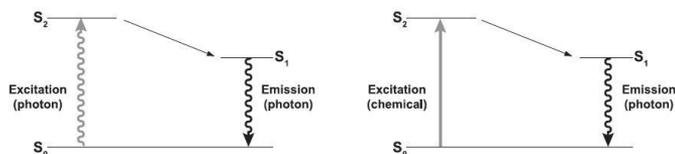

Figure 2.4: **Comparison of fluorescence (left) to luminescence (right). S_0, ground state; S_1, excited state after vibrational relaxation; S_2, excited state.**

difference fundamentally affects assay features and performance. Fluorescent assays tend to be much brighter since the photons generating the excited states can be introduced into a sample at a very high rate.

However, because of the high influx of photons, background is higher and then sensitivity is affected. Notably, in chemiluminescence light intensities are much lower because of the slower rate by which excited states can be created: then assay backgrounds are virtually absent since no photons need to be introduces into the samples. This feature leads to higher sensitivities in the screening assay. In cellular microscopy optics requirements - for resolving sub-cellular microstructures - impose limits in photon detection, with brightness becoming the dominant consideration for good performance. Consequently, fluorescence is preferred over chemiluminescence. In macroscopic samples like microwell plates, since more photons can be collected, the reduction in the background associated with the assay method becomes fundamental. For this reason, chemiluminescent assays often outperform analogous fluorescent assays. The low background inherent in chemiluminescence allows for a better signal to- noise ratio and thus better assay sensitivity [21]. The main obstacle to the use of chemiluminescence in HTS has been the lack of available assay methods. But, new capabilities in chemiluminescence, particularly in bioluminescence, are now changing this trend. Bioluminescence is a special form of chemiluminescence found in living organisms. As a class, it is characterized as being an enzyme-catalyzed process, where the high efficiency of photon emission is derived through natural evolution. The enzymes that catalyze this process are called luciferases, and the photon-emitting substrates are luciferins. Bioluminescent chemistries have evolved from multiple independent origins, and thus comprise many distinct molecular structures. Of the many natural forms, only three have been widely used in HTS: firefly luciferase, *Renilla* luciferase, and aequorin. Of these Firefly luciferase is the most

diffused in screening applications. Firefly (*Photinus pyralis*) luciferase is a monomeric enzyme of 61 kDa that requires no post-translational modifications for activity. It acts by first combining beetle luciferin with ATP, to form luciferyl-AMP as an enzyme-bound intermediate. This intermediate reacts with O_2 to create another bound intermediate, oxyluciferin, in a high-energy state. The subsequent energy transition to the ground state yields yellow-green light with a spectral maximum of 560 nm.

Together with fluorescence and chemiluminescence, colorimetric methods are a low-cost alternative detection way whose use is increasing. Colorimetric-based detection methods are attractive because the experimental setups are relatively low-cost and simple. Colorimetric detections can be carried out with inexpensive imaging equipment such as a CCD camera and a computer software for data analysis. While these aspects are beneficial because they drastically reduce the cost and procedural complexity of the experimental setup, colorimetric methods sometimes suffer from lower detection limits, respect to fluorescence methods. As a proof-of-principle experiment, Liang et al. [22] used a colorimetric nanogold probe coupled with silver enhancement to produce black image of microarray spots, which can be easily detected with a commercial CCD camera. Their studies reveal that for this method, the detection limit for protein immobilized on microarray slides (human immunoglobulin G, IgG) can be as low as 1 pg and for protein in aqueous solution (anti-human IgG, anti-IgG) 2.75 ng/ml, a detection sensitivity comparable to fluorescence methods. In another method paper, Jiang et al. [23] employed protein microarray methodology for the serodiagnosis of IgM antibodies directed against different TORCH pathogens. They

found out that while signal amplification of fluorescence-based detection was more sensitive, the immunogold-based microarray was simpler but having worse detection.

2.1.3 High-Throughput Screening by Chemical Microarrays

Chemical microarrays (also called small-molecule microarrays) are devices composed of different chemical compounds arrayed on a surface [24]. They are capable of evaluating the activity of a large number of chemical structures against hundreds of biological targets. The development of these devices has been a slow process. One of the major problems for their development is that compounds with different structures and properties are screened in a solution phase, and individual reactions need to be isolated in wells. When reactions are reduced to microarray size, no automatic liquid handling system can process these reactions individually, separately and sequentially if each reaction is still kept in a solution phase. Therefore, chemical microarray technology, which directly links chemicals to the chip surface, was introduced [25]. However, differently from DNA and protein microarray technologies, no general linking chemistry can be established to immobilize compounds having different structures and functional groups on the same chip surface. To avoid the potential complicated immobilization process, microarrays with dry compounds have been developed. This technology can deposit any chemical compound library on the same chip surface in a dry form. However, different compounds possessing different dissolution rates can create problems with reaction uniformity and endpoint data comparison. Given that there are more than 10^{40} potential low molec-

ular weight chemical compounds available in theory, one might imagine that many difficulties could be encountered with the approaches outlined above.

To avoid these problems, a new solution-phase chemical compound microarray was created in which each compound is individually arrayed on a glass surface - with a reaction buffer containing a low concentration of glycerol to prevent evaporation. Therefore, as in conventional well-based screening, the chemical compounds and biological targets are always in reaction solutions, which are activated with biological targets by delivering analytes using non contact deposition technology. With this approach all compounds and peptide libraries can be microarrayed, and activated by biological targets in the form of pure protein or cell lysate. By performing assays in solution, the enzyme reaction can be performed in a more native-like environment, and the proteins will retain their native structure and activity. This approach was firstly developed by Gosalia et al. [26] who arrayed chemical compounds inside nanoliter droplets of glycerol and by aerosol deposition, added reagents and water to assemble different multiple biochemical reactions without requiring chemical linkage of the protein to the surface. They were able to execute kinetic profiling of protease mixtures, protease-substrate interactions and high throughput reactions showing the suitability of the method by the identification of an inhibitor of caspases 2, 4 and 6. They also profiled [27] human blood serine proteases using a 722-member peptide library microarray of fluorogenic protease substrates with the general structure Ac-Ala-X-X-(Arg/Lys)-coumarin, identifying cooperative interactions between substrate sub-sites. Moreover, Mugherli et al. set-up a robust microarray platform in which multiple reactions are

conducted in piezo deposited nanoliter droplets maintained on a glass slide for the in situ preparation of derivatives of thousands of derivatives of phenylboronic acid and their successive activity screening on the NS3/4A protease of the hepatitis C virus [28] and, in another paper they were able to identificate new type of fluorescent pharmacophores by multicomponent reactions using combinatorial synthesis and screening of chemical libraries in droplet microarrays [29]. In particular, the assembly by a multicomponent reaction is a unique potential for synthesizing thousands of structurally different fluorescent molecules. Since they are based upon a druglike scaffold, these fluorophores maintain their molecular recognition potential and, thus their suitability as bioimaging probes.
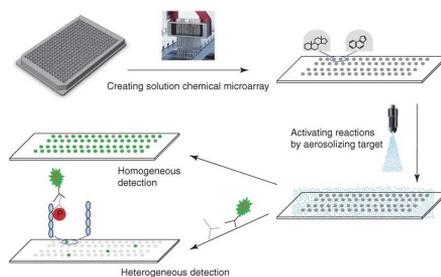
Figure 2.5: **Example of a solution-phase chemical microarray. Chemical compounds in assay buffer containing dimethyl sulfoxide (DMSO) and glycerol are arrayed on the surface of the microarray. In order to perform homgeneous reactions, biological target and substrate are added into each reaction dot by aerosol deposition technology. The reaction products are detected by a laser scanner or imager.**

2.2 Single cell arrays

2.2.1 Live cellular assays

Living cells are a remarkably complex system. To unravel this complexity, living-cell assays are being developed to allow delivery of experimental stimuli and measurement of the resulting cellular responses. High-throughput adaptations of these assays, known as living-cell microarrays, which are based on microtiter plates, high-density spotting, microfabrication, and microfluidics technologies, are being developed for two general applications: (a) to screen large-scale chemical and genomic libraries and (b) to systematically investigate the local cellular microenvironment. These emerging experimental platforms offer exciting opportunities to rapidly identify genetic determinants of disease, to discover modulators of cellular function, and to probe the complex and dynamic relationships between cells and their local environment [30].

Living-cell assays can be divided into three parts: (a) the inputs, (b) the outputs, and (c) the cells under investigation, as illustrated in Fig. 2.6. High-throughput cell assay platforms are designed to systematically vary one or more of these components between elements of the array while holding the remaining assay variables constant.
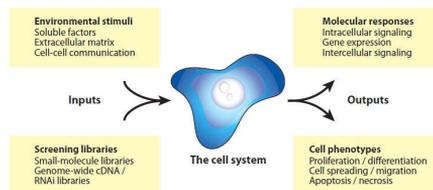

Figure 2.6: **Attributes of a cell assay.**

The inputs of a cell assay span all aspects of the cellular micro envi-

ronmentsoluble, insoluble, and cellular. Soluble inputs consist of standardized culture medium, metabolic substrates, and other unspecified additives derived from animal serum. Another important group of assay inputs are insoluble factors, such as extracellular matrix (ECM). The ECM provides mechanical and biochemical cues that modulate the shape, migration patterns, and overall phenotype of associated cells [31].

Cell responses can be measured and quantified in many ways. Western blotting or enzyme-linked immunosorbant assays (ELISAs) can be employed for monitoring with molecular specificity in microtiter plates using bulk fluorescence, luminescence, or absorbance as a readout. Alternatively, microscopy can be used to gain spatial resolution either at fixed time points using fixed and stained cells or by real-time monitoring dynamic responses of living cells in order to quantify and analyse morphological features to study phenotypes such as proliferation, migration, or differentiation. The development of live-cell imaging tools, such as the genetically encoded green fluorescent protein (GFP) and its variants, represented a major advance in the ability to study intracellular molecular events across space and time [32].

Conventional cell assays measure average responses of large cell populations: an implicit assumption of this approach is that the average response is representative of a typical cell within the population. In many cases, however, this is an oversimplification. One of the most striking examples is encountered when examining cells that exhibit all-or-none responses [33]. Since activation occurs in a stochastic way, such cells become activated asynchronously, and the average population response increases gradually, whereas at the single-cell level, responses are abrupt but exhibit a distribution of activation times. Notably, by ex-

amining the distribution of single cells midway through the response, no individual cell will exhibit the response level predicted by the average population. Instead, there will be only fully activated and non-activated cells [34]. Accurately characterizing single-cell responses as a function of space and time can play an important role in understanding the variations and emergent properties of cell populations: in this sense, efforts to profile cell responses at the single cell level are growing increasingly common [35].

2.2.2   Microtiter plate technologies

The standard for high-throughput living-cell assays consists in the microtiter plate (96-, 384- and 1536-well format), a miniaturized version of a conventional tissue culture dish. Advanced laboratory automation equipments, including plate-handling robotics, high-precision fluid dispensers, nanoliter-scale transfer pipettes, multiwell plate scanners, and automated microscopes have been developed and optimized [36]. Automated liquid dispensers dispense cells from suspension into the wells of a microtiter plate. They attach and spread, and nanoliter volumes of experimental compounds are transferred from wells of the library storage plate into the cell-seeded wells of microtiter plates: cells are then incubated with the compounds for a specified duration, and the experiment is quantified using either a fluorescence or luminescence plate reader or using high-throughput microscopy with image-based quantification. The repeatability of the assay can be parametrized by the Z factors, a quality measure for an assay, defined in [37]. However, although microtiter plate technologies represent the standard for high-throughput screening, they also place several limitations on the attributes of a living-cell as-

say that can be controlled. For example, time-varying stimuli, such as transient chemical exposures used in pulse-chase experiments, are difficult to control because they require complete removal of the soluble stimulus, followed by multiple washing steps. Similarly, it is difficult to deliver spatially heterogeneous stimuli, such as gradients of chemotactic factors, and to control the delivery of one stimulus with respect to another in time or space. Microtiter plate experiments are also not well suited for studying phenomena that occur on short time-scales because stimulation and measurement are performed using different equipment. These limitations, combined with the need for additional scaling, have motivated the development of several next-generation living-cell arrays.

2.2.3 High-density spotting technology

In an effort to improve upon the miniaturization and parallelization provided by multiwell plates, researchers took inspiration from printing strategies used to create DNA and protein microarrays and applied them to living-cell assays. This platform, which is illustrated was termed cell microarrays [38]. This technology has been extensively reviewed [39, 40] involving culturing cells in confluent monolayers over high-density arrays of nanoliter droplets preprinted on glass slides. Compared with microtiter plates, the approach offers reduced assay volume, increased assay density and throughput, compatibility with long-term storage, and eliminates the need for high-throughput fluid transfer equipment once the spotted array is created. Applications of these technologies are the Cell Genomic Microarrays [41] - devices that permit to miniaturize and parallelize genome wide gain- and loss-of-function studies on living cells-; Small Molecule Microarrays - for screening small molecule activity on

single cells - and Microenvironment Arrays - platforms in which elements of the extracellular matrix are printed beneath single cells.

The cellular micro-environment consists of a strikingly diverse collection of soluble factors, extracellular matrix cues, and cellular networks [42]. These have proven difficult to experimentally control using conventional techniques, in large part due to the wide range of length- and timescales involved. In this sense, micro- and nano- fabrication, technology originally developed for integrated circuits fabrication, offers precise reproducible spatial control and can be adapted to achieve temporal control as well.

The most commonly used method for constructing microfabricated cell-based devices is soft lithography (for details consider reference [43]). Microwell geometries have been optimized for single cells, allowing large numbers of individual cells to be stimulated in a massively parallel fashion [44]. Recently, a new approach has been shown by Liberski et al. [45] who prepare arrays of sessile droplets of living single cell cultures using a liquid hydrophobic barrier to prevent the samples from dehydrating thus allowing for statistical quantitative single cell studies in spatially addressable arrays. With the careful advancing of a thin layer of mineral oil on the substrate over the droplets during the printing, dehydration of the droplets can be prevented, and the vitality of the cells can be retained. Another approach is the combination of microfabrication with surface-modification strategies to indirectly pattern cells by controlling the spatial localization of biochemical cues that affect the adherence of cells. Microstructured films are coated with biomolecules and used to stamp or transfer them to the culture surface wherever raised microscale features are present. Wheter the printed molecules are more

adhesive - like for instance fibronectin or collagen -, or less adhesive - as for example polyethylene glycol or albumin -, than the surrounding culture substrate, the cells will preferentially localize onto or avoid the stamped regions, respectively. The transfer of molecules to the surface can be achieved by physical absorption, but more commonly, covalent bonding strategies based on self-assembled monolayer methodologies to achieve high-density surface modification [46]. Recently, R.A. Desai and coworkers showed a clever microcontact printing-based strategy namely, stamp-off printing - to pattern multiples extracellular matrix proteins that bind distinct integrins in order to study how multiple types of integrins might interact in a spatially confined manner [47]. In their approach, proteins are firstly adsorbed to a PDMS stamp and the selectively de-inked. By employing this approach, it is possible to overcome typical issues of microcontact printing as pattern fouling associated with stamp collapse and limited biological functionality of the surface patterns. The approach is shown in Fig. 2.7. A plane PDMS stamp is first inked with a protein solution. In parallel, a PDMS template is cast against a master (prepared by photolithography) to create features in relief and is cleaned and activated by ultraviolet ozone (A2). The inked stamp is then rinsed, dried, and placed in contact with the template, so transferring protein from the stamp to the template at the points of contact. Then, the stamp surface (initially featureless) can print a pattern corresponding to the features of the template (A3). Finally, the pattern is transferred to a substrate, as in normal microcontact printing (A4). Interestingly, although different types of integrins can segregate to their corresponding ECM spots, they show that cells were able to coordinate a simultaneous engagement of $\alpha v \beta 5$ and $\beta 1$-based integrins for

the cooperative assembly of focal adhesions (signal of cell adhesion and migration) shown by the co-localization of $\alpha v \beta 5$ integrin to vitronectin and $\beta 1$ integrin to collage type I.
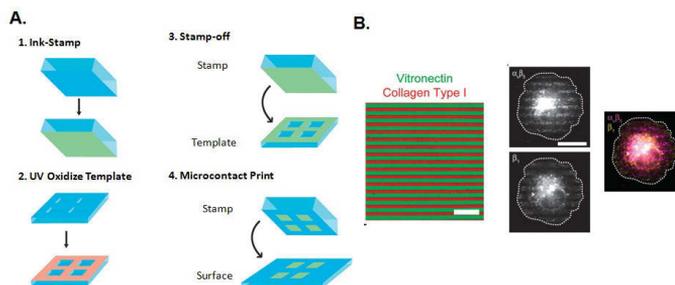

Figure 2.7: **(A.) Scheme of the stamp-off process: see text for details. (B.) Endothelial cells seeded on patterned substrates. Scale bars are 20 μm. Pictures adapted from [47].**

References

[1] Resnick R.; Halliday D. and Krane K.S., *Overview of Microarrays in Drug Discovery and Development, Current Protocols in Pharmacology* (John Wiley & Sons, Inc., Hoboken, New Jersey, 2003).

[2] Hughes J.P.; Rees S.; Kalindjian S.B. and Philpott K.L., *Brit. Journ. of Pharmacol.* **162**, 1239 (2011).

[3] D.A. Pereira and J.A. Williams, *British Journ. of Pharmacol.* **152**, 53 (2007).

[4] Hong J.; Edel J.B.; deMello A.J., *DDT* **14**, 134 (2009).

[5] Fernandes T.G; Diogo M.M.; Clark D.S.; Dordick J.S. and Cabra J.M.S., *Trends in Biotechnol.* **27**, 342 (2009).

[6] Keith C. T.; Borisy A. A. and Stockwell B. R., *Nat. Rev. Drug Discov.* **4**, 71 (2005).

[7] Yang Y.; Adelstein S.J. and Kassis A.I., *DDT* **14**, 147 (2009).

[8] Bertram L.; Tanzi R.E., *Biochem. Pharmacol.* **69**, 1133 (2005).

[9] Zheng C.; Han L.; Yap C.W.; Xie B.; Chen Y., *DDT* **11**, 412 (2006).

[10] Rask-Andersen M.; Almen M.S.; and Schioth H.B., *Nat. Rev. Drug Discov.* **10**, 579 (2011).

[11] F. Zhu; Z. Shi; C. Qin; L. Tao; X. Liu; F. Xu; L. Zhang; Y. Song; X. Liu; J. Zhang; B. Han; P. Zhang and Y. Chen, *NAR* **39**, 1 (2011).

[12] F. Zhu; Z. Shi; C. Qin; L. Tao; X. Liu; F. Xu; L. Zhang; Y. Song; X. Liu; J. Zhang; B. Han; P. Zhang and Y. Chen, *Curr .Opin. Chem. Biol.* **10**, 294 (2006).

[13] van der Greef J.; McBurney R.N., *Nat.Rev.Drug Discov.* **4**, 961 (2005).

[14] Hultschig C.; Kreutzberger J.; Seitz H.; Konthur Z.; Büssow K.; Lehrach H., *Curr. Opin. Chem. Biol.* **10**, 4 (2006).

[15] Nielsen U.B.; Cardone M.H.; Sinskey A.J.; MacBeath G.; Sorger P.K., *PNAS* **100**, 9330 (2003).

[16] Gulmann C.; Sheehan K.M.; Kay E.W.; Liotta L.A.; Petricoin E.F., *J. Pathol.* **208**, 595 (2006).

[17] Hall D.A.; Ptacek J.; and Snyder M., *Mech. Ageing Dev.* **128**, 161 (2007).

[18] Schröder H.; Niemeyer C.M. Jonkheijm P.; Weinrich D.; and Waldmann H., *Angew. Chem. Int. Ed.* **47**, 9618 (2008).

[19] Huang J.; Zhu H.; Haggarty S.J.; Spring D.R.; Hwang H.; Jin F.; Snyder M.; and Schreiber S.L., *PNAS* **101**, 16594 (2004).

[20] Zhu H. and Snyder M., *Curr. Opinion in Chem. Biol.* **7**, 55 (2003).

[21] Cali J.J.; Niles A.; Valley M.P.; O' Brien M.A.; Riss T.L. and Shultz J., *ASSAY and Drug Development Technologies* **5**, 127 (2007).

[22] Liang R.Q.; Tan C.Y.; Ruan K.C., *Journ. of Immunol. Methods* **285**, 157 (2004).

[23] Jiang L.; Yu Z.; Du W.; Tang Z.; Jiang T.; Zhang C.; Lu Z., *Biosens. Bioelectron.* **24**, 376 (2008).

[24] Hong J.; Edel J.B.; deMello A.J., *DDT* **11**, 661 (2006).

[25] Gosalia D.N.; Diamond S.L., *PNAS* **100**, 8721 (2003).

[26] Gosalia D.N.; Diamond S.L., *PNAS* **100**, 8721 (2008).

[27] Gosalia D.N.;., Salisbury C.M.;, Maly D.J.;, Ellman J.A., and Diamond S.L., *PROTEOMICS* **5**, 1292 (2005).

[28] Mugherli L.; Burchak O.N.; Balakireva L.A.; Thomas A.; Chatelain F.; Balakirev M.Y., *Angew. Chem. Int. Ed.* **48**, 7639 (2009).

[29] Mugherli L.; Burchak O.N.; Balakireva L.A.; Thomas A.; Chatelain F.; Balakirev M.Y., *J. Am. Chem. Soc.* **133**, 10058 (2011).

[30] Yarmush M.L. and King K.R., *Annu. Rev. Biomed. Eng.* **11**, 235 (2009).

[31] Yarmush M.L. and King K.R., *Int. J. Dev. Biol.* **50**, 255 (2006).

[32] Wang Y.; Shyy J.Y.; Chien S., *Annu. Rev. Biomed. Eng.* **10**, 1 (2008).

[33] Bastiaens P., *Nature* **459**, 334 (2009).

[34] Di Carlo D.; Lee L.P., *Anal. Chem.* **78**, 7918 (2006).

[35] Loo L.H.; Wu L.F.; Altschuler S.J., *Nat. Methods* **4**, 445 (2007).

[36] Blow N., *Nat. Methods* **5**, 109 (2008).

[37] Zhang J.H.; Chung T.D.; Oldenburg K.R., *J. Biomol. Screen.* **4**, 67 (1999).

[38] Ziauddin J.; Sabatini D.M., *Nature* **411**, 107 (2001).

[39] Angres B., *Expert Rev. Mol. Diagn.* **5**, 769 (2005).

[40] Wheeler D.B.; Carpenter A.E.; Sabatini D.M., *Nat. Genet.* **37**, S25 (2005).

[41] Carpenter A.E.; Sabatini D.M., *Nat. Rev. Genet.* **5**, 11 (2004).

[42] Scadden D.T., *Nature* **441**, 1075 (2006).

[43] Xia Y.; Whitesides G.M., *Angew. Chem. Int. Ed. Engl.* **37**, 550 (1998).

[44] Rettig J.R.; Folch A., *Anal. Chem.* **77**, 5628 (2005).

[45] Liberski A.R.; Delaney J.T. and Schubert U.S., *ACS Comb. Sci.* **13**, 190 (2011).

[46] Folch A.; Toner M., *Annu. Rev. Biomed. Eng.* **2**, 227 (2000).

[47] Desai R.A.; Khan M.K.; Gopal S.B. and Chen C.S., *Integr. Biol.* **3**, 560 (2011).

Part II

Experimental Part

3

Enzymatic arrays by Inkjet printing

This chapter reports on the employment of Ink-jet printing as of a general methodology for drug screening purposes. In the field of drug screening ultra-rapid and low-cost high-throughput screening devices are needed for the discovery of suitable drug molecules by screening entire chemical libraries against hundreds of biological targets. In this chapter we show a microarray-based ink-jet printing realized drug screening platform featured with a low-cost, simple and easy-to-generalize optical red-out. We show the working principle of this approach on a model enzyme/substrate couple (Glucose Oxidase/D-glucose) showing enzymatic competitive inhibition by its known inhibitor compound (D-glucal). Finally we envisage the extension of the presented methodology to systems like Cytochrome CYP3A4 which are of clear interest for medicinal chemistry being one of the most important enzymes for Phase I drug metabolism.

Glossary and list of acronyms:

Luciferins: Class of small-molecule substrates that are oxidized in the presence of the enzyme Luciferase to produce oxyluciferin and energy in the form of light.

Luciferase: Generic term for the class of oxidative enzymes used in bioluminescence. One famous example is the firefly Luciferase from the firefly *Photinus pyralis*.

CYP3A4: Acronym for Cytochrome P450 3A4, a member of the cytochrome P450 mixed-function oxidase system, one of the most important enzymes involved in the xenobiotics metabolism in the body.

GOx: Acronym for Glucose Oxidase (GOx), an oxido-reductase enzyme which catalyzes the oxidation of glucose to hydrogen peroxide and D-glucono-δ-lactone.

CCD-camera: Acronym for charge-coupled device, an instrument for the movement of electrical charge, usually from within the device to an area where the charge can be manipulated, for example conversion into a digital value.

Drug-Drug-Interactions:

3.1 Glucose Oxidase Screening Microarrays

Glucose Oxidase covalent immobilization and surface characterization

Glucose Oxidase (GOx) is a homodimeric enzyme [1] which catalyses the oxidation of β-D-glucose by molecular oxygen to δ-gluconolactone and hydrogen peroxide. In this work, GOx was dissolved in phosphate buffer (PBS; Na_2HPO_4 + NaH_2PO_4; 0.1 M; pH 6.5) in order to prepare a 1 mg/ml solution.

GOx was covalently liked to modified Silicon Dioxide (SiO_2) surfaces thermally grown on Si by an oxidation process at $950\,^{\circ}C$ for 30 min in O_2 ambient conditions. The reagents employed in the experiments were: 3-Aminopropyl triethoxysilane (APTES), glutharaldeyde

Figure 3.1: **Biological assembly of Glucose Oxidase assigned by authors in [1].**

(GA) solution (grade II), glucose oxidase (GOx, type X-S, Aspergillus niger), disodium hydrogen phosphate anhydrous (Na_2HPO_4), sodium dihydrogen phosphate (NaH_2PO_4), D-glucal (96%) and glycerol. They were all purchased from Sigma Chemical Co.
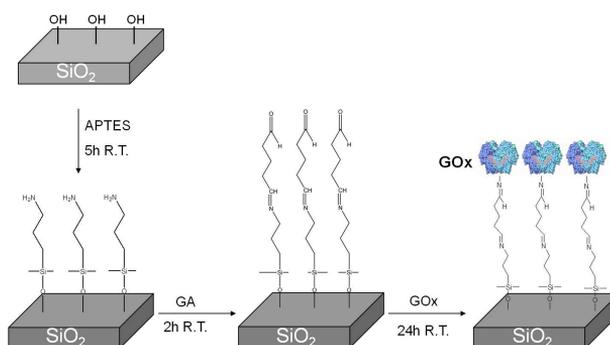

Figure 3.2: **Protocol for the covalent immobilization of Glucose Oxidase on Silicon Dioxide surfaces.**

Silicon oxide substrates and functionalized silicon oxide-based substrates (SiO_2/APTES/GA) were employed for the experiments. The latter were prepared with an immobilization procedure which involved:

- Oxygen plasma treatment: 10 min 75 W 1 mbar (March Barrel Plasmod)

- APTES silanization: 5 hours soaking in APTES solution (10% in ethanol) at room temperature and following heating (1 hour 100 °C under N$_2$ flux)

- GA derivatization: solution (2.5% in PBS) 2h at room temperature (the sample up to this functionalization step is called UP TO GA).

Finally the functionalised substrates were immersed in a GOx solution in PBS (2 mg/ml pH 6.5) overnight at room temperature. They were rinsed and dried under a gentle nitrogen flow before the prints. The above explained procedure showed to permit to obtain a functional enzyme monolayer with significant biological activity. In figure 3.2 a scheme for the immobilization protocol is given. GOx is a homodimeric glycoprotein of molecular weight 160 kDa, with one tightly but noncovalently bound flavin adenine dinucleotide (FAD) cofactor per monomer. It is is a flavin-dependent enzyme which catalyses the oxidation of β-D-glucose by molecular oxygen to δ-gluconolactone and hydrogen peroxide. The action mechanism is described as ping pong with two different enzymatic states: the oxidized (having oxidized FAD cofactor) and the reduced state (having reduced FAD). The mechanism is made up of two semi-reactions: the oxidative semireaction of glucose and the reductive semi-reaction of molecular oxygen. The reductive semi-reaction with β-D-glucose takes place by proton abstraction from OH-1 glucose group to a imidazolic nitrogen of a His residue (His559 or His516) and the following direct hydride transfer from the C-1 carbon atom of the sugar to N-5 atom of the FAD molecule. In the oxidative semireaction, $FADH^-$ is reoxidized to FAD by molecular oxygen that reduces to hydrogen per-

oxide. The enzyme is highly specific for β-D-glucose, but a few other monosaccharides, e.g., 2-deoxy-D-glucose, D-mannose, and D-galactose, exhibit low activity as substrates [2].

Surface characterization was conducted by employing XPS, AFM and contact angle measurements. XPS analyses were carried out using a Kratos AXIS-HS spectrometer. The Mg $K\alpha_{1,2}$ of 1253,6 eV was used at the conditions of 10 mA and 15 keV with a pass energy of 40 eV. During the analysis the residual pressure in the chamber was on the order of 10^{-7} Pa. AFM measurements were conducted in air using a Multimode/Nanoscope IIIa, Digital Instruments, equipped with a phase extender. Etched-silicon probes with a pyramidal shaped tip having a nominal curvature of 10 nm and a nominal internal angle of $35\,^{\circ}$ were used. During scanning, the 125 μm long cantilever, with a nominal spring constant in the range 20- 100 N/m, oscillated at its resonance frequency (330 kHz). To control and enhance the range of the attractive forces interaction regime, the instrument was equipped with an additional feedback circuit, called Q-control [3].

GOx enzymatic assay

The enzymatic activity of Glucose oxidase was monitored by using the enzymatic kit K-GLOX 01/05 (Megazyme, Ireland). The assay consists in a procedure exploiting the quantitative formation of a red quinoneimine dye, namely, 1,5-dimethyl-4-(4-oxo-cyclohexa-2,5-dienyldeneamino)-2-phenyl-1,2-dihydro-pyrazol-3-one (see fig. 3.3). By such method, hydrogen peroxide is produced as a result of the GOx catalyzed oxidation of β-D-glucose. Hydrogen peroxide then reacts with p-hydroxybenzoic acid and 4-aminoantipyrine in a reaction catalysed
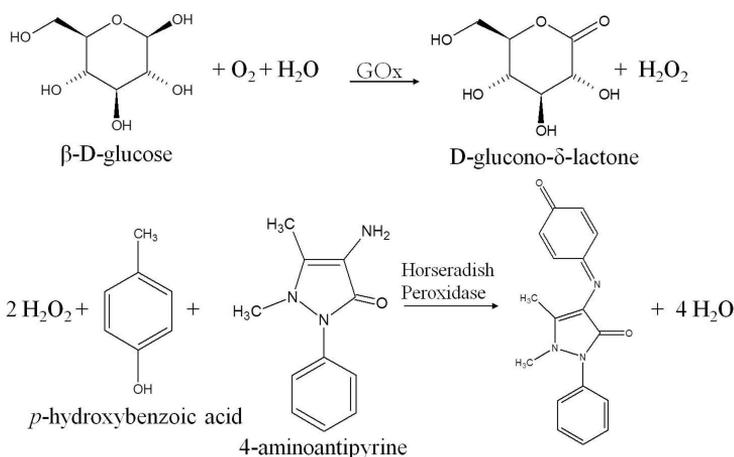
Figure 3.3: **Scheme of the colorimetric method for detecting Glucose Oxidase enzymatic activity on Silicon Dioxide surfaces.**

by a peroxidase enzyme to form the dye complex.

3.1.1 Molecular ink-jet dispensing

The biological inks used in this work consisted of β-D-Glucose and/or D-glucal (1,5-Anhydro-2-deoxy-D-arabino-hex-1-enitol) solubilized in the above described kit solution. β-D-Glucose concentration was mantained constant (0.071 M), while D-glucal concentrations was varied in a ratio ranging from 1:3 to 1:7. Inks containing only β-D-Glucose or D-glucal were printed too. All the biological printed inks contained glycerol at 30% v/v. Glycerol is suitable for the achievement of high quality printed biological drops, due to its effects on the physical-chemical properties (such as viscosity and surface tension) of the printed patterns.

The bioink drops were dispensed on GOx functionalised silicon dioxide substrates using a Dimatix Materials Printer (DMP-2800, Fujifilm). This instrument was equipped with user fillable piezo-driven inkjet print

cartridges, each with 16 nozzles 254 μm spaced and 21.5 μ m in diameter. In addition, by using an integrated heater within the cartridge allowed for temperature control in order to maintain it at 30 °C during dispensing.

Optical images of the patterns were obtained by a Nikon Eclipse ME600 Microscope and managed by employing the software Lucia G on Mutech v 4.60 (Nikon, Italy).

Due to the GOx catalyzed oxidation of β-D-glucose, the above considered red quinoneimine dye complex was formed. In order to measure the enzymatic activity per each spot, the medium intensity of red color per each spot was measured by determining the medium number of red color pixels inside it. For this reason, using software provided Trace Histogram tool, a rectangle region around each spot was defined such that the size of the net background was similar to or slightly larger than the signal area. This was obtained by taking a rectangle that exactly circumscribed the spot. A double peak distribution was obtained: an histogram is associated to the spot signal (foreground signal or F) while the other histogram is due to the immediately surrounding background signal (B). The signal due to the background was subtracted from the foreground to get a normalized signal: only by normalizing the signal it was possible to compare data from different microarrays.

3.2 Cythorocrome CYP3A4 Microarrays

In order to extend the method above reported to a biological meaningful target enzyme, we showed the suitability of the approach by employing human Cytochrome P450 3A4. Cytochrome P450 3A4 (abbreviated CYP3A4) is a 56 kDa membrane-associated protein, fundamental

member of the cytochrome P450 mixed-function oxidase enzymatic system. It is able to metabolize a wide range of endogenous compounds and xenobiotics, such as pollutants, environmental compounds, and drug molecules. CYP3A4 is involved in the oxidation of the largest range of substrates of all the CYPs. In humans, the CYP3A4 protein is encoded by the CYP3A4 gene which is part of a cluster of cytochrome P450 genes on chromosome 7q21.1. Cytochrome P450 3A4 (CYP3A4) metabolizes more drug molecules than all other isoforms combined [4, 5]. It is the most important enzyme for Phase I drug metabolism this meaning that almost every new drug is involved in interactions with CYP3A4 [1].

Figure 3.4: **Biological assembly assigned by authors [4] and generated by PQS software. The structure of CYP3A4 exhibits a relatively large substrate-binding cavity that is consistent with the various sizes of substrates that are oxidized by the enzyme.**

---

[1]The microsomal, membrane-associated, P450 isoforms CYP3A4, CYP2D6, CYP2C9, CYP2C19, CYP2E1, and CYP1A2 are responsible for the oxidative metabolism of more than 90% of marketed drugs.

Cytochrome P450 CYP3A4 droplet microarray realization

CYP3A4 enzyme was purchased from PROMEGA as Screening System containing the Luciferin Detection Reagent (i.e. Luciferase enzyme, Luciferin-IPA, namely 2-(4-(diisopropoxymethyl) - 4,5 - dihydrothiazol-2-yl) benzo[d]thiazol -6-olOMP and Luciferase Buffer with Esterase), CYP3A4 (1pmol/μL) + P450 Reductase, Cytochrome b5, NADPH Regeneration System consisting in Solution A having NADP$^+$ and glucose-6-phosphate (G6P) supplied as a 20X concentrate and Solution B containing glucose-6-phosphate dehydrogenase (G6PDH) at a 100X concentration. Potassium Salt D-luciferin, namely potassium (4S)-2-(6-hydroxy-1,3-benzothiazol-2-yl) -4,5-dihydrothiazole -4-carboxylate, was purchased at PROMEGA too. MTMOS (methyltrimethoxysilane), glycerol and erythromicin were purchased at Sigma Aldrich. Droplets of different chemical composition all contained glycerol at 30% v/v in order to achieve high definition spots and to alleviate evaporation problems. Spots were sequentially ink-jet printed on surface modified silicon surfaces according to the below explained protocol. Thermal silicon dioxide substrates (80 nm thermal oxide thickness) were washed with millipore water thoroughly. Subsequently, oxygen plasma cleaning was carried out (1 mbar 75 W, 10', March Barrel Plasmod) and finally MTMOS (Methyltrimethoxysilane) was spincoated (30 μL, 1000 RPM, 30", TP 6000 Dispense and Spinning System, Sulzer Electro Technique) in order to slightly increase surface hydrophobicity (measured water contact angle was 23-25 degrees) and also for facilitating the easy attachment of individual microarray spots and preventing local spreading and merging of printed spots [6]. Moreover, it is known that CYP activity may be inhibited nonspecifically by binding of CYP membranes and/or substrates

to a surface that has been treated for enhanced hydrophobicity. Accordingly, the slight hydrophobicity of such prepared surfaces doesn't affect enzymatic activity (as shown by Sukumaran et al. [7]). Before use, the MTMOS-coated slides were stored in the dark at $-20\,^{\circ}$C. The sequential ink-jet process was carried out according the assay-in-micro-droplets approach: this approach consists in the execution of enzymatic reaction in liquid phase [7] without the need of covalent binding of the enzyme on the surface. Droplets of different biological materials were printed according the following sequential order:

- PBS buffer (0.7 M - pH 7.4)

- Test inhibitor (concentration between 10 μM- 1 μmM),

- CYP3A4 (2 nM) + Luciferin-IPA (3 μM)

- Regeneration System (NADP^{+}, G6P, G6PDH)

- Luciferase Detection Reagent

In between each new biomolecular printing step, since a different cartridge is required for each dispensed biomaterial, MEMS Alignment procedure was executed in order to address droplets on spots printed in the previous printing steps with a positional repeatability of 25 μm. After the printing of the CYP3A4 enzyme, incubation between the enzyme and inhibitor occurred together with substrate Luciferin-IPA for at least 10 minutes. Then enzymatic reaction started by adding Regeneration System: the reaction occurred at room temperature for 15 minutes. Finally, spots were addressed with Luciferase Detection Reagent in order to start the Luminescent Reaction. After 10 minutes of incubation, bright field images were captured with a SONY Exwave HAD Color

Video Camera Digital mounted on a Nikon Eclipse ME600 optical microscope. The acquisition time for all the images was set-up as 40 ms.
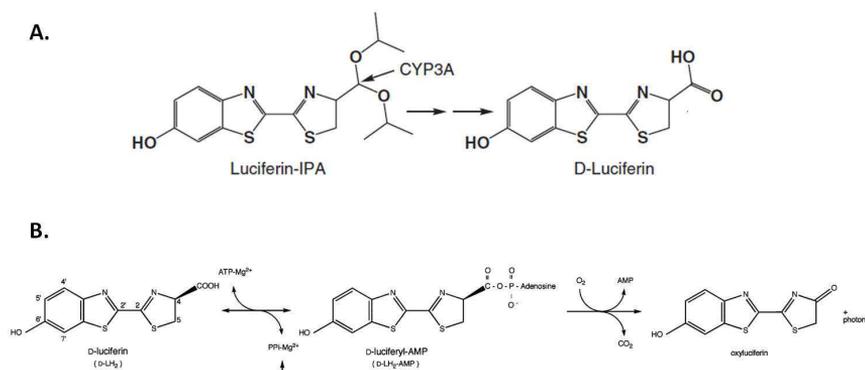

Figure 3.5: **Luminescent cytochrome P450 assay by employing Luciferase enzyme. (A.) Luciferin-Isopropylacetal, namely 2-(4-(diisopropoxymethyl)-4,5-dihydrothiazol-2-yl)benzo[*d*]thiazol-6-olOMP, is a substrate for CYP3A4 enzyme: the product of the reaction is D-Luciferin [8]. (B.) In presence of ATP-Mg^{2+}, D-luciferin products light upon reaction with oxygen in a reaction catalyzed by Luciferase enzyme [9].**

3.3   GOx screening arrays by Inkjet printing

The experimental procedure used for the screening methodology is here briefly reported. Picoliter volume drops containing tens of picograms of molecules (either D-glucose or a mixture of D-glucose/D-glucal) are ink-jet printed on a glucose oxidase monolayer immobilized on a silicon oxide surface. Upon hitting the solid surface, the dispensed drops form regular rounded spots. A colorimetric detection based on the horseradish peroxidase method probes the interaction between the dispensed molecule and the enzymatic target at the single spot: accordingly, whenever the enzymatic reaction occurs, the red dye complex forms. The more the spot is colored, the higher becomes the grayscale optical contrast of the spot with respect to the background. We finally verified that the solid-supported enzymatic surface can be reused for this screening purposes several times by simply rinsing with water. Moreover, the enzymatic activity of the array was only partially affected by aging in air for three months at room temperature.

3.3.1   Substrate characterization

The characterization of glucose oxidase (GOx) immobilization procedure on silicon dioxide surfaces was carried out by employing techniques like X-Ray photoelectrons spectroscopy (XPS) and Atomic Force Microscopy (AFM).

XPS

XPS measurements were conducted on UP TO GA and full process samples.
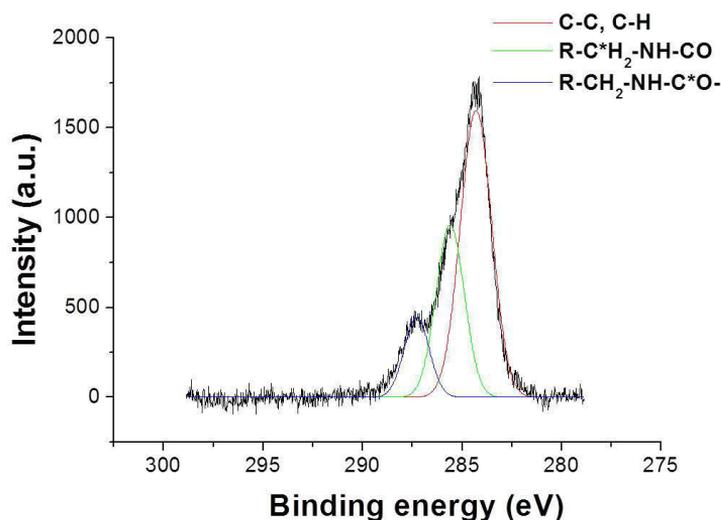
Figure 3.6: **C_{1s} XPS spectra of Glucose Oxidase monolayer chemisorbed on Silicon Dioxide surfaces.**

The X-ray photoelectron spectroscopy confirms that Glucose Oxidase is covalently bounded to the silicon dioxide surface. In particular, the N1s signal, centered at about 400 eV was detected in the full processed sample and was barely visible (only 0,4%) in the UP TO GA sample. This is due to the fact that GA doesn't have N as component and that GA may form an uniform layer on APTES, almost completely shielding its N signal. The C1s peak, centered at 285 eV (see fig. 2.6), is easily detectable in the full process sample and it is due to the enzyme deposition on its surface. The C1s peak shows at least three components. The first at 285,0 eV is assigned to C-C and C-H groups, the second at 286.3 eV is assigned to $R - CH_2^* - NH - (CO)-$ and the third at 288.1 eV is assigned to $R - CH_2 - NH - (C^*O)-$ chemical groups respectively. These groups are all typical of protein molecules,
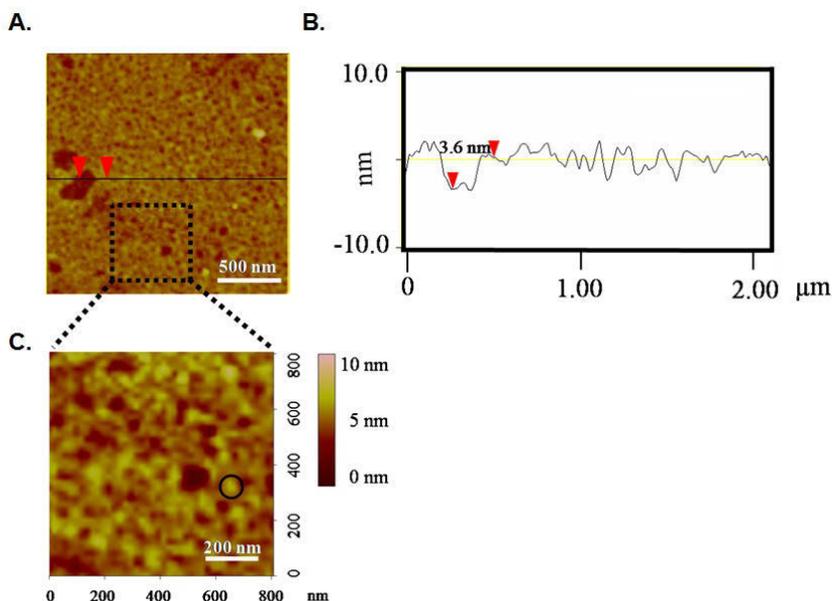
Figure 3.7: **Atomic Force Microscopy investigation of the GOx monolayer chemisorbed on Silicon Dioxide Surfaces. In (A.) height image on a region with some enzyme vacant zones, that has been chosen just to measure the surface thickness by section analysis; in (B.) section analysis along the line marked in (A.) figure; in (C.) zoom of a restricted region (800 nm scan size) showing single proteins along with high-protein packing (see the one by the circle).**

as expected if the enzyme is present at the surface. The UP TO GA sample exhibited only the C-C, C-H related peak at 284.8 eV. Due to sensitivity reasons of the XPS technique, phosphorous of the FAD group and sulfur in the protein were not detected.

AFM

The AFM section analysis in Fig. 3.7 shows that the height of the protein layer resembles the diameter of an individual GOx molecule (3.6 nm). This indicates that the system consists of a compact pro-

tein monolayer covalently liked to the silicon dioxide surface. The zoom
of the image permits to visualize individual protein molecules as single
round features at the surface. The shape of the features is approxima-
tively round: this can be explained being GOx a globular protein [10].
We also evaluated a protein surface coverage of about 90% as measured
on different sample regions on the GOx chemisorbed monolayer.

RMS roughness value for the full process sample is 0.87 nm for a 1 μm
scan size image. This value is higher than the one obtained by Libertino
et al. [10] (0.59 nm). However the authors employed a different silicon
dioxide activation and a different silanization procedure.

Contact angle measurements gave important information about func-
tionalization steps for the achievement of the GOx monolayer covered
surfaces. UP TO GA samples gave contact angle values approaching
50 degrees (49.6 ± 0.6). These values are in agreement with GA self-
assembled monolayer surfaces prepared in our previous work, in which
functionalized SiO_2 surfaces were obtained according to the Libertino et
al. [11] method in which APTES silanization was conducted by vapour
deposition. Full process samples (i.e. GOx functionalized) contact an-
gles were approaching 57 degrees (56.4 ± 2.4). This higher value is
reasonable because globular protein molecules are hydrophobic systems
and so their self assembled monolayers make surfaces more hydrophobic
than UP TO GA surfaces, so determining a higher contact angle value.

3.3.2 Printing conditions

The first goal of the experiments is the optimization of the printing
conditions. This was achieved by considering the experimental features

for setting up the experiments (waveforms, jetting voltage effects, drop shapes). In a work we published on Langmuir [12], it was shown that jetting voltage has dramatic effects on the drop formation since it affects its own dimensions, the droplet average speed after the pinch-off from the nozzle exit and the speed at which it impacts on the surface. We also found out that the addition of glycerol to the molecular ink allows for the achievement of high spot definition and resolution (tens of micrometers wide; one molecule tall), but in spite of its well-known structural stabilizing properties, in dynamic conditions it may lead to increased protein stresses. By realizing printing without glycerol, spots showed no regular shape and dimension along with spot misalignment and numerous spread small features, probably due to the formation of satellites during the droplet ejection. On the other side, by adding glycerol at concentrations higher than 30 %, it was possible to achieve good spot morphology and alignment (see Fig. 3.8). Glycerol helps in raising viscosity in order to a higher stability in the liquid column ejected from the nozzle that typically contracts into a single drop without significantly breaking it up.
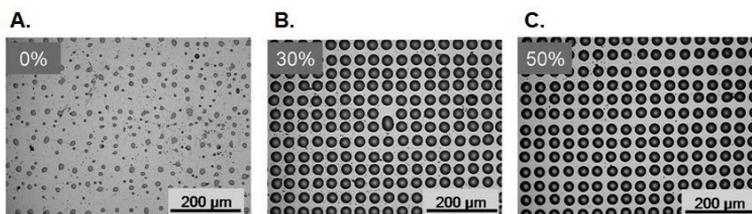

Figure 3.8: **Microarrays with 40 μm spot spacing obtained by ink-jet printing GOx solutions at different glycerol concentrations: (A.) 0% glycerol, (A.) 30% glycerol, (C.) 50% glycerol. Picture reproduced from [12].**

In all the experiments, the same pulse length (11,52 μs) was em-

ployed because this pulse length gave the possibility to get a quite speed ejected drop at low jetting voltages; while if the longer pulse waveform (23,04 μs) was employed a higher voltage (with consequent higher related compressive stress) would have been required to have the same drop speed. The length of the liquid thread while pinching off at the nozzle exit varied with the voltage. For the lowest ejecting voltages, 12-13 V, the thread was shorter than 100 μm or even it was not evident because of the sudden formation of spherical droplets in order to minimize surface energy. At high ejecting voltages, the length of the liquid thread was higher, being more than 700 μm at 40 V. When the length of the pinch-off was high, the drop underwent high stretching that finally lead to the creation of a system having high surface to volume ratio. This finally lead to wave-like instabilities along the thread. As the amplitude of the capillary wave increased, the liquid thread was able to break up at several locations at slightly different times, forming several satellites of different sizes. The higher was the ejection voltage, the longer was the liquid thread and more satellites were formed. In our experimental conditions (ink having 30% glycerol v/v), multiple breakups evolving from the wave-like instabilities were evident only at the highest ejecting voltages (36-40 V). Instead, at intermediate voltages, more controllable end-pinching phenomena occurred. These observations were justified by considering the effect of glycerol in raising the viscosity of the ink-jetted inks, so determining an increase in liquid thread stability in our experimental conditions. In fig. 3.9, stroboscopic images of a drop ejected in the jetting voltage range 15-40 V are shown. The ejecting voltage (20 V) was the one typically used for the experiments, since it gave sufficient droplet ballistic accuracy of the droplet not determining satellites due

to multiple-breakups phenomena.
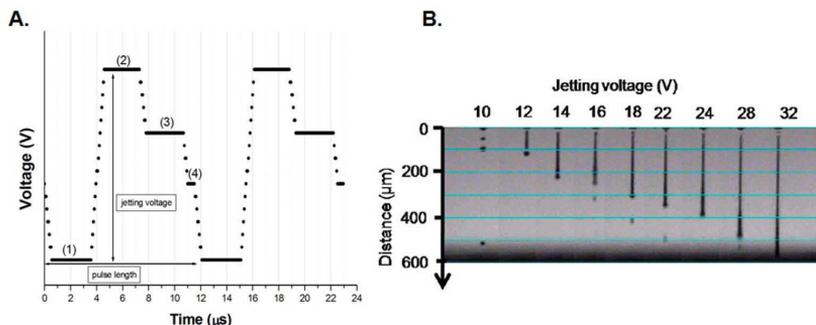
Figure 3.9: **On the left, scheme of the four-segments driving waveform having a single pulse length of 11.52 μs; On the right stroboscopic images showing droplets of D-glucose:D-glucal mixtures with 30% glycerol pinching off at the nozzle at increasing voltages.**

Printing speed strongly depends on the pinch-off time: the time which is needed for the ejected fluid to stretch and pinch off from the nozzle exit. If the pinch-off time increases, the printing speed of a single spot decreases. The pinch-off time doesn't depend upon the ejection voltage but is strongly correlated to the viscosity of the ink. In our experiments, the typical pinch-off time was about 19 μs. This result means that tens of microseconds were needed in order to eject a single drop and justifies the capabilities of inkjet printing technique for the high throughput and high speed fabrication of microarray (few minutes are needed in order one microarray to be realised). On the other hand, ejection speed was the effective rapidity with which the ink-jetted drop pinches-off at the nozzle and hits the substrate. What it has been found in our experiments is that the drop speed linearly goes with the ejecting voltage, as can be see from fig. 3.10, where the correlation between drop speed to ejection voltage is shown. The speed range was between 10 and 22 m/s.
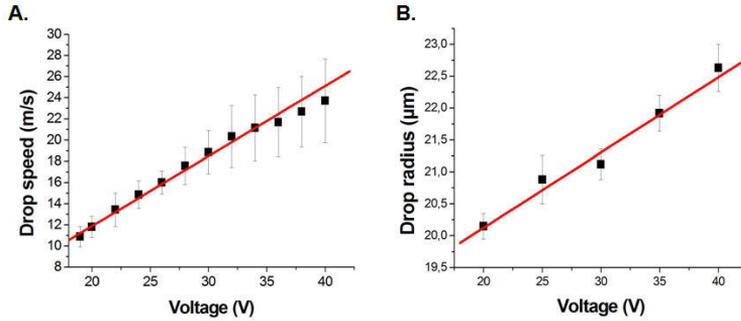
Figure 3.10: **Correlation between jetting voltage and drop velocity/radius at the GOx functionalised surface. The inkjetted liquid consits in a D-glucose solution (0,071 M) containing 30 % glycerol v/v..**

The higher is the ejection speed, the higher is the speed at which the drop hits the substrate and then higher is the final radius of the spot. In addition, it has been found a linear correlation between jetting voltage and spot radius at the GOx functionalised surface (see Fig. 3.10). The covered radius range is 20-23 μm for a voltage range between 20-40 V. In these impact conditions, the role of kinetic energy prevails on the capillary forces: the impact regime is type I (inviscid like fluid impact for which $O(10) < Re < (10^3)$ and $O(1) < We < O(10^2)$)) according to Schiaffino and Sonin classification [13].

In two cases, a single droplet (without satellites) was produced: when the satellite and the primary droplet recombined to form a single drop or when the liquid thread ejected from the nozzle contracted into a single drop without breaking up. In the first case, without taking into account the action of the surrounding air, the necessary condition for their recombination is that the axial speed away from the nozzle, v_s , should be higher than that of the primary drop, v_p . At the same time, the recoil speed of liquid thread separated from the primary drop

must be higher than the speed of the satellite. In other terms, necessary condition for the coalescence of the satellite drop with the primary drop is given by:

$$av_{ca} \approx v_r > v_s > v_p \tag{3.1}$$

where v_r, v_s, v_p are respectively the recoil speed, the satellite speed, the primary drop speed.

The second possibility is the drop formation without breakups generation. In this situation, the liquid column ejected from the nozzle will contract into a single drop without breaking it up if the length of liquid thread at pinch-off, l_b/R_{noz} doesn't exceed a limiting value l_b^*/R_{noz} :

$$\frac{l_b}{R_{noz}} < \zeta\frac{1}{\alpha_{max}^*} + 2 = \frac{l_b^*}{R_{noz}} \tag{3.2}$$

where $\zeta = (C_2 - C_1)a.C_1$ depends strongly on the waveform (in particular higher is the frequency, higher results the t_{b1}). On the other hand, C_2 doesn't depend on the waveform. From this result, two general main considerations can be derived:

(1) Signal waveform must be opportunely designed in order to get a t_{b1} (pinch-off time) the lowest as possible to avoid the formation of satellites.

(2) Liquid properties (viscosity and surface tension) must be tuned

in order to lower the value of α^*_{max} by employing viscogenic additives and/or surfactants.

3.3.3 Spot morphology and signal analysis of the microarray

The first step in the microarray image analysis was the feature extraction of the microarray image, in order to measure the signal intensity for each spot. The processing of a typical image was separated in three phases:

- Coordinates addressing: the process of assigning grid coordinates (**i,j**) to each of the spots.

- Segmentation: the classification of pixels as foreground (spot of interest) or as background (enzymatic layer).

- Intensity evaluation: the calculation, for each spot in the array, of the foreground and background intensities.

Spot morphology and positional accuracy were measured by employing the microarray quality parameters defined below:

- **Scale Invariance (S.I.)**: The ratio of the radius of the largest circle contained by spot i,j to that of the smallest circle containing the same spot i,j. This parameter is a measure of the spot roundness and its value is comprised between 0 to 1.

- **Size Regularity (S.R.)**: The ratio of the real spot area to the area of the smallest circle that circumscribes the spot. This parameter is influenced by the size of the spot.

- **Spot Alignment error**: The difference between the spot positions in an ideal grid structure ($I_{i,j}$) and the real spot positions in the realized microarray grid ($R_{i,j}$).

3.3.4 Colorimetric microarray detection for drug screening

Experimental set-up for signal detection at the microspot

The first step in image analysis is the feature extraction of the microarray image, in order to measure the signal intensity for each spot. The processing of a typical image was separated in three phases: the addressing (i.e. the process of assigning coordinates to each of the spots), segmentation (i.e. the classification of pixels as foreground - that is, as corresponding to a spot of interest - or as background), intensity extraction (i.e. the calculation, for each spot in the array, the foreground and background intensities) [14, 15]. The signal intensity of any given spot is the collective or statistic measurement of pixel intensities or grey values within the spot. Optical images usually had bright spots on a dark background (i.e. the grey levels in spot pixels are higher than those in background). This is a normal feature of spot signal in protein microarrays [16]. Once the spot was identified, background correction was needed to estimate the true amount of the product of the GOx catalyzed enzymatic reaction [17, 18]. Background correction methods include global, local, regional and morphological opening correction, etc. The motivation behind background adjustement is the belief that a spot's signal is due not only to the product of the chemical reaction but also to nonspecific adsorption and other chemicals on the slide. The goal is to measure this contribution and subtract it in order to get a more

accurate measurement. A regional background approach was used: the pixel intensity value of the surface immediately surrounding the spot was subtracted from the intensity value of the spot.

The extraction of the pixel intensities values was executed inside a rectangle surrounding a single spot: the signal at each spot was visualized as a double peak distribution - due to Foreground and Background pixels histograms - of red pixel versus a grey scale corresponding to the red colour. Both Foreground and Background signals (composed of thousands of pixels) could easily be fitted as normal distributions for which values as mean, median, mode, area, standard deviation or even certain percentile values can be calculated.

The total amount of the enzymatic catalyzed β-D-glucose oxidation reaction at each spot is proportional to the total Foreground signal. The Foreground signal had the highest density at the central region and a slow declining density at the region farther from the center [19]. The Foreground area is a measure of the amount of the substrate occupation on the enzymatic sites present at the protein monolayer surface at each spot. In this sense, the most appropriate measure of the reaction is the sum of the pixel intensities within the spot (i.e. the foreground area signal). The medium value of the pixel Foreground distribution (minus the mean Background signal) is a measure of the most frequent grey value inside the spot, and it gives the quantity of the dye complex formed by the detection reaction between hydrogen peroxide with p-hydroxybenzoic acid and 4-aminoantipyrine. The mean of the Foreground distribution is dependent upon the brightness of the microscope source illumination to which the microarray is exposed. The higher is the lightning, the higher is the Foreground mean (in gray values). In

order to have a signal that is independent on the absolute illumination power, it is mandatory to subtract from the Foreground mean the Background mean.
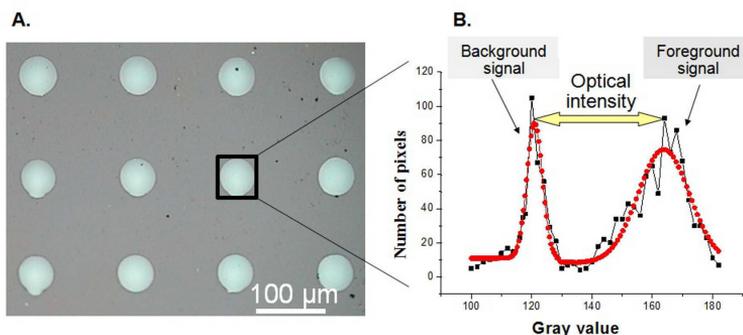

Figure 3.11: **(A.) Optical image of β-D-Glucose microarray printed on GOx surfaces with rectangle surrounding a spot; (B.) Background and Foreground pixel intensity distributions as function of gray value for the selected spot.**

For a typical ink-jet printed glucose microarray printed on GOx covered silicon dioxide surfaces, the mean foreground value after background subctration was characterized by a quite small variability (calculated as the error respect to the mean value) - about 3% - as calculated on 25 spots on the same microarray after 90 min incubation time. The coefficient of variation was 16% for the mean foreground data. These data is an indication of the potentially high quality obtainable data from this kind of microarray. In effect, typical protein microarrays usually have high variability in data between the same slide due to the fragility of such biomolecular systems at the surface that can in principle partly lose their biological activity. On the other hand, high variability has been found for the Foreground area values - that is 30% for 25 spots of the same array. The mean value was about 3700 pixels with a standard

deviation of 2800 for 25 spots. This being explained since the Foreground area is a high-sensible measurement of the substrate occupation on the enzymatic sites at the surface. The protein monolayer can be easily contaminated due to air exposure and this can determinate a certain variability in the enzymatic active area per spot: this could justify the high variability that has been found for this parameter. In this sense, the mean Foreground value after background subtraction seems to be a more suitable for studies dealing with molecules/drugs interactions with surface linked enzymatic targets.

Colorimetric methods similar to the one used in this work were employed by Ulyashova et al. [20] who showed that a colorimetric detection based on a horseradish peroxidase was suitable for DNA Microarray hybridization analysis. Up till now, microarrays detection technology typically involves a fluorescent label without an enzymatic signal amplification. However, expensive instrumentation has limited the wide applications of DNA and protein microarrays technologies, especially in clinical diagnosis. In this way, colorimetric methods like the one employed in this work can be a good candidate as alternative of fluorescence detection for producing inexpensive analytical devices. The advantages of colorimetric microarray-based assays are their sensitivity, reproducibility, rapidity, simplicity, portability, and cost-effectiveness [21].

Drug Screening Platform

In Fig. 3.12 a typical image of the drug screening platform is reported. Picoliter volume drops containing tens of picograms of molecules (either D-glucose or a mixture of D-glucose/D-glucal) are ink-jet printed on a glucose oxidase monolayer immobilized on a silicon oxide surface.

Upon hitting the solid surface, the dispensed drops form regular rounded spots with dimensions of about 40-50 μm. The colorimetric detection based on the horseradish peroxidase method [12] allows one to probe the interaction between the dispensed molecule and the enzymatic target at the single spot. Accordingly, whenever the enzymatic reaction occurs a red dye complex forms. The more the spot is coloured, the higher becomes the gray-scale optical contrast of the spot with respect to the background. We verified that the solid-supported enzymatic surface can be reused for this screening purposes several times by simply rinsing with water. In Fig. 3.12.A and 3.12.B optical images of alternated D-glucose rich (absence of D-glucal) and D-glucose/D-glucal (χ-D-glucal = 0.88) rich spotted lines, as freshly printed and after 90 minutes of incubation are shown, respectively. The spots had diameters of 38.8 ± 1.5 μm along with a coefficient of variation as low as 4% to be compared with those reachable by solid pin printing and by the widely used stealth pin printing techniques of about 2% and 12%, respectively [22].

We verified the microarray spot definition to be of high quality if compared to that obtainable by pin printing methodologies [18], and a scale invariance of the spot roundness of 0.91 ± 0.04 along with a size regularity of 0.84 ± 0.09 were evaluated. Moreover, the spot alignment error was 10.0 ± 4.8 μm. By comparing the two figures, one can easily observe that, in absence of D-glucal, the brightness of the D-glucose rich spots is largely increased after 90 minutes of incubation on the Glucose Oxidase monolayer at room temperature. On this respect, Fig. 3.12.C reports gray-scale colour distributions (gaussian fits) for two representative spots marked in Fig. 3.12.B as 1 and 2. Spot 1 is rich in D-glucose and shows a double-peak distribution with the foreground
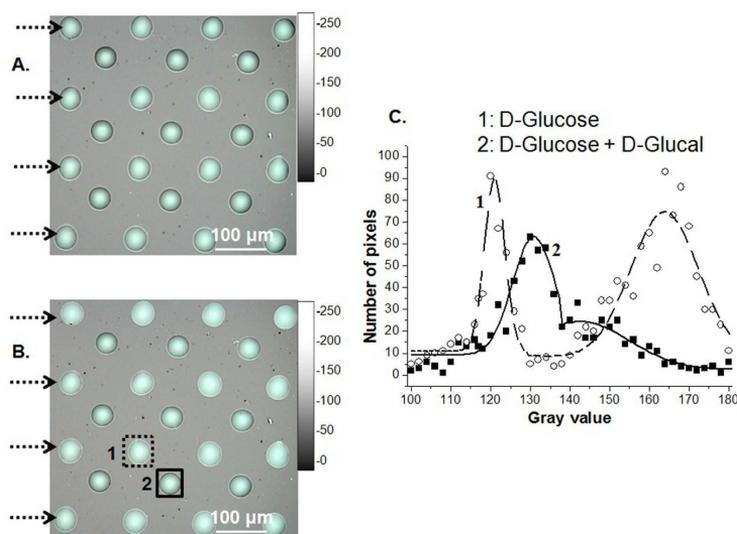
Figure 3.12: **Optical images of a model screening array made of alternated β-D-glucose and β-D-glucose/D-glucal rich spotted lines (A.) immediately after ink-jet printing operation. The lines 1, 3, 5, and 7 marked by the arrows consist each of four D-glucose rich spots; (B.) the same sample region after 90 min; (C.) gray-scale pixel intensity distribution with Gaussian fits for the regions marked by rectangles 1 (solid line) and 2 (dashed line) in part B enclosing representative β-D-glucose and β-D-glucose/D-glucal rich spots, respectively.**

signal well distinguishable with respect to the background. As to Spot 2 (β-D-glucose/D-glucal rich) the foreground results in a shoulder of the background signal, i.e. only a scarce optical contrast is detected. For each spot we defined as Optical Intensity value (O.I.) the difference between the average foreground and the average background gray-scale values. It is remarkable to observe that the greatest optical intensity differences are found around the dots perimeter forming well contrasted halos. This can be likely explained by considering a solute transport to the ring periphery under drop evaporation, [23, 24] that according to our detection method results in light and dark perimeters for β-D-glucose

rich and D-glucal rich drops, respectively. Unlikely, due to the low number of pixels O.I. values cannot be calculated at the dot perimeter with a significant statistics so that hereafter O.I. related to whole spots are reported.
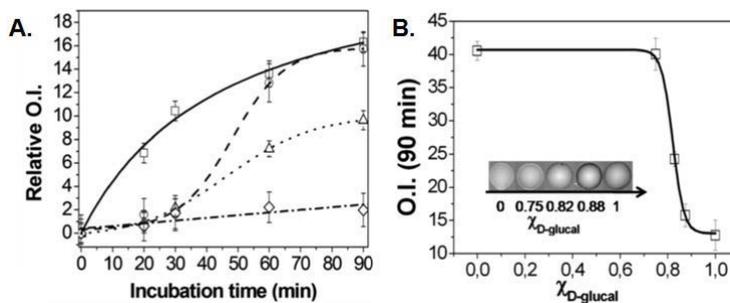

Figure 3.13: **(A.) Relative O.I. vs. incubation time for different χ-D-glucal [$\square$] 0, $\bigcirc$) 0.75, $\triangle$) 0.83, $\Diamond$) 0.88]. No significant O.I. increase has been found by employing χ-D-glucal of 0.88. (B.) O.I. at 90 min vs. χ-D-glucal in D-glucose:D-glucal rich spots. A sequence of spots having increasing χ-D-glucal is inserted. Both in parts (A.) and (B.), each value is averaged by five different spots.**

Fig. 3.13 reports a graphic showing relative O.I. vs. time for different χ D-glucal values as measured at a single spot level on the arrays. Relative O.I. values refer to the O.I. values at time t minus O.I. values at time zero. Note that reproducibility of measurements was quite good as demonstrated by the small error bars as well as by the coefficient of variation which was 11.4 % as measured on about 40 different D-glucose rich spots. The signal variation is almost similar to that typically obtainable by fluorimetric detection methodologies [25, 26]. As expected, in absence of D-glucal, O.I. increases hyperbolically ($R^2 = 0.9939$) with time due to the progress of the enzymatic reaction. The addition of D-glucal at χ D-glucal = 0.75 allows to observe a different trend, which is well fitted by a sigmoidal curve ($R^2 = 0.9959$) matching

the O.I. values of the above D-glucose spots after about 60 minutes of incubation. Such a behavior indicates that, in spite of possible problems occurring during hetero-phase assays, at our solid-supported enzymatic surface, D-glucose out-competes the D-glucal inhibition as it arises from a competitive inhibition mechanism [27].

The inhibition occurs at similar concentration values already observed in the solution-phase [28]. This out-competing effect is observed to be gradually lost by further increasing χ D-glucal and seems to completely disappear at a molar fraction of 0.88 where no significant O.I. increase in time is observed. In Fig. 3.13.B we show the effect of the inhibitor concentration on the GOx enzymatic activity at a fixed D-glucose concentration (0.071 M). In particular, we report O.I. values averaged on five different spots obtained after 90 min of incubation as a function of the χ D-glucal. A clear sigmoidal trend ($R_2 = 0.9995$) is observed with an inhibition threshold at a χ D-glucal of 0.75. The phenomenon obtained at our solid/liquid interface well agrees with already reported literature dealing with such a enzyme-substrate/inhibitor system working in solution [28]. Moreover, our single spot-based assay shows acceptable quality factor, Z = 0.65 (calculated on a 20 positive control assays - D-glucose rich spots- and 20 negative control assays - D-glucal rich spots) thus indicating the suitability of our method for high-throughput screening [29].

In order to generalize the here employed colorimetric detection method via peroxidase oxidation one can for instance refer to ligand biotinylation and streptavidin-peroxidase conjugates [20] as already shown for DNA hybridization (see Fig. 3.14).
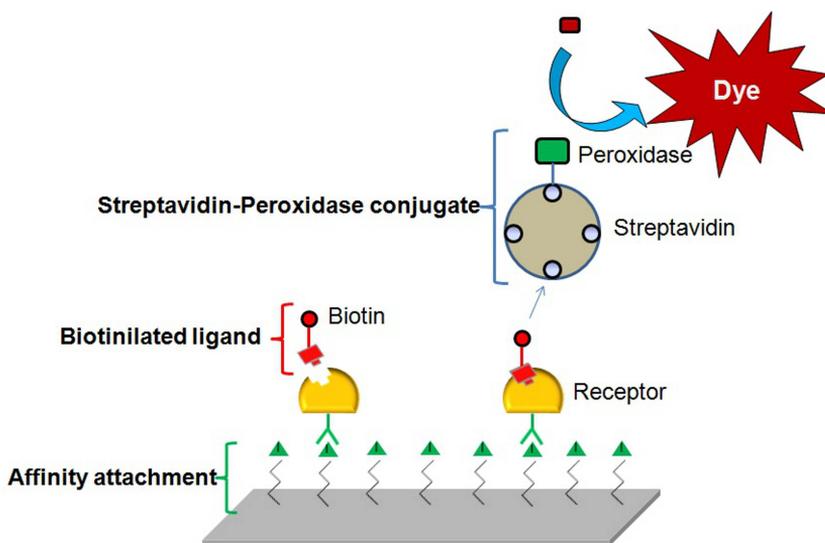
Figure 3.14: **Generalization of the colorimetric detection method by employing Streptavidin-Perozidase Conjugated and a Biotynilated Ligand.**

Aging effect

In Fig. 3.15 the effect of three months aging on the performance of a microarray stored in air is reported. The graph shows the O.I. as a function of the number of washes for a D-glucose microarray stored in air for three months. We observed a certain loss in the enzymatic activity which was quantified to be about 40%: albeit this evident decay in activity, still significant O.I. values were obtained (from 40 to 24 in terms of gray scale). This phenomenon is well in agree with observed with enzyme monolayer storage [30].
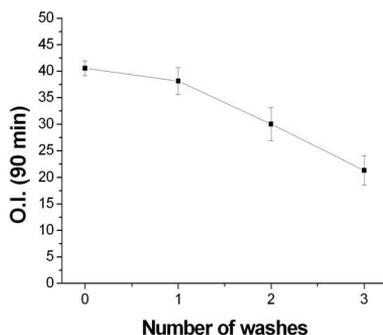
Figure 3.15: **Optical Intensity values reported as a function of washes in three months device storage. Each point is given by the average by five indipendent O.I. measurements on different spots.**

3.4 CYP3A4 arrays by Inkjet printing

3.4.1 Optimization of the printing conditions

As explained in Fig. 3.16, the approach we employed for the generation of the arrays was the one of droplet microarrays. Droplets of inhibitor molecules (volumes ranging from 0 to 180 pL) combined with buffer solution droplets (volumes ranging from 180 to 0 pL) in order to generate spots having different concentrations of inhibitor molecules in solution. Then, by printing CYP3A4, its substrate Luciferin-IPA and the enzymatic Regeneration system the reaction at the droplets occurred in a final volume of 240 pL. As final step, an equal volume of Luciferase enzyme was deposited on the previous spots in order to quantify production of Luciferin was quantfied by Luminometri measurments. Consider that the final droplets dimensions had diameters of about 150 μm.

The sequential ink-jet process was carried out according the assay-in-micro-droplets approach: this approach consists in the execution of enzymatic reaction in liquid phase [7] without the need of covalent binding

A.

	1.	2.	3.	4.	5.
Buffer	180	170	120	90	0
Inhibitor	0	10	60	90	180
CYP3A4 + LIPA	30	30	30	30	30
Reg. System	30	30	30	30	30
LUX detection	30	30	30	30	30

B.

(1): CYP3A4 + Substrate
(2-5): CYP3A4 + Substrate + [Inhibitor]
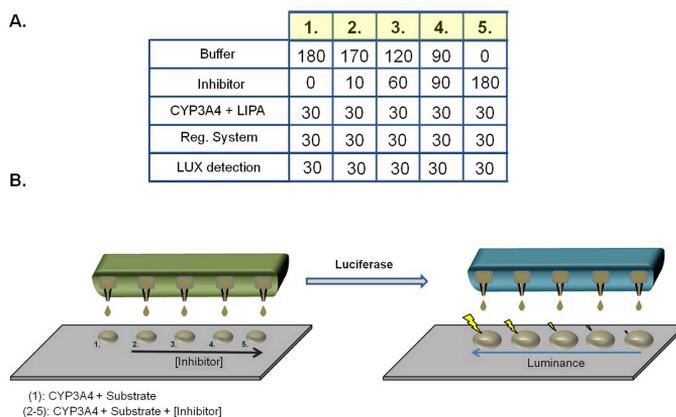
Figure 3.16: **Principle for a Luminometric Droplet Microarray for Drug Screening on CYP3A4 enzyme. In (A.) volumes of the droplets (in picoliters) inkjet printed on a MTMOS-covered silicon dioxide surface. In (B.) inkjet printing of droplets containing CYP3A4 enzyme, inhibitors and finally Luciferase enzyme for the luminometric detection.**

of the enzyme on the surface. Droplets of different biological materials were printed according the following sequential order:

- PBS buffer (0.7 M - pH 7.4)

- Test inhibitor (Erythtomycin concentration in the spotted solution was 20 μM, while 1-Aminobenzotriazole was 150 μM),

- CYP3A4 (2 nM) + Luciferin-IPA (3 μM)

- Regeneration System (NADP$^+$, Glucose-6-Phosphate and Glucose-6-Phosphate dehydrogenases)

- Luciferase Detection Reagent

The printed voltages were typically around 12-20 V in order to avoid shear and compression stresses on the fragile enzymatic systems dissolved in the solution [31]. Importantly, the droplet velocity after the

pinching-off at the nozzle was always kept higher than 5-6 m/s in order
to permit the formation of well directioned droplet with few unwanted
satellites. In contrast, higher speed resulted with long tails and higher
number of satellites, whereas at lower speeds, droplets could not be
ejected. These findings are in accordance with the results from Feng et
al [32]. Finally, such velocities permitted to achieve liquid coalescence
in the droplets with a certain liquid mass movement under the impact
site (i.e. conditions of droplet spreading) but without the formation of
unwanted liquid crowns consisting of a thin sheets having unstable free
rims at the top, from which numerous small secondary droplets would
be ejected [33].

The inhibitors spotted solution were diluted in the droplets to con-
centrations depending on the total final number of droplets. Specifically,
Erythormycin was diluted to final concentrations in solution of 0 μM;
0.83 μM; 5.0 μM; 7.5 μM and 15 μM. 1-Aminobenzotriazole was diluted
to final concentrations of 0 μM; 6.2 μM; 37.3 μM; 56 μM and 112 μM.

3.4.2   Set-up of a CCD camera for luminance detection

Conventionally, measurement of enzymatic activity via Luciferase
bioluminescent methodology are executed by employing Luminometer
devices integrated in expensive Plate Readers (see [34, 35] for instance).
These devices are specially manufactured for measuring with very high
requirements; due to high-precision solutions these cameras are very
expensive and are not commercially viable for many image-resolving
measuring tasks. Therefore, it would be desirable to measure luminance
with digital cameras which are much cheaper and easier to use. The
approach of image resolving luminance measurement represents a sim-

plification of such measuring tasks. W$\ddot{u}$ller and Gabele showed a clever method for utilizing digital cameras as luminance meters independent of the exposure settings [36]. They performed a calibration of the camera by employing an OECF (opto-electronic conversion function) measurement calculating luminance with the camera's digital RGB output values. This approach would permit to correlate optical digital values with luminance. This being said, in the following we show that a simple digital optical signal extracted with a CCD-camera is able to measure enzymatic activity

After the prints of the spots, optical images of the printed spots are extracted via a CCD camera. The 2D output pixel intensity signal for each spot is plotted inside a rectangle (or even more conveniently on a circle that is circumscribed by a spot) to extract the optical integrated density value which is the sum of the values of the pixels in the image or selection. From Fig. 3.17, it is evident that the integrated pixel density measured in the rectangle circumscribed by a single spot decreases by increasing the inhibitor concentration. This phenomenon can be ascribed to the minor production of Luciferin by CYP3A4 enzymatic reaction on the substrate Luciferin-Isopropylacetal (Fig. 3.5) in presence of the specific inhibitor erythromycin. The minor is the concentration of Luciferin, the minor is the total amount of photons generated by subsequent Luciferase enzymatic reaction (Fig. 3.5), thus leading to a minor brightness of the spots and then to a lower integrated density.

If taken together, these results show the possibility to detect CYP3A4 inhibition at the single spot in a easy and straightforward approach. However, the typical hurdle consisted in the difficulty in imaging only small fields of view so limiting the maximum number of spots in the
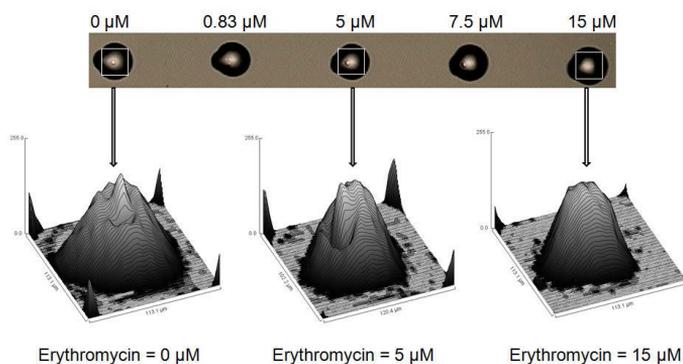
Figure 3.17: **Optical detection of enzymatic inhibition on CYP3A4 droplet microarrays by selective inhibitor erythromycin at different inhibitor concentrations (0 μM - 15 μM). The graphs represent the 2D pixel intensity distribution in the rectangles inscribed inside the selected spots.**

array that can be imaged simultaneously. As a result, an X-Y moving stage with multiple movements and numerous camera exposures always had to be used in order to cover all the slide and the resultant images must be assembled to yield a composite image. Finally, CCD cameras have been used with some degree of success in enzyme microarray imaging. Gosalia and others [37] employed a 12-bit CCD camera with a fluorescence microscope for the high-throughput screening of proteases in fluid phase nanoliter-scale arrays. Rupcich and others [38] obtained images of enzymatic reactions in sol-gel microarrays using a bright-field microscope equipped with a CCD camera. Similarly, Lu and Yeung [39] used a plano objective lens attached to a CCD camera for 10 X magnification of horseradish peroxidase arrays in high-throughput kinetic studies.

3.4.3 Inhibition assay on CYP3A4

After the set-up of the optical detection, we could quantify CYP3A4 inhibition on microarray format by erythromycin and 1-aminobenzotriazole. CYP3A4 and the inhbitors were left in incubation in droplets in presence of Luciferin-IPA substrate for at least 10 minutes or 20 minutes at room temperature in order to allow the inhibitors to interact with the enzyme. It is remarkable the fact that we observed reproducible optical signals only when employing 10 minutes incubation: this incubation time being the one preferibly employed in conventional luminescence assays.
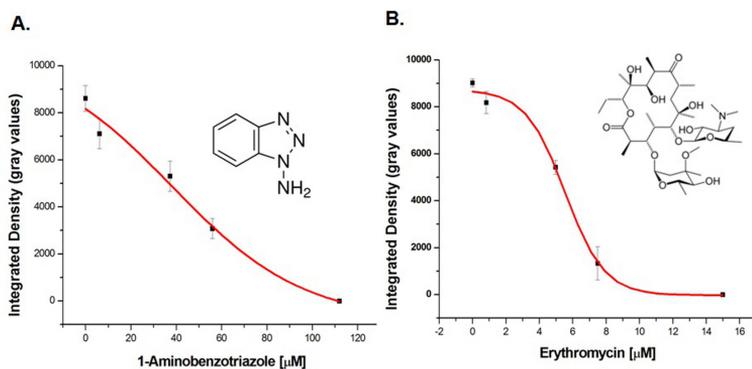

Figure 3.18: **Relative Integrated density measured on CYP3A4 droplet microar-rays inhibited with 1-aminobenzotriazole (A.) and erythromycin (B.) at different inhibitor concentrations (respectively 0 μM - 112 μM and 0 μM - 15 μM). The inhibitors were incubated 10 minutes with CYP3A4 at room temperature.**

From the plots of Fig. 3.18, it is evident that both inhibitors deter-mine a diminution of enzymatic signal by increasing their concentration. The inhibition plot for 1-aminobenzotriazole (1-ABT) is not a such clear sigmoid ($R^2 = 0.98453$) but anyway permits to evaluate a IC_{50} equal to 46.20996 ± 10.28692 μM. The inhibition concentration is so high since 1-Aminobenzotriazole is a nonselective mechanism-based inactivator of

both human and nonhuman cytochrome P450 (P450) enzymes with few difference in the inhibition affinity with different enzymes. Thus, 1-ABT can be used when conducting in vitro reaction phenotyping studies with new chemical entities in drug discovery to decipher P450 from non-P450-mediated metabolism and it exploits its activity only at high concentrations [40]. On the other side, Erythromycin inhibition curve has a clearly sigmoidal shape ($R^2 = 0.99125$) with a IC_{50} calculated as 5.55 ± 0.35 μM which is in accordance with values obtained from conventional solution-assays in microtiter plates [41]. Importantly, this value has to be compared with conventional 96- and 1536-well fluorescence detection inhbition studies [42] which give IC_{50} values below 1 μM. From structural studies [43], it is known CYP3A4 undergoes dramatic conformational changes upon ligand binding with an increase in the active site volume by $> 80\%$. The conformational changes induced by erythromycin are relatively extensive determining an $rmsd$ for all ordered C_α atoms of 1.2 $\overset{\circ}{A}$ when compared with the ligand-free structures. The most prominent differences are localized in the F-G region of CYP3A4 [43]. Moreover, it is known that erythromycin localizes its position close to the heme group in one of the molecules in the asymmetric unit.

CYP enzymes are the major catalyst of oxidative drug metabolism. Among the 57 human genes that encode CYP enzymes, five (CYP1A2, -2C9, -2C19, -2D6 and -3A4) account for most CYP-dependent drug metabolism. Among these, CYP3A4 is the the most prominent, being known to be the most promiscuous of the human CYP enzymes and able to contribute to the metabolism of about 50% of marketed drugs. Compounds that are rapidly metabolized or converted to toxic products
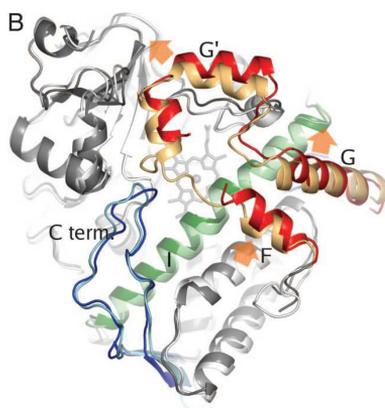
Figure 3.19: **Erythromycin binding to CYP3A4. Erythromycin is shown in orange stick representation. The heme is shown in magenta. Secondary structure and stick representations of side chains within 4 $\overset{\circ}{A}$ from the ligand are shown in green. Picture reproduced from [43].**

by CYPs may be poor drug candidates. On the other side, compounds that either inhibit or induce CYP activities can cause Drug-Drug Interactions. A first drug that induces expression of a CYP and which metabolizes a second drug may accelerate clearance of the second drug to the point of reduced therapeutic efficacy [44]. In contrast, a first drug that inhibits a CYP and which metabolizes a second co-administered drug can cause the second drug to accumulate to a toxic level due to slowed metabolism. These effects are amenable to bioluminescent probe investigation via CYP substrates, which are available for numerous CYPs [44]. CYP enzyme activities can be increased or decreased by many drugs, which is a major reason for drug-induced toxicity via drugdrug interactions (DDIs). According to the current state-of-knowledge, CYP3A4 can adopt multiple ligand bound protein conformations and accommodate simultaneous ligand binding even of relatively large compounds. Thus, the evaluation of potential DDIs is a key aspect of new drug dis-

covery and development [45]. The inhibition assay here proposed is a simple, low cost and rapid platform for evaluating possible inhibitors for such a fundamental metabolic enzyme. Moreover, the additive nature of a fabrication process via inkjet would enable direct studies of drug-drug interaction in single droplets by spotting different drug candidates on spots containing CYP3A4. Importantly, the here employed solution phase microarray technology also has great potential especially in hit identification and confirmation and also for lead optimization. Ma et al. [46] were among the first to report on the commercial applications of this approach by revealing the details of aerosol technology and its application in fabricating homogeneous-based screening formats for enzymes such as caspase, matrix metalloproteinases, thrombin, factor Xa, histone deacetylases and protein kinase A. Because of the homogeneous reaction systems, time-dependent and dose-dependent reactions can also be performed on microarrays, delivering kinetic parameters such as K_m, V_{max}, and k_{cat}. In fact, the authors demonstrated that these microarray-generated parameters were quantitatively similar to those derived from conventional well-based assays. For example, both technologies yielded similar IC_{50} values for caspase-6 when the same reaction conditions were used. Furthermore, taking advantage of miniaturization pays off in larger scale HTS: the total cost of microarray-based reactions could be significantly reduced compared with standard low volume 384-well-based assays [46] finally reducing the cost for the discovery and the optimization of a suitable drug compound.

References

[1] Wohlfahrt G.; Witt S.; Hendle J.; Schomburg D.; Kalisz H.M.; Hecht H.J., *Acta Crystallogr D Biol Crystallogr.* **55**, 969 (1999).

[2] Gibson Q.H.; Swoboda B.E.I.; Massey V., *JBC* **239**, 3927 (1964).

[3] Pignataro B.; Chi L.F.; Gao S.; Anczykowski B.; C. M. Niemeyer C.M.; M. Adler; D. Blohm; H. Fuchs, *Appl. Phys. A* **74**, 447 (2002).

[4] Williams P. A. et al., *Science* **305**, 683 (2004).

[5] Yano J.K.; Wester M.R.; Schoch G.A.; Griffin K.J.; Stout C.D. and Johnson E.F., *JBC* **279**, 38091 (2004).

[6] Sukumaran S.M.; Potsais B.; Lee M.-Y.; Clark D.S. and Dordick J.S., *J. Biomol. Screen.* **14**, 668 (2009).

[7] Chiu D.T.; Lorenz R.M. and Jeffries G.D.M., *Anal. Chem.* **81**, 5111 (2009).

[8] Li A.P., *DMD* **37**, 1598 (2009).

[9] Fraga H., *Photochem. Photobiol. Sci.* **7**, 146 (2008).

[10] Giannazzo F.; Aiello V.; Scandurra A.;Sinatra F.; Renis M.; Fichera M. Libertino S.;, *Langmuir* **24**, 1965 (2008).

[11] Libertino S. et al., *Appl. Surf. Sci.* **253**, 9116 (2007).

[12] Arrabito G.; Musumeci C.; Aiello V.; Libertino S.; Compagnini G.; Pignataro B., *Langmuir* **25**, 6312 (2009).

[13] Schiaffino S.; Sonin A. A., *Phys. Fluids* **9**, 3172 (2003).

[14] Khan F.; Zhang R.; Unciti-Broceta A.; Diaz-Mochón J.J.; Bradley M., *JALA* **19**, 35243528 (2007).

[15] Hong J.; Edel J. B.; deMello A.J., *DDT* **14**, 134 (2009).

[16] Mugherli L.; Burchak O.N.; Balakireva L.A.; Thomas A.; Chatelain F.; Balakirev M.Y., *Angew. Chem. Int. Ed.* **48**, 7639 (2009).

[17] P.G.; Park K.; Cho H.G., *Internat. Journ. of Inform. Tech.* **11**, 117 (2005).

[18] Dufva M., *Biomol. Eng.* **22**, 173 (2005).

[19] Zhu H. and Snyder M., *BMC Bioinform.* **8**, 485 (2007).

[20] Ulyashova M.M.; Rubstova M. Yu.; Batchmann T.; Egorov A.M., *Moscow Univ. Chem. Bullettin* **63**, 75 (2008).

[21] Mascini M.; Guilbault G.G; Lebrun S.J.; Compagnone D., *Anal. Lett.* **40**, 1386 (2007).

[22] M´uller U. R.; Papen R., *Microarray Technology and Its Applications* (Springer - Verlag, Berlin Heidelberg, Germany, 2005).

[23] Deegan R.D.; Bakajin O.; Dupont T.F.; Huber G.; Nagel S.R.; Witten T.A., *Nature* **389**, 827 (1997).

[24] Blossey R.; Bosio A., *Langmuir* **18**, 2952 (2002).

[25] Jiang L.; Yu Z.; Du W.; Tang Z.; Jiang T.; Zhang C.; Lu Z., *Biosens. Bioelectron.* **24**, 376 (2008).

[26] Litten B.; Smith R.; Banfield E., *JALA* **15**, 58 (2010).

[27] Rowlands A.R.; Panniers R.; Henshaw E.C., *J. Biol. Chem.* **263**, 5526 (1988).

[28] Rogers M.J.; Brandt K.G., *Biochemistry* **10**, 4624 (1971).

[29] Zhang J.H.; Chung T.D.; Oldenburg K.R., *J. Biomol. Screen.* **4**, 67 (1999).

[30] Liang R.Q.; Tan C.Y.; Ruan K.C., *Journ. of Biosc. and Bioengin.* **87**, 1389 (1999).

[31] Nishioka G. M.; Markey A. A.; Holloway C. K., *J. Am Chem. Soc.* **126**, 16320 (2002).

[32] Feng J.Q.J., *Imaging Sci. Technol.* **46**, 398 (2002).

[33] Anderson D. M., *Phys. Fluids* **17**, 087104 (2005).

[34] Cali J.J.; Niles A.; Valley M.P.; O' Brien M.A.; Riss T.L. and Shultz J., *Expert Opin. Drug Metab. Toxicol.* **4**, 103 (2008).

[35] W*ü*ller D.; Gabele H., *DMD* **37**, 1598 (2009).

[36] W*ü*ller D.; Gabele H., *Proc. of SPIE-IS&T Electronic Imaging* **6502**, 65020U (2007).

[37] Gosalia D.N.; Diamond S.L., *PNAS* **100**, 8721 (2003).

[38] Rupcich N.; Goldstein A.; Brennan J.D., *Chem. Mater.* **15**, 1803 (2003).

[39] Lu G.X.; Yeung E.S., *Isr. J. Chem.* **47**, 141 (2007).

[40] Linder C.D. et al., *DMD* **37**, 10 (2009).

[41] Cohen L.H. et al., *DMD* **31**, 1005 (2003).

[42] Trubetskoy et al., *J. Biomol. Screen.* **10**, 56 (2003).

[43] Ekroos M. and Sj*ö*gren T., *PNAS* **103**, 13682 (2006).

[44] Cali J.J.; Niles A.; Valley M.P.; O'Brien M.A.; Riss T.L. and Shultz J., *Expert Opin. Drug Metab. Toxicol.* **4**, 103 (2008).

[45] Lee K.S. and Kim S.K., *J. Appl. Toxicol.* **10**, DOI: 10.1002/jat.1720 (2011).

[46] Ma H.; Horiuchi K.Y.; Wang Y.; Kucharewicz S.A.; Diamond S.L., *ASSAY and Drug Development Technologies* **3**, 177 (2005).

4

Single Cell Interaction Arrays by DPN

In this chapter we demonstrate Dip Pen Nanolithography as powerful patterning methodology for the direct deposition of multiple single-strand DNA oligonmers in ambient conditions via a liquid ink protocol based on Polyethylene glycol (PEG) as carrier material. Combining such approach with DNA-directed immobilization i.e. the hybridization of the deposited sequence with a complementary ssDNA sequence conjugated with a strep-tavidin conjugate and a biotinylated polipeptide ligand, allowing for the realization of a protein biochip for single-cells experiments, in particular cell-adhesion and single cell assays. We optimize the liquid ink deposition conditions by analyzing the effects of relative humidity, dwell time, surface energy of the receiving substrate and molecular weight of the PEG on the printing efficiency and hybridization efficiency.

Glossary and list of acronyms:

PEG: acronym for Polyethylene glycol (general structure HO-CH_2-(CH_2-

O-CH$_2$-)$_n$-CH$_2$-OH), oligomer or polymer of ethylene oxide. Historically PEG has tended to refer to oligomers and polymers with a molecular mass below 20,000 g/mol.

DDI: acronym for DNA-Directed Immobilization, powerful and chemically mild procedure to immobilize biotinylated macromolecules conjugated with a single-strand DNA oligomer at solid substrates bearing covalent conjugates of a complementary single-stranded DNA oligomer and streptavidin.

R.H.: acronym for Relative Humidity (R.H. or also ϕ), term used to define the ratio of the partial pressure of water vapor (H$_2$O) (e_w) in a mixture to the saturated vapor pressure of water (e_w^*) at a given temperature. Relative humidity is normally expressed as a percentage and is calculated according to the following equation:

$$\phi = \frac{e_w}{e_w^*} x 100\%$$

4.1   Single cell interaction arrays by DPN

4.1.1   Preparation of oligonucleotide solutions

Here are shown the oligonucleotides sequences employed for the preparation of DNA-protein conjugates and the relative amino modified complementary capture oligomers in the 5′ to 3′ direction:

- **tF5** GGT CCG GTC ATA AAG CGA TAA G (5′ thiolink)

- **tF10** GGA CGA ATA CAA AGG CTA CAC G (5′ thiolink)

- **acF10** GTA CTT CCT TAA ACG ACG CAG G (5′ thiolink)

- **acF5** CTT ATC GCT TTA TGA CCG GAC C (5′ thiolink)

- **dt12-cF5** TTT TTT TTT TTT CTT ATC GCT TTA TGA CCG GAC C (5′ thiolink)

Before performing any experiment, an oligonucleotide sample was doubly purified by using gravity flow columns typically employed for the purification of small DNA fragments, desalting and buffer exchange (NAP5 / NAP10 columns GE Healthcare). The purification was executed as follows. Firstly, the oligonucleotide aliquot was diluted in 500 μL in water. Then the following operations were performed.

- Preparation and equilibration of NAP 5/ NAP 10 Columns (water allowed to flow through the columns for 10-20 minutes at room temperature)

- Oligonucleotide sample (500 μL solution) loading into NAP 5 column

- NAP 5 elution with 1000 μL water (NAP 5 and NAP 10 columns were placed on top of each other, so that the purified sample was collected in NAP 10 column)

- NAP 10 elution with (750 μL + 750 μL) water and immediate collecting of the sample.

- Sample collecting (1500 μL)

- Sample concentration till total water evaporation in Eppendorf Concentrator 5301 (4 h)

- Sample reconstitution with 0.1 TE buffer (1 mM Tris, 0.1 mM EDTA) in a volume of 10-15 μL.

Importantly, before and after the utilization of NAP columns, columns are washed three times with water in order to clean them from previous

oligonucleotide solutions. The concentration of the oligo in the recon-
stituted sample was determined by using UV-vis spectrophotometer. In
this regard, an aliquot of the sample (typically from 0.5 μL to 5 μL)
was diluted till approximatively 1-2 μM (150-300 fold dilution factor).
Then a UV-vis spectra was recorded in the wavelength range between
200 nm and 500 nm. The absorption at 260 nm (absorbance due to the
nucleotide bases) was measured: this value is divided by the extinction
coefficient ($L \cdot mol^{-1}\mu \cdot cm^{-1}$) and multiplied for the dilution factor to
retrieve the concentration of the oligonuclepotide solution (x) diluted in
the 0.1 TE buffer solution. (Lambert-Beer law $A = E \cdot c * d$, d = 1 cm)
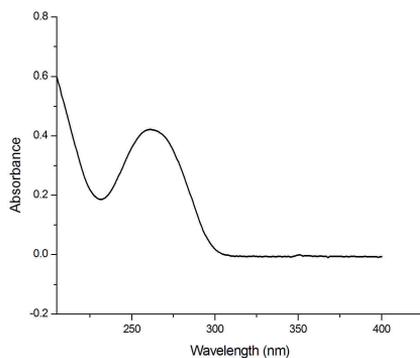
Figure 4.1: **Typical UV-vis spectra of an oligonucleotide solution. The high ab-
sorption at approximately 260 nm is due to the nucleotide bases.**

4.1.2 Preparation of capture oligonucleotides Arrays by Liquid DPN

Preparation of oligonucleotide solutions in PEG hydrogel matrix

In all the experiments ink was deposited by DPN in liquid conditions. In this sense, a PEG/glycerol water is employed as matrix to facilitate the transportation of different nanomaterials on various substrates. The PEG carrier solution was prepared by dissolving PEG in the water/glycerol mixture. 5 μL is the typical final volume of the solution for the DPN. Defining x the concentration of the oligo dissolved in 0.1 TE buffer solution, the final solution typically had 0.05 TE buffer, x (μM) oligo, 30% w/v PEG, 30% v/v glycerol and then it contained:

- PEG 1.5 mg

- Glycerol 1.5 μL

- Oligo solution (500/x) μL

- TE buffer (0.25 - 50/x) μL

- Water (3.25 - 450/x) μL

In order to minimize the errors in weighting PEG and glycerol and also to prepare several DPN solutions with the same PEG/glycerol solution, a 1000 fold higher quantity of the PEG/glycerol mixture without oligo in water was prepared as follows:

- PEG 1.5 g

- Glycerol 1.50 mL

- TE buffer $1000 \cdot (0.25 - \frac{50}{x})$ μL

- Water $1000 \cdot (3.25 - \frac{450}{x})$ μL

PEG and glycerol are soluble in water: in order to facilitate the dissolution of PEG in water/glycerol mixture, the solution was heated till $60-70\,^{\circ}$C and then equilibrated to room temperature. Then 5 - 500/x μL of this solution were added to the 500/x μL of the oligo solution. This final solution is suitable for DPN and can be added to the Inkwells.

DPN Instrumentation

All Dip Pen Nanolithography experiments were performed by using a commercial DPN instrument (Nscriptor, Nanoink Inc., USA). Arrays were designed using $InkCAD^{TM}$ software 3.7.1. version. DPN writing was carried out with the 1D type M passive DPN Pen array (NanoInk Inc., USA), which is featured with 12 silicon nitride tips 66 μm spaced each one with a Spring Constant of 0.6 N/m . Tips were plasma cleaned (Flecto 10 USB instrument, Plasma Technology GmbH, Germany) before each experiment (O_2 gas, 30-40 s, 50 W, 0.5 mbar) in order to remove organic contaminants and increase the density of hydroxyl groups on their surface. The hydrophilic tips were then immersed in the ink by using the microfluidic ink delivery system (M-12MW Inkwell Arrays-IWL-0031-01, Nanoink Inc., USA), which was also plasma cleaned with O_2 gas (30-40 s, 5 W, 0.5 mbar) only after the first use in order to slightly increase the hydrophilicity of the ink channels. The inkwells were filled with the capture oligonucleotide solution (25- 150 μM, 0.3 μL per reservoir, 30% v/v glycerol, TE buffer 0.05 -0.5 mM Tris, 0.05 mM EDTA-, 30% w/v PEG of varying molecular weight, ranging from

400 to 4000 kDa). The top surface of inkwells is hydrophobic since it
has a Teflon coating; on the other side, the surface of microchannels
and wells is hydrophilic. This helps keeping the ink inside the channels.
Pen-surface contact and pen array leveling were executed via optical in-
vestigation of the cantilever deflection identified by a marked increase of
its reflectivity upon contact with the glass surface. In these conditions,
the DPN deposition process is force independent.
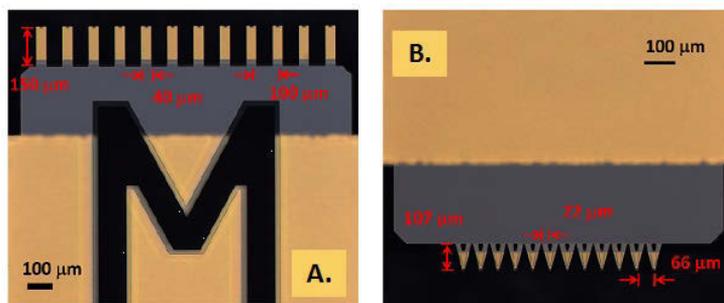
Figure 4.2: **Optical image of a M-type pens (made of twelve pens 66μm spaced)
Array. (A.) Side $M-1$ has "diving board" shaped cantilevers and
(B.) Side M-2 has "A-frame" shaped cantilevers.**

Tips were ink loaded by dipping for 5 - 10 s in the end part of the
6 μm wide ink loaded microchannels of the inkwell substrate. Prior
to the printing of arrays, excess ink was removed from freshly coated
tips by making some bleeding spots in a non-essential area of the glass
slide. All patterning experiments were carried out at room temperature
at varying relative humidities (R.H.), ranging from 25-70 % R.H and at
dwell-times in a range between 0.01 s and 10 s in order to perform the
liquid ink calibration studies. The minimum possible dwell time (0.01 s)
was chosen for the fabrication of all the cellular adhesion studies arrays.
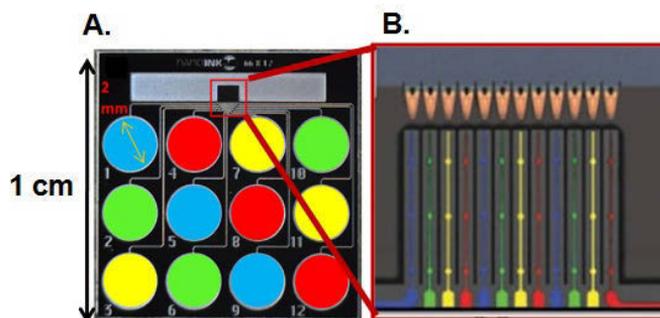
Figure 4.3: **Optical microscope images showing (A.) Optical image of the twelve reservoir M-12MS Inkwell each one inked with a different coloured solution and (B.) zoom on the pen ink loading area showing the microchannels and the microwells inked with the solutions. Figures reproduced from www.nanoink.net.**

4.1.3 Protein biochip by DNA-directed Immobilization

Microscope coverslips (18 x 18 mm) were cleaned with abs. EtOH for 30 minutes. Afterwards, they were soaked into a 3-aminopropyltriethoxy-silane solution (APTS, Sigma-Aldrich) containing 93% EtOH, 5% ddH2O and 2% APTS for 4 h. Subsequently, the functionalised slides were washed thoroughly with EtOH and acetone for 10 min. Then they were dried for 15 minutes at $110\,^{\circ}$C and stored at $-20\,^{\circ}$C over night. Finally, the coverslips were coated with PBAG (Sigma-Aldrich) 1:1 in aceton (w/w) or covered with dendrimer by employing the sandwich method [1] overnight. After coating with PBAG the slides were washed with acetone and dried under nitrogen. Capture oligonucleotides ($5'$ amino-modified acF5 and acF10) were dispensed on PBAG-activated coverslips. The slides were incubated overnight at RT and then mounted under a prepared culture dish having a 1mm diameter hole at the center. The covalent DNA-STV conjugates (F5 and F10) were synthesized,

purified by anion-exchange chromatography and subsequently coupled with the biotinylated dyes Atto488 (b488) and Atto565 (b565) and the biotinylated epidermal growth factor (bEGF) according to experimental strategies described in detail in [2] Before hybridization experiments, the capture oligonucleotide array was pretreated with MESTBS buffer for 30 minutes and subsequently washed for 15 minutes with TETBS buffer in order to reduce non-specific binding of oligonucleotides to he glass substrate. Then DNA-STV-b488/b565 or DNA-STV-bEGF conjugate solution (25 nM) were allowed to hybridize for 60 minutes at room temperature in a humidity chamber (VWR). After hybridization of the conjugates the DNA array was washed with sterile PBS. The cells employed in the adhesion experiments were the stable transfected MCF-7 (human breast adenocarcinoma) cells with an eGFP tagged epidermal growth factor receptor (eGFP-EGFR).

Fluorescence microscopy pictures were taken with an inverse fluorescence TIRF microscope (Olympus IX81). Images were taken with the software $Cell^R$ version 2006 and processed with *MacBiophotonics ImageJ* software. The cell pictures were taken by using the TIRF-filter for GFP (TGFP) and the 60x TIRF objective to localize the GFP-tagged receptor on the attached cell membrane. Wide-field pictures of the spots were taken with the RFP-filter and for the cells the GFP-filter was used. MacBiophotonics ImageJ software was employed for analysing microscope data. For ink calibration, arrays with seven rows of six spots were realized, each row having spots with a fixed dwell time (0.01-0.1-0.5-1-2-5-10 s). Areas of spots were measured from the fluorescence images to calculate spot diameter. In order to determine the effects of the surface chemistry, total fluorescence signal intensity of the

spotted DNA is measured by selecting its position and measuring the integrated signal density, which is the product of the area and the mean gray value.

4.2   Results and Discussion

The goal of our approach was to develop a robust strategy to couple the DPN-mediated micro-structuring and the DNA-directed immobilization (DDI) functionalization, such that DPN-based patterning is executed via a single type of molecular adaptors (that is oligonucleotides) which can be deposited under constant solution conditions but at the same time are featured with specific recognition properties for immobilizing polypeptides in mild conditions. This fabrication methodology is aimed at the fabrication of microstructured cell-specific proteic ligands with lateral dimensions below one single cell: these such generated surfaces are suitable for single-cell culture studies. As shown in Fig. 4.4, the fabrication of such surfaces is divided in a micropatterning part (Parts A and B) realized by liquid DPN in which two different ssDNA are firstly loaded at single tips on a 1D-pen array (for sake of simplicity only three adjacent pens are shown) and then are deposited on modified glass surface onto which they are covalently bounded while retaining their functionality. Then the functionalization part occurs (Parts C and D) by hybridization with the complementary ssDNA sequence conjugated with streptavidin conjugate and a biotinylated polipeptide ligand (see in Fig. 4.4 the proteins P_1 and P_2) that result in spots displaying specific interactions with living cells.
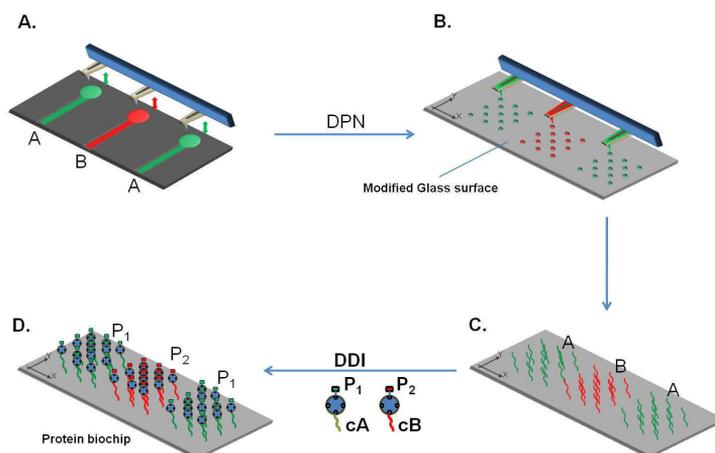
Figure 4.4: **General scheme for multi-ligands patterning below single-cell scale by employing a combination of Dip Pen Nanopatterning and DNA-directed immobilization. See the text for an explanation of the figure.**

4.2.1   Optimization of multiplexed liquid ink DPN

As first achievements, the optimization of the liquid DPN process was achieved. At the very beginning of each experiment, it was found out that a precise leveling of the pens array with respect to the substrate has to be fulfilled. This can be easily achieved by iteratively tilting and rotating the imaginary plane of the 1D pen array on the surface of the substrate. It has to be ensured that the plane of the array of pens is as parallel as possible to the plane of the surface in a way that all the pens exert the same amount of force on the surface. By simple looking by an optical camera, it was possible to execute this fundamental task. When in contact conditions, tips that exerted more force on the substrate reflected more light and then were brighter than the ones which exerted less force. After a certain number of rotations around the axis

outgoing from the pen array, when all the pens - being in contact with the substrate surface - reflected the same amount of light, then they exerted the same amount of force on the surface and the 1D pen array was leveled to the surface 4.5.

The leveling procedure also permits To avoid damaging the pens in a multi-pen array and to obtain equivalent amounts of ink on the cantilevers, finally resulting with uniform spot sizes across the array and extended periods of writing time.
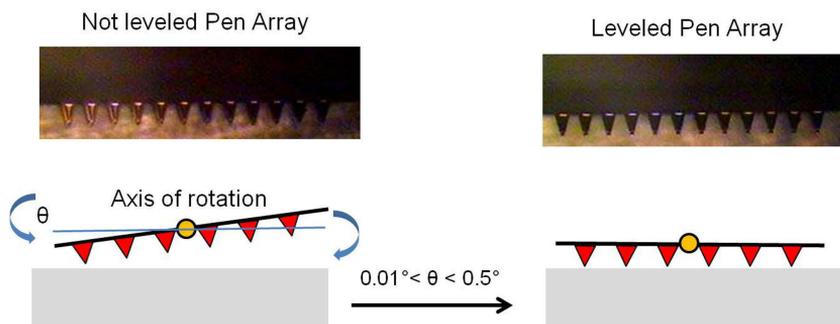

Figure 4.5: **Leveling procedure for a generic 1D pen array. On the left the case of not-leveled M-type pen array is presented: after some rotations, the pen array is leveled and the pens reflect the same amount of light when they touch the surface. The central dot represents the axis of rotation of the 1D pen array.**

It was found out that the optimization of the ink loading at the tips of the pen array was fundamental in order to get reproducible results. Actually, the amount of ink available on a pen determinates the quantity of features that can be written reproducibly without size deviations. Typically a twelve pen arrays was dipped into micron-sized cavities or microwells, containing two different oligonucleotide solutions arranged in a alternated manner. we found out that a better methodology consisted in pens dipping at the edge of the microchannels in order

to minimize the problem of ink contamination between adjacent pens. Being microfluidics elements in open configuration, they are relatively clog-free and easy to fabricate and it should be possible to reuse them by appropriate cleaning procedures. Anyway by cleaning them with polar solvents like ethanol, it is easy to cause cross-contamination between different microwells and microchannels. For this reason, inkwells can be considered an almost single experiment devices: efforts are needed in order to gain more expertise in cleaning protocols that might enable multiple inkwell usage. In principle a 1D pen array should be aligned on the inkwell surface in order that all the pens are dipped in the same way at the same time. For the inking the 1D pen array was lowered down to the inkwells by employing Z-stage motors and Z-piezo motor. The M-type pens array wa usually leveled on the inkwell before dipping to make sure that all the pens are dipped in the same time. Afterwards, inking was executed: both Z-motors and Z-piezo can be used for precise approaching to inkwell, and dipping the pens. After having inked the pens, the cantilevers were lifted up, and looked for checking the ink loading and wetting. Then the humidity was set to the target value, allowing the system to come to equilibrium (10-15 minutes). The sample surface was firstly approached, and the tip gently contacted the surface and then was withdrawn. After withdrawing, spots of ink transferred from the cantilever to the substrate were visible. This operation, named spot bleeding, was executed till two-three times on areas of the substrate which are not to be used for the patterns in order to remove the excessive ink solution from the pens. After bleeding in two-three points, the pattern typically resulted in quite uniform spots.

4.2.2 Effects of substrate surface energy on printing conditions

We experimentally investigated the feasibility of direct writing of oligonucleotide-PEG ink by DPN by initially comparing two different surface chemistries for the covalent immobilization of the capture oligonucleotides. On the one hand, we employed a chemically activated organic layer of polyamidoamine dendrimers. This surface is hydrophilic and contains amino-reactive epoxy- groups, which are used for covalent immobilization of the amino-alkyl modified capture oligomers. On the other hand, hydrophobic surfaces were used: these were prepared by coating the 3-aminopropyltriethoxy-silane (APTS) activated coverslips with poly-bisphenol-A-glycidyl (PBAG) (Sigma-Aldrich) 1:1 in aceton (w/w) by using the sandwich method as described for the dendrimer coating overnight [1]. Initially we compared the amount of oligonucleotide transferred by DPN to these two different surfaces. The ink we employed was dT12-cF5-Alexa546 at varying concentrations ranging from 25-150 μM in TE buffer containing 30% v/v glycerol and 30% w/v PEG 1000 was used and DPN was carried out with a dwell time of 0.01 seconds in 30 % relative humidity (R.H.). Subsequently, the slides were stored at room temperature and analysed by fluorescence microscopy. In order to remove the non covalently bounded molecules, the slides were washed carefully with TEBTS/PBS buffers and dried by a gentle nitrogen flux, and finally the fluorescence signals were determined. In Fig. 4.6, averaged integrated total fluorescence intensity of spots is shown. From the figure it is clear that the concentration of the oligonucleotide in the liquid ink effects the total amount of the DPN-deposited material. Saturation of signals occurs at an oligonucleotide

concentration of 100 μM. Although further increase to 150 μM leads to a slight increase in deposited material, this addition is removed upon washing. These results suggest that DPN depositing of inks containing 100 μM oligonucleotide leads to saturation of reactive epoxy groups present on the surface. Moreover, hydrophobic PBAG surface modified slides showed significantly higher signals with respect to hydrophilic dendrimer slides smaller loss of material due to washing than the hydrophilic dendrimer slides. This result is in agreement with PEG-known induced macromolecular crowding effect [3]. PEG polymer experiences a significative steric hindrance along the three-dimensional dendrimeric structure of the hydrophilic slides, thus finally affecting the DNA diffusion inside the dendrimeric structure and the binding on the epoxy groups. Instead, on the PBAG surface, epoxy groups are accessible on an almost 2D surface, thus PEG doesn't affect DNA binding.

Finally, by optically measuring the droplet height (h) and radius (r) and by assuming the spherical cap approximation, the volume of a single droplet was calculated to be in the order of 10^1-10^2 fL. To verify the above results, we conducted similar experiments by piezo-depositing known amounts of the fluorescently labeled oligonucleotides on dendrimer- and PBAG-coated glass slides. For details, please consider this paper [4] in which we also estimated the absolute amount of oligonucleotide transferred during DPN by calibration of the fluorescence signal intensity. Similarly as observed with DPN deposition, hydrophobic PBAG slides determined higher fluorescence signals in comparison to hydrophilic dendrimer slides.
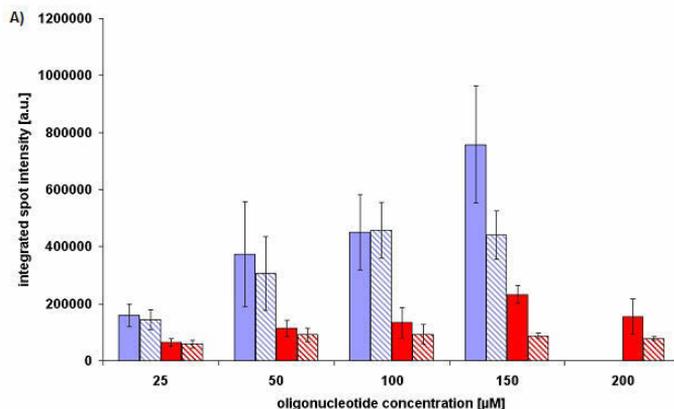
Figure 4.6: **Effects of surface chemistry and washing on the amount of surface-immobilized oligonucleotide for DPN inks with varying concentrations of oligonucleotides. The height of the bars is the total fluorescence signal intensities of a Cy5-labeled oligonucleotide deposited on either dendrimer- (red) or PBAG-coated (blue) glass surface. The filled bars represent slides directly after oligonucleotide deposition while the hatched bars denote signals determined after washing to remove non-covalently bound materials.**

4.2.3 Effects of Molecular Weight of PEG on printing conditions

Subsequently, we conducted a more detailed analysis of the DPN deposition of oligonucleotide-PEG inks on PBAG slides (see Fig. 4.7). To this end, deposition of oligonucleotide-PEG inks was tested in dependence of relative humidity, dwell time and molecular weight of the PEG. Subsequent to DPN deposition, the patterned slides were incubated overnight at room temperature and a complementary ssDNA-STV conjugate fluorescently labeled with biotinylated Atto488 dye was allowed to hybridize with the covalently immobilized capture oligonucleotides. Hybridization efficiency was determined by fluorescence microscopy, as described above. Remarkably, different molecular weights

PEGs have different physical properties (e.g. viscosity, hygroscopicity) due to chain length effects, while their chemical properties are almost identical. For example, viscosity increases with increasing molecular weight. Moreover, glycerol is used as co-solvent because of its high hygroscopic features: it permits to absorb water from the surrounding in a way dependent on the humidity. Its hygroscopicity is higher than PEG and permits the ink to remain liquid on the tip for a lot of time.
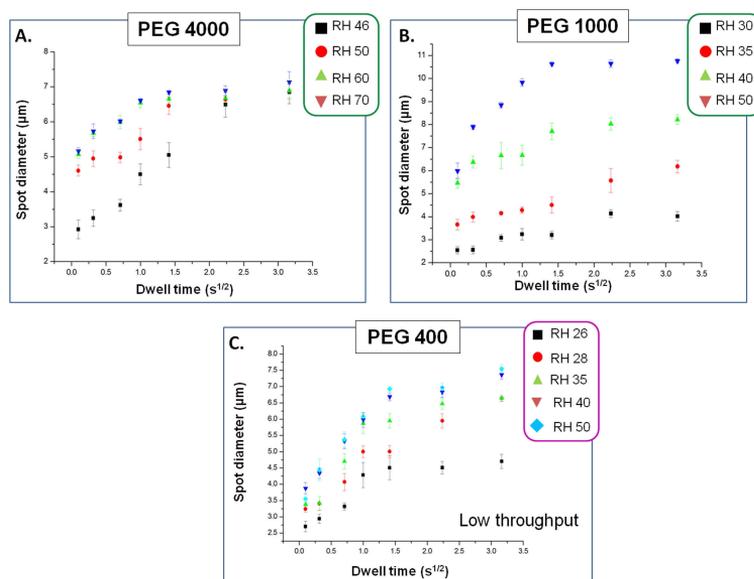

Figure 4.7: **Control of spot diameter size for PEG-oligonucleotide liquid ink by DPN. Effect of dwell time (ranging from 0.01 s to 10s) on spot diameter size obtained at varying relative humidities (R.H.) and molecular weights of PEG: (A.) PEG 400, 26 - 50 % R.H.; (B.) PEG 1000, 30 - 50% R.H.; (C.) PEG 4000, 46 % - 70% R.H.. Each value represents the average of at least five different spots. Data were extracted from fluorescence images subsequent to hybridization of the oligonucleotide arrays with dye-labeld complementary DNA-STV conjugate.**

It is evident from Fig. 4.7 that the spot diameters increase with

increasing dwell times. In particular, the spot size linearly increased for short dwell times ($< 2s$) reaching a plateau for longer dwell times after about 2 seconds. This observation is in agreement with an earlier study on liquid ink deposition [5], and it can be attributed to the lower ink transportation rates for larger spots as one would expect from diffusive ink transport at long dwell times [6]. Notably, the increase of spot dimensions by augmenting dwell times is typical for diffusive inks, in which the diffusing molecules on substrates are assumed non-interacting, and therefore their behaviour is described by a 2D Fickian diffusion model [7]. However in contrast to the diffusive mechanism where the spot diameter linearly goes with the square root of the dwell time, we found out that in case of PEG-based inks, the diffusion reaches the maximum at at dwell time of two seconds, after which the ink behaves as non-diffusive.

Relative humidity plays a crucial role for the inks viscosity and thus the deposition efficiency, as we observed by measuring spot sizes. We found that more viscous PEG inks, i.e. those containing higher molecular weight PEG, can be deposited only at higher R.H.. In particular, PEG 400 ink can be easily deposited even at low humidity around 25% R.H. while PEG 1000 requires at least 28 % R.H. and PEG 4000 cannot be deposited at humidity lower than 45 % R.H.. These findings clearly indicate that relative humidity (R.H.) thresholds increases with PEG molecular weight, this being attributed to the lower fluidity of inks having higher molecular weight PEGs. In addition, it was also observed that the thresholds are particularly critical for loading of the tip: this meaning that at humidity lower than the above reported threshold, ink was not fluid enough for the inking the pens at the microwells. At short
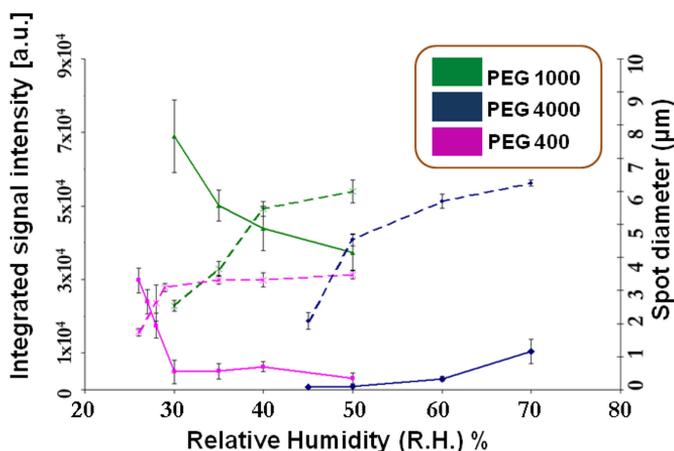
Figure 4.8: **Control in DDI-based integrated fluorescence signal intensity (lines) and spot diameter (dashed lines) for liquid oligonucleotide inks containing PEG 400 (magenta), PEG 1000 (green) and PEG 4000 (blue).**

dwell times, PEG 400, PEG 1000 and PEG 4000-based inks showed a linear increase in spot size upon increase in R.H. from 30 % to 60 %, as one would expect from an ink with less viscosity and also enhanced liquid adhesion receiving surface because of the higher humidity [8]. At fixed dwell times of 0.01 s, spot diameters increased with relative humidity for all PEG inks (dashed lines in Fig. 4.8). However, the curves indicate that further increase in R.H. did not lead to significant increase in spot size, this suggesting that transport at high R.H. (that is at high ink fluidity), is no longer driven by viscosity but by contact time along

with surface energy. Accordingly, in this high-fluidity conditions, surface energy tends to slightly reduce the ink meniscus spreading on the surface, as already reported for 1-octadecanethiol patterning at R.H. higher than 40% via diffusive DPN on gold surfaces [9]. Nonetheless, dwell times of greater than two seconds did not increase the spot size further, as indicated by the plateau of the curves in Fig. 4.7. The writing throughput by Liquid DPN strongly depends upon viscosity of the liquid ink: the higher is the viscosity of the ink, the higher is the number of spots that can be written by a single pen. Generally, the best writing conditions were attained by employing PEGs 1000 and 4000: they both permitted to attain extended DNA writing (at the best writing typically on 2-3 mm^2 by employing 1D pen array at 30 % R.H. for PEG 1000 and 50 % for PEG 4000). On the other side, PEG 400 permitted to attain only moderate writing throughput, with at the best only half a mm^2. These data are not reported.

To further optimize the DPN process towards generating smallest possible spots with highest possible concentration of chemically bound DNA oligomers, we also studied the dependency of signal intensity from ink composition and R.H. (continuous lines in Fig. 4.8). From the graph we obtained, it is clear that R.H. strongly affects the hybridization capacity of the oligos at the spots. Each of the different inks showed distinctive maximum signal intensity at a particular R.H.. PEG 400 ink produced highest signals at low R.H. of 26%, PEG 1000 at 30% R.H., while PEG 4000 led to highest signals at higher humidity as 70% R.H. PEG 1000 produced the highest signals in absolute, followed by PEG 400 and PEG 4000. Two competing mechanisms are responsible for these humidity-dependent changes in hybridization capacity. On the

one hand, increased R.H. leads to increasing spot size due to decrease viscosity of the ink as the consequence of water uptake from the air. On the other hand, water uptake leads to dilution of the oligonucleotides ink solution, and thus decrease in binding capacity. These results are in accordance to previous studies on diffusive inks [9], in which humidity plays a double role for DPN writing onto bare gold surface: on the one side water molecules increase the size of the meniscus and then the amount of the transported ink, on the other side water behaves as resist layer on the metal surface impeding molecules to adsor on it.

Taken all together, these data interestingly show that the best conditions between small feature sizes and high density of immobilized oligonucleotide are obtained by PEG 1000 inks showing enough fluidity to permit DNA oligonucleotide solution to flow from the tips at lower-intermediate humidity, with a capture oligonucleotide concentration of 100 μM and 0.01 s as dwell time..

4.2.4   Dual oligos array by DPN

Multi-features arrays are the ultimate goal of DPN fabrication. However, simultaneous parallel patterning of different chemical entities via DPN methods at sub cellular scales ($< 10~\mu$m) is still quite awkward [10]. Anyway, this capability is of tremendous importance for fundamental cell-biology studies [11]. We set-up a robust and rapid method to generate micro-scale arrays of two capture oligonucleotides - corresponding after DDI to two biological different ligands - at dimensions below a single cell in a high throughput fashion by using the optimized conditions discovered in the methodological studies: that is the deposition by employing PEG 1000-based oligonucleotide inks at 30 % R.H. and

employing 0.01 s as dwell time in order to write as many array as possible with the smallest spot dimensions and the smallest. We realized the double-oligo array as follows.
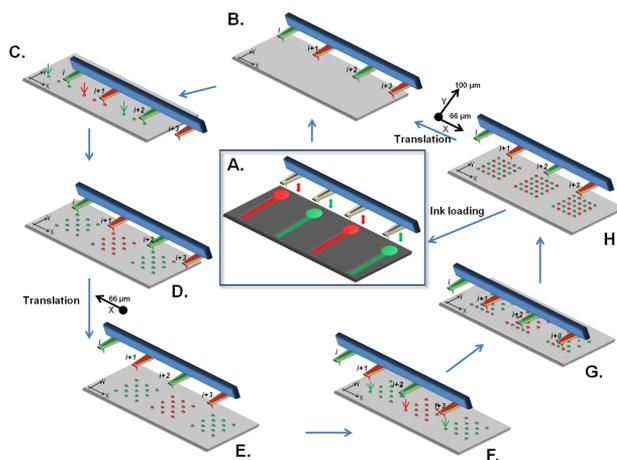

Figure 4.9: **Scheme for DPN fabrication of double-oligonucleotide arrays - respectively red spots for acF5 and green spots for acF10 - using 1D M-type pens array. For sake of simplicity, only four adjacent pens of the pen array are shown as pens writing three arrays. In A, the pen array is alternately inked with the two oligonucleotides in a single step by a microfluidic inking device. At the outset the first sub-array is written (parts B-C), then after a translation along the X-axis (parts D-E) and a pens microscale alignment on the previous pattern (part F), the double-oligonucleotide array is completed with the second sub-array (parts G-H). The pen array is translated along the X-axis of 66 μm to the right and along the the Y-axis of 100 μm on to write new arrays. The process is repeated as long as ink is present at the pens.**

We considered one generic 1D M-type pens array having twelve pens 4.9. These are marked by a i index for i comprised between one and nine (both included). All the pens are inked at once with the two oligonucleotides acF5 and acF10 in an alternated manner - i.e. pen i is inked with acF10 (green colour), pen $i + 1$ with acF5 (red color), pen $i + 2$ with acF10 and so on- by employing microfluidic inkwell loading

(see A-B). The double oligo array is constituted of two different partial arrays each one corresponding to one capture oligo. The first sub-array is realized by dispensing lines of spots with 24 μm pitch (see C-D) - each pen starting by the spot marked by an arrow. Then the pen array is translated of 66 μm to the left on the x-axis by the stage motor (see E). Afterwards, microscale alignment via the Alignment software tool is executed: the pens inked with oligo acF5 are aligned in the position held in the previous step by pens inked with acF10 before writing the prime sub-array - i.e. on the spots marked with arrows - and vice versa for the pens inked with oligo acF10. The positional error is of approximately $\pm$ 3 μm on the plane (see F). Time consuming nanoscale alignment is not executed since feature sizes are in the micrometer scale range: then an optical alignment is sufficient. The second sub-array is then fabricated via depositing the remaining spots with 24 μm pitch in between the spots of the other oligo (G). The final result is an array of alternated oligo spots having ideally 12 μm pitch (H). Being the feature alignment on the micron scale, spots of the two oligos are not exactly aligned on the plane (as shown in the picture) but tend to be a bit staggered. In the ideal case, it is possible to get 11 dual-oligo arrays per M-type pen array, being the subarray written by the twelfth pen not completed with the second one. Subsequently, the pen array is translated on the X-axis of 66 μm to the right and 100 μm on the Y-axis by stage motors in order to repeat the procedure until there is enough liquid at the pens; otherwise new ink is loaded (A) and the process is repeated. The above explained process takes advantage of the high-throughput writing capabilities of the optimal conditions we found previously (PEG 1000 as carrier, oligo concentration 100 μM, 30 % R.H., 0.01 s dwell time) to

write quite rapidly (times of minutes) dual features array on mm^2 areas
(see Fig. 4.13).
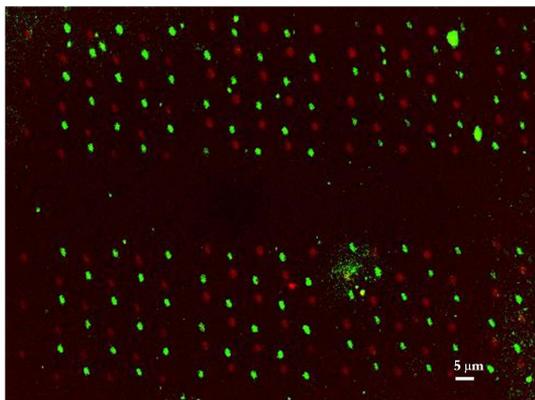
Figure 4.10: **Fluorescence image of oligonucleotide arrays containing two different oligonucleotides (acF5, acF10) hydridized with fluorophore-tagged complementary sequences (cF5-STv-biotinAtto564 and cF10-STV-biotinAtto488) in the same array.**

4.2.5 Applications as Single Cell Arrays

The methodology we implemented is a general strategy to create complex protein biochips for cell biology applications: we showed this for cell adhesion properties on these arrays. Moreover this methodology can also be applied to the generation of an innovative intracellular biosensor via fluorescence red-out [12, 13]. In the following section, hints concerning the application of the above optimized biochip arrays will be briefly reported.

In order to prove the generation of a protein biochip featured with cell ligands recognized by cellular receptors we chose epidermal growth factor (EGF) as model system [1]. The biotinylated epidermal growth factor (EFG) was coupled with covalent ssDNA-STV conjugates by employing biotin-STV interaction; subsequently it was hybridized with its complementary ssDNA sequences spotted by DPN on glass surface. This surface-immobilized EGF was used for the recruitment and clustering of EGFR by lateral diffusion in the plasma membrane. The recruitment of concentration of eGFP-EGFR is clearly visible on spots functionalized with the biotinEGF-STV-DNA conjugate by DDI. For more details concerning the results of these experiments, please consider the paper [4] and the Ph.D. thesis from S. Reisewitz [15].

Geometrical arrays for cell topology studies

As firstly shown by Chen et al. [16], endothelial cells can switch from growth to apoptosis in presence of micropatterned substrates con-

---

[1]Epidermal growth factor is a growth factor that plays an important role in the regulation of cell growth, proliferation, and differentiation by binding to its transmembrane receptor EGFR which belongs [14]
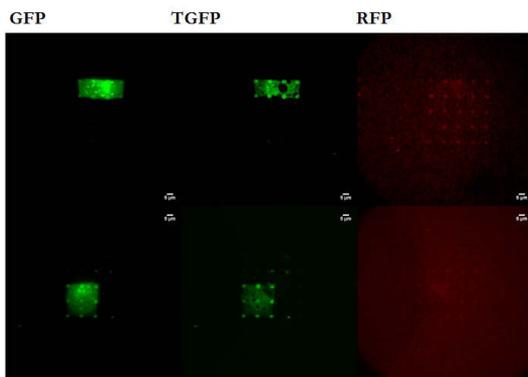
Figure 4.11: **Fluorescence image of single MC7 cells with their eGFP-labeled EGFR adhering to the spots containing biotin EGF-STV-DNA conjugate by combination of DDI and DPN.**

taining extracellular matrix-coated adhesive islands of decreasing size to progressively restrict cell extension. This means that cell shape can in principle govern whether individual cells grow or die, regardless of specific type of matrix protein or antibody. We also tryed to implement this fundamental notion within our experiments by implementing arrays having specific geometrical features: see for instance Fig. 4.12 for two arrays of this type. Studies in the future will deal with the employment of such type of arrays for for cell topology studies.
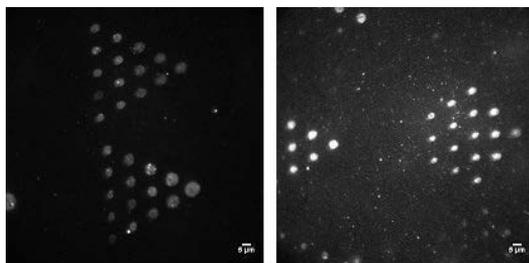
Figure 4.12: **Geometrical feature (triangle, hexagon) arrays by DPN. Patterns of cF5 were deposited on surfaces, subsequently F5-STV-b488 was used for visualization.**

Single-cell interaction array

As last application, these protein chips acting have been used as a intracellular biosensors able to measure intracellular levels of cAMP [17]. In particular this system consists of immobilized ligands onto which designed receptors are selectively recruited. Each receptor presents an intracellular protein domain of interest acting as a bait (regulatory subunit of PKA). A cytosolic tagged binding partner (i.e. the catalytic subunit of PKA) works as prey. The recruitment of artificial receptors for single-cell interaction arrays was performed via a strategy analogous to that of EGFR-based experiments. As a proof-of-principle, alterations in the interaction between these two proteins, the catalytic and regulatory subunit of the cAMP-dependent protein kinase (PKA) in living cells following manipulation by pharmacological treatment on the β-adrenergic receptor signaling, were measured via Total-internal reflectance fluorescence microscopy. Briefly, as to the perturbations of cAMP levels following pharmacological treatments on the β-adrenergic receptors, the expected dynamic responses were retrieved. A receptor agonist permitted to transiently dissociate the bait/prey complex, while an irreversible receptor antagonist prevented receptor stimulation. Finally, Adenylate Cyclase agonist (Forskolin) in combination with Phosphodiesterase inhibitor (IBMX) reversibly induced dissociation of the bait/prey complex.

4.2.6   Sub-micron protein arrays by DPN

The ability to fabricate protein arrays with sub-micron scale structures is highly desirable for applications in proteomic analysis, diagnostic, drug screening, biological sensors and cell cultures due to a lower
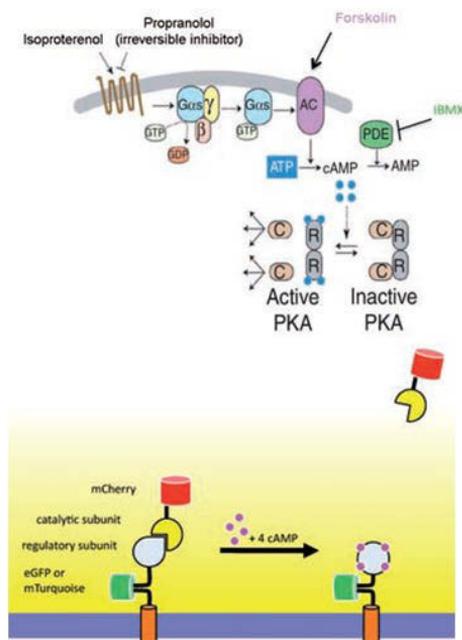
Figure 4.13: **On the top: scheme for the signal transduction mechanism of β-adrenergic receptors and the influence of pharmacological treatments. The signal pathway depiction is modified from Zamir et al. [18]. On the bottom: intracellular cAMP bio-sensor based on the modulated interaction between regulatory and catalytic sub-units of PKA. The scheme is modified from Gandor S., planned dissertation, TU Dortmund (2012) [13].**

sample volume consumption as well as an increase sensitivity of a smaller spot when both sample volume and analyte concentration are limited. But in the specific case of cell-culture applications, which require analysis of co-operative patterning and geometric effects on individual cell surfaces, there is an additional size requirement in that more than one functional protein must be patterned together on a scale below the size of a single cell [19]. If this is achieved, the response of the cell to the surfaces is usable as a readout of the biological function of the pattern. The cellular environment is by definition a complex system of chemical,

topographic, and mechanical signals, all of which can influence intracellular tension, cell migration, cytoskeletal organization, and ultimately cell fate. For example, interactions between the extra cellular matrix proteins and cell surface receptors, primarily the heterodimeric proteins known as integrins, initiate or modulate a wide range of signaling pathways. The ability of integrins to cluster on the nanometer length scale is also critical for activating these pathways, as well as forming the basis of focal adhesion development, the initial structure required for polymerization of the actin cytoskeleton. Nanometer scale spatial control of the extra cellular matrix proteins or peptides that associate with integrins will be paramount to mechanistically examining the effects of integrin clustering, focal adhesion size and spatial arrangement, and ligand density on cell fate and function [20].

Protein patterning via DPN techniques at feature sizes smaller than a single cell have shown great potential applications for use as tools to control cellular activity at the single cell level. For example, Hoover et al. [21] prepared symmetric and asymmetric cell adhesive peptide nanoarrays for the study of single cell polarization by Dip pen nanolithography of hydroquinone terminated alkanethiol on gold substrates. In [22] Y. Mei and coworkers developed an automated printing technique microscale direct writing (MDW) technology for the generation of complex extracellular matrix protein arrays at subcellular feature size (6-9 microns spot size) with multiple components: the first component is a mixture of laminin and collagen, the second is Fibronectin. The cell adhesion properties of these two systems are sufficiently different in order to observe a clear difference in cell adhesion and spreading of a model cell line, mouse fibroblasts. More recently, Sekula et al. [19] employed

1D pen arrays to execute the simultaneous patterning of multicomponent micro- and nano- structured supported DOPC lipid membranes and multilayers containing various amounts of biotin and/or nitrilotriacetic acid functional groups. Adsorption of functionalized proteins based on streptavidin or histidine affinity tags permits to generate model peripheral membrane bound proteins. These membrane patterns are then used as substrates for cell culture: this was demonstrated with the selective T-cells adhesion and activation by functional proteins (anti-CD3/anti-CD28 antibodies) bound to phospholipid multilayer patterns via streptavidin. Recently, by employing DPN techniques, J. M. Collins and S. Nettikadan were able to generate sub-cellular patterns of fibronectin and laminin to show [23] the binding dynamic of two different cell types (3T3 fibroblasts and C2C12 myoblasts) respectively with respect to fibronectin and laminin with a spatial control at single cell level (see fig. 4.14). The need for a clarification of the individual effects of these signals has driven the development of new techniques to control the distribution of biomolecules and topographic features at length scales below one single cell. A major hurdle in fabricating submicron-patterned substrates by standard photolithographic techniques is the high costs associated with the fabrication processes become prohibitively expensive as the scale of the patterns moves below the diffraction limit of the processing light. Importantly, unavoidable UV exposure, time consuming multiple baking steps, cleanroom access and solvent development pose potential threats to biological materials. Microcontact printing cannot easily translate well into the nanoscale, as the low modulus of the elastomeric stamps affects pattern fidelity. On the other side, *in vitro* patterning of biomolecules using Dip Pen Nanolithography allows

for a simplification of the deposition processes. By delivering inks to a surface in a molecular format, DPN permits to integrate in parallel functional biomolecules on subcellular length scales due to its constructive nature, high resolution and high throughput capabilities if executed in parallel manner by employing pen arrays.
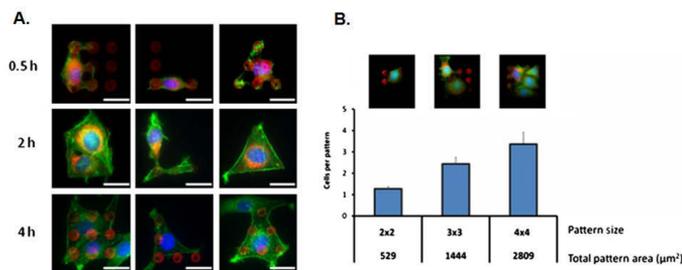

Figure 4.14: **Single cells on arrays fabricated by Dip Pen Nanolithography methodologies. (A.) Cells attach to fibronectin and spread over time. At 2 h, cell morphology clearly coincides with the protein patterns. Actin filaments become more defined, and spreading and migration occur through 4 h. Scale bar = 20 μm. (B) Larger patterns allow more cells to bind, and single cell levels can be achieved by employing 529 μm^2 patterns of fibronectin. Pictures adapted from [23].**

As previously explained in Chapter 1, at the current state of knowledge liquid DPN is not sufficient to achieve sub-micro features patterning since their feature sizes are in the micron range. On the other side, diffusive inks easily permit sub-micro patterning resolution. However, albeit being possible in principle as shown by Mirkin et al. [24], printing DNA as diffusive ink is much less effective than printing it as liquid ink, due to large size and low diffusion coefficient of DNA/oligos molecules. Recently, Turri et al. [24] realized high density DNA arrays by by direct deposition with Dip-Pen Nanolithography of acrylamido-functionalized oligonucleotides (23-mer) on spin-coated, flat polystyrene surfaces, looking at the spots in topography and demodulation modes: their findings

prove that it is possible to print single DNA sequences in diffusive conditions. Finally, we performed preliminary experiments to evaluate the feasibility of a diffusive approach by using an ink having a cF9 oligomer at the concentration of 15 μM, with the add of Tween 20 at 1% (v/v) and glycerol at 30% (v/v). We obtained sub-micron resolution spots (lateral dimensions of 750 $\pm$ 50 nm - average of twenty spots) at 40 % R.H on dendrimeric modified glass slides. However, fluorescence imaging showed undesirable halos around the printed features, which might be due to the not optimized drying of the molecular ink prior to the deposition. Additional researches will focus on the optimization of such sub-micrometer DNA molecular dispensing approach in a multiplexing format. A big hurdle to be solved is the ink loading at the tips. Microfluidic ink loading at inkwells for diffusive inks is much more challening than for liquid inks; importantly, the solvent of the diffusive ink should not evaporate too fast from the inkwell's channels, but should evaporate fast form the dipped pen.
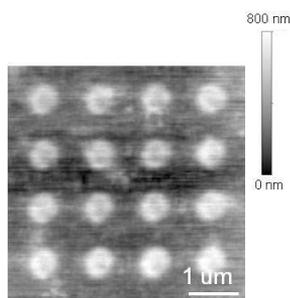
Figure 4.15: **Lateral Force Microscopy Image of a sub micrometer spots oligomers array printed on modified glass slide.**

References

[1] Benters R.; Niemeyer C. M.; Wöhrle D., *ChemBioChem* **2**, 686 (2001).

[2] Niemeyer C.M.; Bürger W.; Hoedemakers R.M.J., *Bioconjugate Chem.* **9**, 168 (1998).

[3] Ellis R.J., *TiBS* **26**, 597 (2001).

[4] Arrabito G.; Reisewitz S.; Dehmelt L.; Bastiaens P.I.; Pignataro B.; Schroeder H. and Niemeyer C.M., *Manuscript in Preparation* (2012).

[5] Senesi A.J.; Rozkiewicz D.I.; Reinhoudt D.N. and Mirkin C.A., *ACS Nano* **3**, 2394 (2009).

[6] Hampton J.R.; Dameron A.A. and Weiss P.S., *J. Phys. Chem. B* **109**, 23118 (2005).

[7] Jang J.; Hong S.; Schatz G.C. and Ratner M.A., *Journ. of Chem. Phys.* **115**, 2721 (2001).

[8] B.L.; Peterson, E. J.; Weeks, De Yoreo J.J, and Schwartz P.V., *J. Phys. Chem. B* **108**, 15206 (2004).

[9] Rozhok S.; and Piner R.and Mirkin C.A., *J. Phys. Chem. B* **107**, 751 (2003).

[10] Sekula S.; Fuchs J.; Weg-Remers Su.; Nagel P.; Schuppler S.; Fragala J.; Theilacker N.; Franzreb M.; Wingren C.; Ellmark P.; Borrebaeck C. A. K.; Mirkin C. A.; Fuchs H.; Lenhert S., *Small* **4**, 1785 (2008).

[11] Kim M.H.; Kinooka M; Taya M., *Biotechnol. Adv.* **28**, 7 (2010).

[12] Gandor S.; Reisewitz S. et al., *Manuscript in Preparation* (2012).

[13] S. Gandor, Ph.D. thesis, TU Dortmund, 2012.

[14] Reynolds A.R.; Tischer C.; Verveer P.J.; Rocks O.; and Bastiaens P.I.H., *Nat. Cell Biol.* **5**, 447 (2003).

[15] S. Reisewitz, Ph.D. thesis, TU Dortmund, 2012.

[16] Chen C.S.;, Mrksich M.; Huang S.; Whitesides G.M.;., and Ingber D.E., Science **276**, 1425 (1997).

[17] Thevelein J.M. and De Winde J.H., *Molecular Microbiology* **33**, 904 (1999).

[18] Bastiaens P.I.H. Zamir E.; Lommerse P.H.M.; Kinkhabwala A., Grecco H.E., *Nat. Metods* **7**, 295 (2010).

[19] Sekula S.; Fuchs J.; Weg-Remers S.; Nagel P.; Schuppler S.; Fragala J.; Theilacker N.; Franzreb M.; Wingren C.; Ellmark P.; Borrebaeck C.A.K.; Mirkin C.A.; Fuchs H. and Lenhert S., *Small* **4**, 1785 (2008).

[20] Schmidt R.C.; Healy K.E., *J. Biomed. Mater. Res. Part A* **90**, (2009).

[21] Diana K. Hoover, Eugene W. L. Chan, and Muhammad N. Yousaf, *J. Am. Chem. Soc.* **130**, 3280 (2008).

[22] Mei y.; Cannizzaro C.; Park H.; Xu Q.; Bogatyrev S.; Yi K.; Goldman N.; Langer R.; Anderson D.G., *Small* **4**, 1600 (2008).

[23] Collins J.M.; Nettikadan S., *Anal. Biochem.* **419**, 339 (2011).

[24] Demers L.M.; Ginger D.S.; Park S.-J.; Li Z.; Chung S.-W.; Mirkin C. A., *Science* **292**, 1836 (2002).

Conclusions

The first main result of the thesis is the establishment of an innovative drug screening platform based on ink-jet printing methodologies coupled with simple optical detection methods and consisting in dispensing chemical libraries on biological targets in a rapid, low-cost, miniaturized (until single spot), and high-throughput manner. In comparison to conventionally used robotic systems coupled with microwell arrays, this methodology allows one to realize at very low cost (no clean room facilities, prompt target-covered surface reusability, picoliter drop consumption) programmable microarrays in a up to two orders of magnitude faster (10 spots/s) fashion (e.g., refer to 0.1 spots/s of pin printing technique), a comparable positional accuracy and spot morphology by tuning only a few parameters like drop viscosity and surface tension, and the advantage to work not only on hard but also on soft surfaces without any risk of damage and with similar results of liquid phase assays. This drug screening approach was firstly proved with a model enzyme system like Glucose Oxidase substrate covalently linked to a function-

alized silicon oxide support. On this support an enzymatic substrate (D-glucose)/inhibitor (D-glucal) couple was accurately dispensed and enzymatic competitive inhibition was observed by employing a simple horseradish peroxidase colorimetric method which is prone to generalization if employing ligand biotinylation and streptavidin-peroxidase conjugates. Afterwards, this drug screening approach was extended to CYP450 enzymes like CYP3A4, one of the main targets for the phase I drug metabolism via a droplet microreactors arrays containing CYP3A4 enzyme mixed with model inhibitors (like erythromycin) and enzymatic chemiluminescent substrates (Luciferin-Isopropylacetate). The enzymatic activity was again detected by using easy and low cost optical measurements of spot brightness to confirm the inhibition at a single spot level. Perspectives are constituted by extension of such drug screening platform using new possible molecular drug candidates with submicromolar potency in order to exploit the real screening abilities of this device on Metabolic enzymes like CYP3A4.

The second main result of this thesis is the set-up of a robust strategy for the creation of complex protein biochips on modified glass surfaces displaying spots of cell-specific ligands with lateral dimensions minor than one single cell. This methodology is constituted by the combination of high-throughput and multiplexed Dip Pen Nanopatterning in liquid format and Proteic Ligand DNA-Directed Immobilization (DDI). Dip Pen Nanopatterning permits to generate oligomer DNA spots features at the sub-cellular scale, while with DDI approach enables ready functionalization of such arrays into corresponding multi-feature ligand arrays for cell capture and cultivation. The response of the cell to such structured surfaces is usable as a readout of the biological function of

the pattern. In a first application the epidermal growth factor (EFG) protein arrays were realized to display specific single cell adhesion activity. As a second application, immobilized proteic ligands were used to recruit designed cellular receptors which presented intracellular protein domain (regulatory subunit of cAMP-dependent protein kinase) whose interaction with a cytosolic binding partner (catalytic subunit of cAMP-dependent protein kinase) was monitored and pharmacologically perturbated. This methodology has a remarkable importance for fundamental research in cell biology and has applications in biomedical diagnostics and nanobiotechnology. Future work will consider the the optimization of sub-micrometer DNA molecular dispensing approach via diffusive approach in a multiplexing format and also geometrical arrays for cell topology studies.

Acknowledgments

In this thesis work, an enormous number of people have to be acknowledged for what they gave me with their help. I would like to start this important part saying thanks to all those I will forget! The first I have to acknowledge are my parents: without their continuous efforts I wouldn't have reached the conclusion of my PhD. I needed them to feel secure and calm about my future and my life telling me that I have to look to the future with confidence. I have to acknowledge prof. Bruno Pignataro because he has always trusted in me and in my capabilities also when the things were not as good as we wanted they to be (or at least as if he wanted them to be). During all the thesis activities he continuously gave me tons of advises for how I had to manage in difficult situations: without his efforts we wouldn't have reached the proposed results. I hope I will continue my collaboration with him after the PhD experience. I have to acknowledge prof. Salvatore Pignataro for his continuous great support as tutor during all the activities not

only during my PhD but also since the first years at University: it was a great honour for me to work in Superlab for my research activities. Many thanks also to prof.ssa Maria Grazia Grimaldi who was very kind in supporting me as tutor during the last year of my PhD. Then I really have to thank prof. Christof Niemeyer since he always trusted in me and in my work on Dip Pen Nanolithography even if he knew that it was a quite difficult subject. He gave me the great opportunity to work in his wonderful group: I found not only great scientists but also very nice and loyal persons that I will never forget. I have to acknowledge all the colleagues of Superlab I met during the great years of work I spent in the lab. Special thanks have to go to Simone Fabiano: we frequented the same places from the Bachelor thesis till the PhD. It was great having him as colleague since he is a determined and wilful person: I hope the best for his future. I have to acknowledge Chiara Musumeci, a great scientist and also a nice person: I learn a lot from her. I cannot forget Alessandro Luzio: I have to say thank to him if I learnt AFM. I cannot forget Sebastiano Cataldo: I will always remember the numerous discussions about the role of Chemistry in Cultural heritage preservation. Special thanks go to Giuseppe Indelli, the great technician of Superlab: it is thanks to him if the machines inside the lab work. I cannot forget Antonino Scandurra, always able to give me wise advises.

I have to acknowledge all the fantastic people of the group of Biologisch-Chemische Mikrostrukturtechnik of prof. Christof Niemeyer in Technical University of Dortmund: Anna König, Katrin Vogel, Katja Prjadko, Stephie Reisewitz, Rebecca Meyer, Petra Alhorn, Kathrin Kiko, Jens Reiber, Britta Dettweiler, Philipp Ochtrop, Hendrik Schröder, Thomas Kampe, Joschi Müller, Stefan Michelke, Max Glettenberg, Dennis Bauer,

discussions about enzyme kinetics. I miss Holger Schmitte because he was really fundamental to solve the complicated bureaucracy stuff we had to manage with when in Dortmund. And I cannot forget Josipa Brglez because I spent nice times with her especially when we went at lunch and I complained about the food I had in Menza. Of course a "grazie!" wouldn't be enough to thank Barbara Saccá, one of the nicest and smartest persons I have ever met. She was very friendly with me; I remember the moments in which we laughed loudly when I tried to talk to her in our sicilian dialect. I really felt to be at home when I talked with her: I hope the same for her.

A special thank I have to address is to the marvelous people of the Max-Planck Institute of Molecular Physiology of Dortmund. I have to say thanks to Leife Dehmelt, Tomas Mazel, Janos, Silke Gandor, Julia Arens, Katharina Ruf, Melanie and Magda Krejczy. Firstly, I have to acknowledge Leif Dehmelt, a genial and enthusiastic biologist always prone to help me when I wanted to know about cell-biology and fluorescence microscopy. It was great to know Tomas Mazel, I really liked the discussion we had in italian. I am really grateful towards Silke Gandor, a very skilled biochemist and also a very nice person. She was always very helpful especially because she gave me a lot of dark chocolate which I like a lot! I also have to acknowledge Igor Titushkin (Nanoink Inc.), Andreas Bergner (L.O.T.-Oriel GmbH), Wilfried Helle (L.O.T.-Oriel GmbH) for their precious help for fixing up the problems of the DPN instrument. I cannot insert all the people from Central America I met during my stage in Dortmund; but I cannot forget Javier Portillo and Rodrigo Torres since they were two fantastic friends that helped me in so many ways since the first days of my stay. I will never forget

them. Also, I have to acknowledge all the Italian group of Dortmund: I really liked the time we spent together especially when we went at lunch. Great thanks have to go to Consiglio Nazionale delle Ricerche - Sezione Istituto Microelettronica e Microsistemi; in particular to Sebania Libertino and Vera Aiello who gave me the expertise and know-how for managing Glucose Oxidase surfaces preparation. They were very kind and professional colleagues who always helped me when I needed their assistance. Then I have to acknowledge ST-Microelectronics, in particular Clelia Galati and Natalia Spinella who helped me for the preparation of CYP3A4 chips. I found the collaboration with them extremely interesting and involving, I still hope to maintain contacts with them after the PhD.

I also want to say thanks to all the colleagues of the Ph.D. in Nanoscience at Scuola Superiore di Catania: Paolo Cardile, Yana Aleeva and Laura Zanoli. I spent very nice times with them, especially looking back to the Lectures of the First year of our Ph.D. Many thanks to the Bice Immé: she was always helpful with me during all the three years of the Ph.D. and especially when I was in Dortmund and I needed some documents.

I cannot conclude this thesis without mentioning Funding: they are always fundamental. I have to acknowledge Italian MiUR (PRIN program), FIRB-MERIT, FIRB "Futuro in Ricerca 2008", University of Palermo and Laboratorio Pubblico Privato PlastICs for financing the researches concerning drug screening. I have to acknowledge financial support by the International Max Planck Research School in Chemical Biology (IMPRS-CB) for the activities in Dip Pen Nanolithography. Finally, my research period in Dortmund was supported by Contributo

della Scuola Superiore di Catania XXIV ciclo (Contribution of Scuola Superiore di Catania XXIV cycle) and by prof. Christof Niemeyer.

We are living in a period of difficulties due to the economical crisis: many things are changing and we are all worried about the future, me too. I hope the things can be better in next years. But this depends on every one of us that has to do his own part to make this world a better place where to live. With this thesis, even if knowing my great human and technical limits, I tried to give my very small contribution in that, so small that we define it nano, **Nanoscience**.

Giuseppe, Domenico Arrabito

Omnia sol temperat, purus et subtilis. Nova mundo reserat faciem Aprilis.

Come Ulisse hai lasciato la terra natìa desiderando sempre di tornarvi.
Come Itaca del proprio eroe, la tua terra è fiera delle tua gesta.

The ideal situation occurs when
the things that we regard as beautiful
are also regarded by other
people as useful.
Donald Knuth